Titre: Title:	Clean combustion of natural gas in a turbulent fluidized bed reactor
Auteur: Author:	Makoutchou Foka
Date:	1994
Type:	Mémoire ou thèse / Dissertation or Thesis
Référence: Citation:	Foka, M. (1994). Clean combustion of natural gas in a turbulent fluidized bed reactor [Ph.D. thesis, École Polytechnique de Montréal]. PolyPublie. https://publications.polymtl.ca/33315/

UNIVERSITÉ DE MONTRÉAL

CLEAN COMBUSTION OF NATURAL GAS IN A TURBULENT FLUIDIZED BED REACTOR

par

MAKOUTCHOU FOKA

DÉPARTEMENT DE GÉNIE CHIMIQUE

ÉCOLE POLYTECHNIQUE

THÈSE PRÉSENTÉE EN VUE DE L'OBTENTION

DU GRADE DE PHILOSOPHIAE DOCTOR (Ph.D.)

(GÉNIE CHIMIQUE)

NOVEMBRE 1994

ISBN 0-315-99730-3

UNIVERSITÉ DE MONTRÉAL

ÉCOLE POLYTECHNIQUE

Cette thèse intitulée:

CLEAN COMBUSTION OF NATURAL GAS IN A TURBULENT FLUIDIZED BED REACTOR

présentée par: **FOKA Makoutchou**

en vue de l'obtention du grade de: Philosophiae Doctor

a dûment été acceptée par le jury d'examen constitué de:

M. LEGROS Robert, Ph.D., président

M. CHAOUKI Jamal, Ph.D., membre et directeur de recherche

M. GUY Christophe, Ph.D., membre et co-directeur de recherche

M. CHAVARIE Claude, Ph.D., membre

M. CHORNET Esteban, Ph.D., examinateur externe

... to

John Chu Enoh,

Geraldine Jones Smith,

Roy Tembi,

& Gilles Grondin,

...

SOMMAIRE

La technologie du lit fluidisé a connu au cours des dernières années un grand essor dans l'industrie pétrochimique, en génération de chaleur, en minimisation des déchets solides, etc... Cependant, son potentiel comme technologie de combustion propre du gaz naturel reste encore inexploité. La combustion catalytique du gaz naturel peut s'effectuer à basses températures pour générer de l'air chaud et propre à des fins agro–industrielles (séchage) ou domestiques (chauffage de bâtiments) si la taille du réacteur est raisonnable.

Le but de ce travail était d'évaluer expérimentalement la faisabilité de la combustion catalytique du gaz naturel dans un lit fluidisé comme technologie environnementalement douce. Les polluants à éviter étant les oxydes d'azote (NOx) et le monoxyde de carbone (CO). Une méthodologie en quatre étapes a été suivie: (1) détermination du régime hydrodynamique approprié, (2) évaluation des propriétés cinétiques du catalyseur de combustion, (3) caractérisation de l'hydrodynamique du lit fluidisé, (4) combustion catalytique dans le lit fluidisé et couplage de la cinétique et de l'hydrodynamique pour prédire la performance du réacteur pilote.

Afin d'atteindre ces objectifs, nous avons fait une étude bibliographique poussée sur les catalyseurs pour la combustion totale du méthane, sur l'hydrodynamique des lits fluidisés et les modèles de réacteurs à lit fluidisé. Ces informations nous ont permis alors de déterminer les conditions optimales d'opération et le diamètre minimal du réacteur requis pour produire une quantité substantielle de chaleur pour une composition du mélange d'entrée donnée en méthane. Ceci a été possible grâce à la mise au point d'un algorithme de design.

Les résultats de la simulation avec cet algorithme ont clairement indiqué la nécessité d'opérer en régime turbulent afin de réaliser une conversion de 100% tout en générant une puissance substantielle (50–500 kW). Un réacteur pilote de 100 mm de diamètre et de 1.6 m de hauteur a donc été conçu et construit. Il a été équipé pour l'étude hydrodynamique d'un capteur de pression différentielle pour les mesures de fluctuations de pression et des détecteurs à scintillation à cristaux de $NaI(Tl)$ pour détecter le traceur radioactif lors des mesures de la distribution des temps de séjour du gaz. Pour analyser les produits gazeux, un chromatographe en phase gazeuse a été réservé pour le méthane et le dioxyde de carbone, et un appareil *Landcombus* pour la détection des oxydes d'azote et du monoxyde de carbone.

Les paramètres cinétiques des catalyseurs à base de platine (PSA) et de palladium ($PC263$) tous obtenus de la compagnie *Procatalyse* ont été évalués dans un réacteur tubulaire de 7 mm de diamètre dans des conditions atmosphériques entre 400 et 600°C. Leur température d'allumage était de 310°C pour le PSA et de 275°C

pour le $PC263$. La concentration du méthane a été maintenue en dessous de 4% et un modèle cinétique de premier ordre par rapport au méthane a été utilisé pour représenter les données expérimentales obtenues sur une grande plage de temps de séjour. La simulation de la combustion en lit fluidisé turbulent avec le catalyseur PSA a montré que son activité n'était pas assez élevée pour la combustion totale dans ce régime de fluidisation.

Les mesures des temps de séjour ont été effectuées avec l'argon radioactif (^{41}Ar) comme traceur, obtenu par irradiation de l'argon–40 (^{40}Ar) dans un réacteur nucléaire *Slowpoke*. Le coefficient de dispersion axiale a été obtenu à partir des signaux enregistrés par deux détecteurs à scintillation résultant de l'injection imparfaite effectuée en dessous du distributeur poreux et pour trois types de particules (FCC,*sable*,*catalyseur* $PC263$). Les expériences à froid et à chaud ont été effectuées dans deux lits de 100 mm et de 200 mm de diamètre. Le grand lit était muni en plus d'un capteur de pression et d'une sonde à capacitance. Les résultats obtenus avec du sable et du FCC ont montré un changement net de l'amplitude du coefficient de dispersion axiale à la vitesse de transition au régime turbuelnt U_c. L'amplitude du coefficient de dispersion axiale était plus faible dans le lit de 200 mm de diamètre que dans celui de 100 mm de diamètre où l'effet de la paroi paraissait beaucoup plus prononcé. Le coefficient de dispersion axiale obtenu dans le grand lit avec les particules FCC a été corrélé en terme du taux de vide moyen mesuré par la sonde à capacitance et le nombre de Péclet obtenu dans les deux lits en régime turbulent a

été corrélé en terme des nombres adimensionnels caractéristiques du lit fluidisé.

Le modèle à deux phases de *van Deemter* a aussi été utilisé pour analyser nos données expérimentales de mesure des temps de séjour. Le coefficient de transfert de masse entre la phase diluée et la phase émulsion a été estimé et corrélé en terme de la hauteur d'une unité de transfert.

La dernière étape a consisté à faire la combustion catalytique du méthane dans le réacteur de 100 mm de diamètre en régime turbulent avec le catalyseur $PC263$. La conversion du méthane était supérieure à celle obtenue en régime à bulles pour les mêmes nombres d'unités de réaction et un simple modèle piston dispersif a été utilisé pour modéliser nos données expérimentales obtenues entre 450 et 500$°C$. Le modèle parfaitement mélangé s'est aussi avéré satisfaisant pour les données obtenues en régime à bulles. Le modèle de *Werther* a été utilisé avec les données hydrodynamiques estimées à partir du modèle de *van Deemter* pour modéliser les données de combustion du methane. Une combustion auto–entretenue du méthane a été réalisée en maintenant la température du lit inférieure à 550$°C$ avec une conversion de 100% et aucune émission de NOx ou de CO n'a été enrégistrée avec une cellule électrochimique (sensibilité 1ppm).

ABSTRACT

Fluidized bed technology has gained in recent years a high rate of use in petrochemical industry, in heat generation, in solid wastes minimization, etc... However, its potential as a zero NOx and CO emission technology for a clean combustion of natural gas remains untapped. The catalytic combustion of natural gas can be carried out at low temperatures to generate a clean and hot air for foodstuff or for domestic (building heating) use if the size of the combustor is reasonnable.

The aim of this work was to carry out the feasibilty study of the catalytic combustion of natural gas in a fluidized bed as a zero NOx and CO emission technology. A four–step methodology was used: (1) determination of the appropriate hydrodynamic regime of fluidization, (2) kinetic evaluation of the appropriate catalyst, (3) characterization of the bed hydrodynamics, (4) combustion in the fluidized bed and prediction of the reactor performance by coupling the kinetics and the hydrodynamics.

In order to achieve these objectives, we did a comprehensive bibliographical review of complete combustion catalysts, of fluidized bed hydrodynamics, and of

fluidized bed reactors models. Then, the information obtained from the literature was used to estimate the optimal operating conditions and the minimal bed diameter required to produce a substantial amount of heat for a given inlet gas composition. A design algorithm was devised in this respect.

The results of the simulations with this algorithm clearly indicated the necessity to operate in the turbulent regime in order to achieve 100% conversion while generating a substantial power of combustion(50–500 kW). A pilot scale catalytic combustor of 100 mm $I.D.$ and 1.6 m tall was then designed and built. It was equipped for the hydrodynamic studies with a differential pressure transducer used to monitor pressure fluctuations and $NaI(Tl)$ scintillation detectors used to monitor the radioactive gas tracer during residence time distribution (RTD) measurements. For gaseous products analysis a gas chromatograph was envisaged for methane and carbon dioxide and a *Landcombus* device for the detection of NOx and CO.

The kinetic parameters of two catalysts with platinum (PSA) and with palladium ($PC263$) all from *Procatalyse* was evaluated in a tubular flow reactor of 7 mm in diameter at atmospheric conditions and in the temperature range of $400 - 600°C$. Their ignition temperature was $310°C$ for the PSA and $275°C$ for the $PC263$. Methane concentration was kept below 4% and a first order kinetic model was used to fit the data obtained over a wide range of gas residence times. The simulation of the combustion in a turbulent fluidized bed with the PSA catalyst showed that its activity was not suitable for a complete combustion process in this fluidization

regime.

The RTD measurements were performed with ^{41}Ar as the radioactive tracer obtained by irradiation of ^{40}Ar in a *Slowpoke* nuclear reactor. The axial gas dispersion coefficient was derived from the responses recorded by two scintillion detectors as the result of an imperfect input injection below the porous distributor at various gas velocities, and with three different particles (FCC, sand, $PC263$ catalyst). Cold and hot experiments were conducted in two different reactors of 100 mm $I.D.$ and 200 mm $I.D.$ The latter was also equipped with a capacitance probe besides a differential pressure transducer and two $NaI(Tl)$ detectors. The results obtained with sand and FCC particles showed a change in the dispersion magnitude at the onset of turbulence U_c. The magnitude of dispersion was smaller in the 200 mm $I.D.$ bed than in the 100 mm $I.D.$ bed where the wall effect seemed to be more pronounced. The effective axial dispersion coefficient obtained in the larger bed with the FCC particles was correlated in terms of the mean bed porosity measured with the capacitance probe and the Peclet number obtained in both beds in the turbulent regime was correlated in terms of the characteristic dimensionless fluidized bed groups.

The two–phase model of *van Deemter* was also used to analyze the mixing data. The cross–flow mass transfer coefficient between the dilute and the emulsion phases was estimated and correlated in terms of the height of a transfer unit.

The ultimate step consisted of carrying out the combustion of methane in the turbulent regime over the $PC263$ catalyst in the 100 mm I.D. reactor. The conversion

of methane obtained in this regime was higher than the conversion observed in the bubbling regime at similar number of reaction units and a simple plug flow model with axial dispersion was used to model our experimental data obtained between 450 and 500°C. A perfect mixing model satisfactorily predicted the bubbling bed data. The model of *Werther* was used along with hydrodynamic data derived from the model of *van Deemter* to satisfactorily model the methane combustion data. A self–sustained combustion of methane was performed maintaining the bed temperature below 550°C with a conversion of 100% and no NOx or CO were recorded with an electrochemical cell (sensitivity $1ppm$).

RÉSUMÉ

La combustion en lit fluidisé a acquis un statut commercial au niveau mondial au cours des deux dernières décennies et plus. Cependant, la pollution de l'air atmosphérique a constamment induit des changements dans la conception et l'opération des équipements de combustion. Les changements portant essentiellement sur la modification des équipements, la destruction in situ des polluants, et sur le traitement post–combustion.

La combustion sans flamme du gaz naturel en lit fluidisé est une technologie propre en plein essor et dont le potentiel reste encore inexploité. Elle présente des avantages réels par rapports aux brûleurs conventionnels et aux brûleurs catalytiques à lit fixe.

Plusieurs régimes de fluidisation sont observés au fur et à mesure que la vitesse superficielle du gaz augmente dans le lit fluidisé, allant du régime à bulles à la fluidisation rapide en passant par le régime de pistonnage pour les petits lits et le régime turbulent. La détermination des points caractéristiques de bifurcation délimitant les différents régimes d'écoulement est très crucial, surtout avec des sytèmes de com-

bustion catalytique où la conversion du réactif dépend largement de la stabilité du système. Le régime turbulent apparaît comme le régime idéal pour la combustion du gaz naturel. En effet, en plus d'un grand rendement énergétique, la combustion en lit fluidisé turbulent ne développe pas de "points chauds", la température du lit est uniforme, et un bon contact gaz–solide favorable à la réaction est réalisé. Ce régime convient aux particules de groupes A et B de la classification de Geldart. Cependant, le temps de contact dans un lit fluidisé turbulent (LFT) est court par rapport aux lits fixes et son opération requiert un catalyseur très actif. Une caractérisation hydrodynamique est alors cruciale pour des réactions rapides.

L'objectif principal de cette recherche est d'évaluer expérimentalement la faisabilité de la combustion catalytique du méthane dans un lit fluidisé turbulent. Le problème est approché en simulant le procédé avec les données cinétiques et hydrodynamiques tirées de la littérature, et les résultats permettent de déterminer le régime hydrodynamique approprié d'opération et les paramètres de design d'un brûleur pilote expérimental. Deux catalyseurs supportés à base de platine et de palladium sont caractérisés et leurs paramètres cinétiques utilisés pour simuler la combustion dans un lit fluidisé turbulent. Seul le catalyseur à base de palladium s'est avéré suffisamment actif pour la combustion en lit fluidisé turbulent. Les fluctuations de pression et les fluctuations de la dispersion axiale du gaz sont utilisées pour caractériser le début de la turbulence. Enfin, la combustion du méthane est réalisée en régime turbulent avec le catalyseur à base de palladium et les modèles piston dispersif et de

Werther sont utilisés pour représenter la conversion du méthane.

Ce travail est supporté par une étude bibliographique poussée sur les catalyseurs de combustion totale du méthane, sur l'hydrodynamique des lits fluidisés et sur les modèles de réacteurs à lit fluidisé.

Le méthane est parmi les hydrocarbures légers le plus difficile à oxyder. Dans les brûleurs conventionnels, la température de la flamme est de l'ordre de $1200°C$ et il y a une formation intense d'oxydes d'azote (NOx). La combustion catalytique se réalise à basses températures et l'absence de radicaux de méthane empêche la formation des NOx. Bien que les lits fluidisés soient utilisés à grande échelle dans plusieurs procédés industriels, la combustion catalytique du méthane a été jusqu'ici rapportée seulement dans des lits fixes. Seule la combustion homogène a été réalisée dans des lits fluidisés. A cause de la difficulté d'oxyder le méthane, seuls les catalyseurs à base de métaux nobles (platine, palladium) sont généralement utilisés. La recherche est présentement axée sur les catalyseurs non supportés notamment les oxydes mixtes métalliques de type pérovskites. Bien que la réaction de combustion de méthane paraisse simple, le mécanisme de combustion peut être très complexe. Cependant, pour des mélanges pauvres en combustible, un simple modèle de puissance est suffisant pour représenter les données expérimentales pour des fins de design.

Les produits de combustion dépendent des conditions d'opération. Les NOx formés en abondance dans les brûleurs conventionnels à hautes températures peuvent aussi se former dans des dispositifs catalytiques prédisposés aux "points chauds".

Les NOx émanant des sources de combustion stationnaires se forment suivant trois mécanismes bien connus: le mécanisme du NO thermique faisant intervenir l'azote moléculaire présent dans l'air comburant à hautes températures, le mécanisme du NO précoce faisant intervenir les radicaux hydrocarbonés présents dans la zone de combustion et qui réagissent pour rompre la triple liaison de l'azote moléculaire de l'air comburant, et le mécanisme du NO lié qui fait intervenir l'azote lié au carburant (charbon, huiles lourdes, etc...) à des températures modérées. Le gaz naturel n'a pas d'azote lié et ne se prête à aucun des mécanismes de formation de NOx ci–dessus mentionnés à des températures inférieures à $700°C$.

L'autre polluant potentiel issu de la combustion est le monoxyde de carbone. Il est formé lors de la combustion du méthane seulement pour des mélanges pauvres en oxygène. La combustion catalytique du gaz naturel avec un mélange stoichiométrique ou riche en oxygène est donc potentiellement propre aux températures inférieures à $700°C$ dans un système ne développant pas de "points chauds" notamment dans le lit fluidisé turbulent.

L'hydrodynamique des lits fluidisés turbulents est très complexe et a été la pierre angulaire des centaines d'investigations. Trois descriptions du lit fluidisé turbulent sont couramment rencontrées dans la littérature: le lit turbulent est biphasique avec une phase diluée gaz–solide au centre et une phase dense à la paroi; le lit turbulent est homogène et est composé de petites bulles; le lit turbulent a une structure intermédiaire entre la structure du lit fluidisé en régime de pistonnage et la structure du

lit fluidisé circulant. Malgré la controverse sur la description du lit fluidisé turbulent, ses bornes sont bien établies par les vitesses U_c et U_{tr} pouvant être déterminées par les fluctuations de pression, la sonde à capacitance. Et nous montrerons au cours de cet travail que les fluctuations de la dispersion axiale du gaz peuvent aussi être utilisées pour caractériser le début de la turbulence.

Un intérêt prononcé pour l'étude des comportements du solide et du gaz se fait de plus en plus sentir dans la littérature. Le dispersion du gaz dans le lit turbulent est assez faible et le coefficient de rétromélange est presque égal au coefficient de dispersion axiale. Il est aussi bien connu que la dispersion axiale du gaz fluctue aux mêmes conditions opératoires. L'étude de la distribution des temps de séjour du gaz fait appel généralement à un traceur inerte. L'hélium, l'hydrogène et le méthane sont généralement utilisés et sont détectés par prélèvement et analyse des échantillons de gaz à des endroits précis du lit. Cependant, force est de reconnaître qu'un tel échantillonnage peut non seulement affecter l'hydrodynamique du lit mais aussi ne pas être représentatif de la section du lit où la mesure est effectuée. En utilisant par contre un traceur radioactif, les détecteurs à scintillation des rayons γ peuvent être positionnés à l'extérieur du réacteur pour détecter le passage du traceur dans une section donnée du lit.

Les modèles de réacteurs à lit fluidisé sont spécifiques au régime de fluidisation concerné. Le travail au niveau académique a beaucoup mis l'accent sur le régime à bulles avec les particules de groupe B de la classification de Geldart et les modèles

à deux phases rapportés sont légion. Les modèles à deux phases peuvent être classés en modèles à bulles où le diamètre des bulles est un paramètre clé du modèle et en modèles biphasiques simples considèrant la phase diluée comme étant continue. Aux grandes vitesses de fluidisation, la structure du lit diffère significativement de celle du lit à bulles. Le modèle coeur–anneau est généralement utilisé en fluidisation rapide. Malgré la grande utilisation du lit turbulent dans les procédés industriels, l'effort dans la modélisation de ce régime reste très modeste. Seuls les modèles à une phase ont été utilisés: le modèle piston et le modèle piston dispersif.

Cette thèse est présentée sous forme d'articles et structurée en cinq chapitres:

– L'introduction générale présente le canevas du travail et un aperçu des données cruciales de la littérature.

– La première publication traite de la simulation d'un brûleur atmosphérique à lit fluidisé avec les données cinétiques et hydrodynamiques de la littérature. Une revue bibliographique étendue sur les catalyseurs de combustion totale et sur la formation des NOx y est présentée. Un algorithme de design est codé et les principaux résultats indiquent la nécessité d'opérer en régime turbulent avec des particules fines et donnent un bon aperçu des critères de design d'un réacteur pilote pour la génération de chaleur en lit fluidisé turbulent.

– La seconde publication caractérise la cinétique de combustion du méthane sur un catalyseur à base de platine référencé PSA dans un réacteur fixe tubulaire. L'étude de la distribution des temps de séjour du gaz est réalisée à température ambiante sur

un grand intervalle de vitesses dans le lit de 100 mm de diamètre avec des particules de FCC et du sable. Le profil du coefficient effectif de dispersion axiale du gaz croît avec la vitesse et rechute au début de la turbulence. Les paramètres cinétiques du catalyseur PSA sont utilisés pour simuler la combustion en lit fluidisé turbulent. Le nombre d'unités de réaction maximal pouvant être réalisé dans l'installation pilote avec ce catalyseur est d'environ 0.5, ce qui correspond à une conversion du méthane inférieure à 40% et qui est très loin de notre objectif de combustion complète. Un catalyseur beaucoup plus actif est alors requis.

– La troisième publication traite de la combustion du méthane en régime turbulent avec un mélange d'alimentation pauvre en méthane (3%). La combustion est réalisée sur un catalyseur à base de palladium ($PC263$ de la compagnie Procatalyse) dont la cinétique est caractérisée dans un lit fixe tubulaire. Les signaux transmis par la sonde de pression differentielle sont utilisés pour contrôler le niveau des particules dans le lit et la réaction est effectuée jusqu'à $500°C$ en contrôlant le système avec un régulateur numérique $P.I.D$ en régime à bulles et en régime turbulent. La conversion du méthane en régime à bulles est inférieure à la conversion observée en régime turbulent aux mêmes nombres d'unités de réaction. Les études transitoires de mélangeage du gaz sont aussi effectuées entre $300°C$ et $500°C$ et les données sont analysées avec un modèle piston dispersif. La porosité moyenne du lit calculée à partir du temps de séjour moyen du gaz entre deux détecteurs à scintillation est consistante avec les données de la littérature et le modèle est utilisé pour représenter les données

de combustion obtenues en régime turbulent. Dans le régime à bulles le modèle de réacteur parfaitement mélangé représente assez bien les données de combustion. Une combustion autothermique est réalisée avec un mélange contenant 4% de méthane dans les deux régimes et ni les NOx, ni le monoxyde de carbone ne sont détectés avec une cellule électrochimique (sensibilité 1ppm) à la sortie du réacteur jusqu'à $540°C$ pour une convsersion du méthane de 100%.

– La quatrième publication traite de la distribution des temps de séjour du gaz dans deux réacteurs pilotes de 100 mm et 200 mm de diamètre interne. Les fluctuations de la dispersion axiale s'avèrent être un précieux outil de caractérisation du début de la turbulence. Le coefficient de dispersion axiale est plus faible dans le lit de grand diamètre où le rétromélange est moins prononcé. Le nombre de Péclet obtenu à partir des données de dispersion en régime turbulent pour trois différentes particules est corrélé en fonction des grandeurs adimensionnelles caractéristiques du lit fluidisé. Le modèle à deux phases de *van Deemter* est aussi utilisé pour analyser les données de la distribution des temps de séjour et le coefficient d'échange interphasique est corrélé en terme de la hauteur d'unité de transfert. Les paramètres de ce modèle ne peuvent pas être utilisés directement pour modéliser une réaction à hautes conversions parce qu'ils ne tiennent pas compte de l'amplification du transfert de matière dû à la réaction chimique. Cependant, le modèle de *Werther* corrige de façon phénoménologique cette anomalie.

– La conclusion générale et les recommandations résument les principales con-

tributions de ce travail et nos suggestions pour les travaux futurs. L'annexe présente des diagrammes et des graphes complémentaires.

ACKNOWLEDGEMENTS

I am indebted to prof. *Jamal Chaouki* and prof. *Christophe Guy* who initiated and supervised this project. The tremendous efforts deployed by prof. *Danilo Klvana* to unearth an appropriate combustion catalyst are gratefully acknowledged.

Special thanks are due to Dr. *Gregory Kennedy* and Mr. *Jean St–Pierre* of the Département de Génie Energétique who irradiated hundreds of argon samples in the *Slowpoke* nuclear reactor on my behalf.

Without the technical expertise of *Gérald Lafortune*, *Robert Delisle*, *Jean Huard* and *Carol Painchaud*, this work would have been very difficult. I am very grateful to the whole technical staff.

I would also like to acknowledge the catalytic presence of Dr. *Marzouk Benali*, Dr. *Faiçal Larachi*, Dr. *Ahmed Chehbouni*, Mr. *Dushan Kusohorsky*, Mr. *Ali Gonzalez* and the many graduate students I have shared the laboratory facilities with in the Chemical Engineering Department.

Finally, I would like to acknowledge the precious time of the examination committee, Drs. *Robert Legros*, *Claude Chavarie* and *Esteban Chornet*, who agreed to

appraise this work. In particular, I thank Dr. *Esteban Chornet* who had to travel from Colorado despite other pressing demands on his time.

TABLE OF CONTENTS

LIST OF FIGURES

LIST OF TABLES

LIST OF NOTATIONS AND SYMBOLS

Chapter 2

a	Surface de l'interphase par unité de volume, (m^2/m^3)
Ar	Nombre d'Archimède
C_{wp}	Critère de Weisz-Prater
D	Diamètre du lit, (m)
d_b	Diamètre des bulles, (m)
d_p	Diamètre des particules solides, (μm)
E_s	Vitesse minimale d'emportement des particules, (kg/s)
F_{CH_4}	Flux molaire de méthane à l'entrée du réacteur, (mol/s)
g	Accélération de la pesanteur, (m/s^2)
H	Hauteur du lit, (m)
$\Delta H_R(T)$	Chaleur de combustion du méthane à la température T, (kJ)
k_r	Constante de réaction du 1^{er} ordre, (s^{-1})

k_{12} Coefficient d'échange du gaz, (m/s)

N_r Nombre d'unités de réaction

N_α Nombre d'unités de transfert

R_u U/U_{mf}

R_{ut} U_t/U_{mf}

Pu Puissance de combustion, (kW)

Re_{mf} Nombre de Reynolds aux conditions minimales de fluidisation

R_{HD} H/D

T Température du lit, $(°C)$

T_c Température critique de combustion, $(°C)$

U Vitesse superficielle du gaz dans le lit, (m/s)

U_b Vitesse des bulles, (m/s)

U_e Vitesse du gaz interstitielle, (m/s)

U_f Vitesse des bulles aux conditions minimales de fluidisation, (m/s)

U_{mf} Vitesse superficielle du gaz aux conditions minimales de fluidisation, (m/s)

U_s Vitesse des particules solides en mouvement descendant dans le lit, (m/s)

U_t Vitesse terminale de chute libre des particules, (m/s)

W	Masse du catalyseur, (kg)
X	Conversion du méthane

Symboles grecs

α_1	Fraction du solide dans les bulles
ϵ_b	Fraction du lit occupé par les bulles
ϵ_{mf}	Porosité du lit aux conditions minimales de fluidisation
μ	Viscosité dynamique du gaz, $(Pa.s)$
ρ	Densité du gaz, (kg/m^3)
ρ_p	Densité du solide, (kg/m^3)

Chapter 3

C	Unconverted gas concentration, mol/m^3
	Tracer concentration, dimensionless
$c(t)$	Tracer concentration
C_0	Inlet gas concentration, mol/m^3
D_g	Effective gas dispersion coefficient, m^2/s
D_{ax}	Apparent gas dispersion coefficient, m^2/s
E	Activation energy, $kcal/mol$
$(F_{CH4})_0$	Inlet molar flowrate of methane, mol/s
H	Expanded bed depth, m
k	First order reaction rate constant, s^{-1}
k_0	Preexponential factor, $mol/g/s/atm$
L	Distance between two detectors, m
N_D	Number of dispersion
N_r	Number of reaction units
P_{CH4}	Partial pressure of methane, atm
Pe	Peclet number for gas axial dispersion
R_{CH4}	Rate of conversion of methane, $mol/s/gcatalyst$
t	Time, s
T	Temperature, K

U	Superficial gas velocity, m/s
u	Interstitial gas velocity, m/s
U_{mf}	Superficial gas velocity at minimum fluidization, m/s
X	Conversion of methane
y	Axial distance, m
W	Mass of catalyst, g

Greek Symbols

η	Mass of catalyst versus inlet molar flow rate of Methane, $g.s/mol$
θ	Tracer mean residence time /theoretical gas Mean residence time, s^{-1}

Chapter 4

C	Unconverted gas concentration, mol/m^3
D_g	Effective gas dispersion coefficient, m^2/s
D	Reactor diameter, mm
d_p	Average particle size, μm
d_{pi}	Average screen size, μm
E_θ	Activation energy, kK
H	Expanded bed height, m
H_0	Initial bed height, mm
k_r	First order reaction rate constant based on the expanded bed, s^{-1}
K_0	Preexponential factor, $cm^3/g/s$
L	Distance between two gas tracer detectors, m
N_r	Number of reaction units, $k_r H/U$
Pe	Gas Peclet number, uL/D_g
R_{CH4}	Rate of conversion of methane, $mol/s/g\ of\ catalyst$
T	Temperature, K
U	Superficial gas velocity, m/s
U_{mf}	Superficial gas velocity at minimum fluidization conditions, m/s
U_c	Onset of turbulent fluidization, m/s

U_{tr}	Onset of transport fluidization, m/s
u	Interstitial gas velocity, m/s
X_i	Weight fraction, (%)

Subscripts

c	Transition to turbulent fluidization
CH_4	Methane
g	Gas phase

Chapter 5

Ar Archimedes number, $(\rho_p - \rho)\rho g d_p^3/\mu^2$

C Tracer concentration, dimensionless

Unconverted gas concentration, mol/m^3

$c(t)$ Tracer concentration

C_0 Inlet gas concentration, mol/m^3

D Reactor diameter, mm

D_g Effective gas dispersion coefficient, m^2/s

D_v Gas diffusivity, m^2/s

d_p Average particle size, μm

g Acceleration due to gravity, m/s^2

H Expanded bed height, m

Ha Hatta number, $\sqrt{k_r D_v}/k_m$

H_0 Initial bed height, m

k_m Cross–flow mass transfer coefficient, m/s

k_r First order reaction rate constant, s^{-1}

N_D Number of dispersion, $1/P_e$

N_α Number of transfer units, $\alpha_{12}H/U$

N_r Number of reaction units, $k_r H/U$

Pe Gas Peclet number, uL/D_g

Sc	Schmidt number, $\mu/\rho D_v$
t	Time, s
T	Temperature, K
U	Superficial gas velocity, m/s
U_c	Onset of turbulent fluidization, m/s
U_d	Dilute phase interstitial gas velocity, m/s
U_{tr}	Onset of transport fluidization, m/s
u	Interstitial gas velocity, m/s
x	Axial distance, m

Greek Symbols

α_{12}	Cross–flow mass transfer coefficient, s^{-1}
ϵ_m	Mean bed voidage
ϵ_{dm}	Mean dilute phase voidage
ϵ_{em}	Mean emulsion phase voidage
δ	Particle to bed diamter ratio, d_p/D
ρ	Fluid density, kg/m^3
ρ_p	Particle density, kg/m^3
τ	Tracer mean residence time, s
	Dimensionless time

CHAPTER 1

INTRODUCTION

1.1 Introduction

Fluidized bed combustion has gained a worldwide commercial status in the past two decades or so. However, air pollution has constantly altered the design and operation of combustion equipment (*Bartok* et *al.*, 1988). The alteration being focussed on equipment modification (*Kuehn*, 1994), on in situ destruction of pollutants (*Molière* et *al.*, 1989), and on post–combustion treatment (*De Reydellet*,1989).

The flameless fluidized bed catalytic combustion of natural gas is an emerging zero pollutant emission combustion technology whose potential is yet to be tapped. It presents real advantages compared to conventional systems and fixed bed catalytic combustors.

Various fluidization regimes are observed as the superficial gas velocity is increased ranging from the bubbling regime to the slugging regime (for small beds), to turbulence, and to fast fluidization. The location of the characteristic bifurcation

points delimiting the different flow regimes is crucial especially in catalytic combustion systems where the reactant conversion is largely dependent upon the system stability. The turbulent regime appears to be the ideal combustion regime (*Grace*,1990). Besides the high energy throughput, the turbulent fluidized bed catalytic combustion ($TFB2C$) does not develop hot–spots, maintains a uniform temperature and a good gas–solid contact which enhances the reaction (*Avidan*,1982; *Grace*,1990). This regime is suitable for particles of group A and B of *Geldart* (1973). However, the contact time is short in $TFB2C$ compared with that in fixed beds and its operation requires very active catalysts. A good hydrodynamics characterization is also necessary for fast reactions.

The main objective of this research is to assess the experimental feasibility of the combustion of natural gas in a catalytic fluidized bed. The problem is tackled by simulating the process using kinetic and hydrodynamic data from the literature which help to determine the proper regime of operation and the design parameters of a pilot scale experimental combustor. Two platinum and palladium supported catalysts are then characterized and their kinetic parameters are used to simulate the combustion process in the fluidized bed. Only the Pd/Al_2O_3 catalyst is shown to be adequate for turbulent bed operation. Pressure fluctuations and axial gas dispersion fluctuations are used to characterize the onset of turbulent fluidization. Finally, the combustion is performed in the turbulent regime over the Pd/Al_2O_3 catalyst and modeled with a simple dispersive plug flow model and the two–phase model of *van Deemter* (1961).

1.2 Literature Review

Methane is among light hydrocarbons the most difficult to oxidize (*Jones and Salfati*, 1989). In conventional combustors where the temperature level is above $1200°C$, NOx are intensively formed. Catalytic combustion is performed at low temperatures and no methane radicals are formed at these conditions, thus discarding the possibility of NOx formation. Catalytic combustion of methane has been reported so far only in fixed beds (*Salfati* and *van Der Wal*,1989; *Sicardi* et *al.*,1982; *Jones* and *Salfati*,1989) eventhough fluidized beds have been widely used for many commercial processes. The hydrodynamics of fluidized beds is very complex and have been a the cornerstone of hundreds of investigations. Reactor models have also been investigated for different hydrodynamic regimes.

This review will focus on three points: total combustion of methane, fluidized bed hydrodynamics and reactor models.

1.2.1 Complete Combustion of Natural Gas

The complete combustion of methane has been widely performed in fixed catalytic beds (*Mezaki* and *Watson*,1966; *Trim* and *Lam*, 1980; *Sicardi* et *al.* 1982; *Jones* and *Salfati*, 1989). In fluidized beds, only homogeneous combustion has been reported (*Yanata* et *al.*,1975; *van der Vaart*, 1986, 1988, 1992) as far as we know. Since methane is very difficult to oxidize, most experiments have been conducted

on Pt/Pd catalysts (*Firth* and *Holland*, 1969; *Cullis* et *al.*, 1971; *Trim* and *Lam*, 1980; *Sicardi* et *al.*, 1982) and more recently on perovskite–type catalysts (*Wise* and *Quinlan*, 1986; *Klvana* et *al.*, 1994). Eventhough the combustion reaction seems simple, the reaction mechanism is complex as suggest the works of *Mezaki* (1966), *Ahuja* and *Mathur* (1967), and *Sicardi* et *al.* (1982). However, for design purposes, a simple power model can be used to fit experimental data (*Cullis* et *al.*, 1971; *Trim* and *Lam*, 1980; *Sicardi* et *al.*, 1982).

The products of combustion depend on the operating conditions. NOx are intensively produced in conventional combustors where the temperatures near $1200°C$ and can also be formed in catalytic combustors in the presence of hot–spots. The formation mechanisms are well known (*De Soete*,1989): the Thermal NO mechanism involves nitrogen present in the air at high temperatures, the $Fuel–NO$ mechanism involves the fuel nitrogen at moderate temperatures, and the $Prompt–NO$ mechanism involves hydrocarbonated radicals present in the combustion chamber and which react with nitrogen fed with the air. Natural gas being a bounded nitrogen–free fuel, its combustion carried out at temperatures below $700°C$ should produce no NOx since none of the above mechanisms is likely to take place.

Carbon monoxide is another potential pollutant that can be released by the combustion. It is formed only when the combustion is performed off–stoichiometrically (*Wise* and *Quinlan*,1986). The catalytic combustion of natural gas with a stoichiometric or a poor methane mixture below $700°C$ is likely to be clean if carried out in

a system free of hot–spots, for instance in a turbulent fluidized bed.

1.2.2 Turbulent Fluidized Bed Hydrodynamics

The hydrodynamics of turbulent beds is very complex and has been the object of intensive investigations (*Lanneau*,1960; *Kehoe and Davidson*,1971; *Yerushalmi* and *Cancurt*,1979; *Abed*, 1984; *Cai* et *al.*,1989; *Grace*,1990; *Chehbouni*,1993). Three different descriptions of turbulent bed hydrodynamics have been reported: the turbulent bed presents a lean gas–solid phase at the center of the bed and a dense phase at the wall (*Abed*,1984;*Lee* and *Kim*,1989), the turbulent bed is homogeneous with very small bubbles (*Kehoe and Davidson*,1971; *Avidan*,1982), the turbulent bed has an intermediate structure between the slugging bed structure and the fast fluidized bed structure (*Rowe*,1980; *Brereton*,1987). Despite the controversy surrounding the description of turbulent bed, the frontiers of turbulence have been established (*Chehbouni*,1993) to be only the transition velocities U_c and U_{tr} measured by pressure fluctuations and the capacitance probe technique.

The interest in gas and solid mixing is extensive in the literature (*Askins* et *al.*,1951; *May*,1959; *van Deemter*,1961; *Thiel* and *Potter*,1978; *Li* and *Weinstein*, 1989; *Li and Wu*,1990). Gas backmixing is known to be small in the turbulent bed (*Lee* and *Kim*,1989) and the gas backmixing coefficient is equal to the axial gas dispersion coefficient (*van Deemter*,1980). Axial gas dispersion fluctuations have been reported in the literature (*van Deemter*,1980). The most widely used gas tracers

have been hydrogen (*Li* and *Wu*,1990), methane (*Yerushalmi* and *Cancurt*,1979), and helium (*Li* and *Weinstein*,1989) which can be sampled at different locations in the bed and analyzed continuously. This type of sampling is likely to affect the bed hydrodynamics and cannot represent a bed section reality. With a radioactive gas tracer, $NaI(Tl)$ scintillation detectors have been used outside the bed to monitor the gas and solid flow behaviors (*Patience*,1990).

1.2.3 Reactor Models

Reactor models are specific to the fluidization regime of operation. Most works in academia have focussed on the bubbling flow regime using group B particles and the two–phase models developped are legion in the literature (*Grace*, 1986; *Kunii* and *Levenspiel*,1990,1991). The two–phase models can be classified in the bubbling bed models in which the bubble diameter is the key parameter and in the simple two–phase models which consider the lean phase as continuous. At high velocities, the bed structure differs significantly from that of the bubbling bed. The core–annular model has been widely used in circulating fluidized beds modeling (*Brereton* et *al.*,1988; *Kagawa* et *al.*,1991). The turbulent fluidized bed is the regime where the modeling effort has been very modest (*Grace*,1990) despite the widly commercial use of turbulent systems. A simple plug flow model has been used to model a turbulent bed (*van Swaij*,1978). However, despite the fact that this regime is almost bubbleless the conversion level is far from being that of a plug flow reactor. *Avidan* (1982) and

Wen (1984) have successfully used a dispersive plug flow model to describe their data.

1.3 Thesis Structure

This thesis is made up of four publications and is structured in five chapters:

– The general introduction presents the global scope of the work and the related features reported in the literature.

– The first publication deals with the simulation of an atmospheric fluidized bed combustor with the kinetic and hydrodynamic parameters from the literature. A comprehensive review of total combustion catalysts and nitrogen oxides formation is presented. A design algorithm is implemented and the main conclusions indicate the necessity to operate in the turbulent bed as well as a good insight into the design parameters of an experimental pilot scale $TFB2C$.

– The second publication characterizes the kinetics of combustion of methane over a Pt/Al_2O_3 catalyst referenced as PSA in a tubular fixed bed. Gas mixing experiments are also performed at ambient temperature with sand and FCC particles in 100 mm I.D. fluidized bed in a wide range of velocities. The effective axial gas dispersion profile is shown to increase with velocity and to drop at the onset of turbulent fluidization. The kinetic parameters of the PSA catalyst are then used to simulate the combustion in a turbulent bed. The maximum number of reaction

units that can be achieved in the installation with this catalyst is of the order of 0.5, corresponding to a conversion less than 40% and which is very far from our total combustion goal. A more active catalyst is therefore necessary.

– The third publication deals with the combustion of methane in the turbulent regime with a poor inlet mixture of 3% in methane. The combustion is achieved over a Pd/Al_2O_3 catalyst ($PC263$ from $Procatalyse$) whose kinetics is characterized in a tubular fixed bed. The signal from the differential pressure transducer is used to control the catalyst level in the bed and the reaction is achieved at temperatures up to $500°C$ regulated with a numerical $P.I.D$ controller in the bubbling and in the turbulent regimes. The conversion in the turbulent regime is shown to be higher than the conversion in the bubbling bed at the same number of reaction units. Transient gas mixing experiments are also performed between $300°C$ and $500°C$ and analyzed with a dispersive plug flow model. The calculated porosity is consistent with the expected values and the model is used to adequately model the combustion data in the turbulent regime. In the bubbling regime, a perfect mixing model represents well the kinetic data. A self–sustained combustion is achieved with an inlet mixture of 4% in methane both in the bubbling and in the turbulent regime and no NOx and CO are recorded at the reactor exit at temperatures up to $540°C$ and with 100% conversion.

– The fourth publication is devoted to the study of axial gas dispersion fluctuations in two reactors (100 mm and 200 mm $I.D$). They are shown to be a useful

tool for the characterization of the onset of turbulence. The gas dispersion coefficient is shown to be smaller in the larger bed. The Peclet number derived from the turbulent bed data at various operating conditions and with three different types of particles is correlated in terms of characteristic dimensionless groups. A correlation of the dispersion as a function of the mean porosity is also obtained from the data of the larger bed using FCC particles. The two–phase model of *van Deemter* is also used to analyze the mixing data and the cross–flow mass transfer coefficient obtained is correlated in terms of the height of a transfer unit. The parameters of this model cannot be used directly to model a high conversion reaction. This is due to the fact that the parameters derived from tracer experiments do not account for the cross–flow mass transfer enhancement introduced by the reaction. However, the model of *Werther* phenomenologically accounts for this phenomenon by introducing a chemical acceleration factor.

– The general conclusion and recommendations summarize the main contributions of this work and our suggestions. The appendix presents miscellaneous complementary diagrams and graphs.

CHAPTER 2

DIMENSIONNEMENT OPTIMAL D'UN GÉNÉRATEUR DE CHALEUR SANS NOx

M. Foka, J. Chaouki*, C. Guy & D. Klvana

Rev. gén. Therm. Fr., $n°$ 352, pp. 225–232 avril 1991

*Auteur à qui toute correspondance doit être adressée

Abstract

New combustion technologies aiming at protecting the environment require appropriate design methods for catalytic combustors which are their battle horse. This paper presents an algorithm for the design of an atmospheric fluidized bed combustor based on the catalytic combustion of natural gas. It gives optimal design parameters namely the bed diameter, the operating temperature, the particle size, and the superficial gas velocity for a given power and a given methane conversion. Using kinetics data from the literature and hydrodynamic parameters calculated from available equations this algorithm predicts for a required power level of $50kW$ a bed diameter of about $0.25m$ at a temperature of $550°C$ and for a power of 500 kW a bed diameter of about 0.5 m at a temperature of $500°C$.

Résumé

Les nouvelles technologies de combustion visant à protéger l'environnement exigent des méthodes appropriées de design des brûleurs catalytiques qui sont leur cheval de bataille. Cet article présente un algorithme d'optimisation pour le design d'un brûleur atmosphérique basé sur la combustion catalytique du gaz naturel en lit fluidisé. Il permet d'obtenir les paramètres optimaux de design du réacteur qui sont le diamètre du lit, la température d'opération, la taille des particules, et la vitesse superficielle du gaz pour une puissance et une conversion de méthane données. A partir des données

cinétiques tirées de la littérature et des paramètres hydrodynamiques calculés selon les corrélations existantes, cet algorithme donne pour une puissance requise de 50 kW un diamètre optimal du lit d'environ 0.25 m à la température de 550°C et pour une puissance de 500 kW un diamètre du lit de l'ordre de 0.5 m à la température de 500°C.

2.1 Introduction

L'effet de serre, la réduction de la couche d'ozone stratosphérique, les pluies acides et les brouillards oxydants représentent une ménace indéniable à la survie de l'homme et de sa biosphère. Depuis quelques années plusieurs gaz émanant des activités humaines participent directement ou indirectement aux réactions photochimiques dans l'atmosphère qui sont à la base de tous ces phénomènes préjudiciables. Parmi ces gaz, les oxydes d'azote (NOx) provenant des sources humaines (automobiles, engins roulants, foyers fixes de combustion et activités industrielles) et des sources naturelles (orages, feux de forêt, etc...) occupent une place importante. Cette famille de polluants de l'air est constituée de sept oxydes[1] dont les plus courants sont le monoxyde d'azote (NO), le dioxyde d'azote (NO_2), et le protoxyde d'azote (N_2O). Le NO prédomine dans les fumées de combustion (90-95%)[1, 2] et par conséquent la mesure des NOx ne porte que sur lui [3, 4]. Cependant, il s'oxyde facilement en NO_2 au cours de son refroidissement [5]. Le NO peut être formé par plusieurs mécanismes [6]:

– Mécanisme du 'NO thermique' à partir de l'azote moléculaire provenant de l'air comburant à haute température.

– Mécanisme du 'Fuel–NO' à partir de l'azote contenu dans le combustible (cas des combustibles fossiles liquides et solides) à des températures modérées.

– Mécanisme du 'Prompt NO' à partir des radicaux hydrocarbonés (CX) présents dans la zone d'oxydation et de l'azote moléculaire de l'air. Les températures

inférieures à $800°C$ sont défavorables à la formation des radicaux de méthane [7].

L'effet des oxydes d'azote sur l'homme et sur l'environnement n'est plus à démontrer. Le NO_2 est reconnu dommageable pour les fonctions respiratoires [8] et les NOx en contact avec les produits agro–alimentaires, notamment lors des procédés de séchage en direct, peuvent facilement produire des nitrosamines dont certains sont cancérigènes [9]. Par ailleurs, les NOx participent à la formation du smog oxydant [8] et le N_2O contribue pour environ 6% à l'effet de serre [8] et participe à la réduction de la couche d'ozone stratosphérique [10].

Dans les brûleurs traditionnels, la température de flamme est très élevée et dépasse généralement $1200°C$ avec une production intense de NOx dont la réglementation des émissions a fait naître plusieurs techniques visant à les réduire:

– Les techniques primaires permettant une réduction in situ [22, 11],

– Les techniques secondaires appliquées en aval du foyer de combustion [12],

– La combustion catalytique qui permet de valoriser les combustibles de qualité inférieure (huiles à chauffage lourde , charbon, déchets industriels, déchets domestiques et municipaux) tout en minimisant les émissions des NOx et de SO_2 grâce à leur faible température d'opération [13, 14].

2.2 Combustion catalytique du gaz naturel

Ce type de combustion qui peut avoir lieu à basse température présente beaucoup d'avantages par rapport à la combustion vive traditionnelle et est la pierre angulaire des nouvelles technologies gazières. La combustion à basse température exclue d'office la production des NOx par les mécanismes du 'NO thermique' et du 'Prompt NO'. Le méthane ne contenant pas d'azote lié, il n'est pas possible non plus de produire le NO par le mécanisme du 'Fuel–NO'. Bref, la combustion catalytique du méthane est une combustion propre. Ce qui permet de respecter les normes d'émission des NOx qui sont beaucoup plus sévères pour le gaz naturel que pour les autres combustibles fossiles au Canada. A cet avantage s'ajoutent l'absence du risque d'inflammation et d'explosion [15] et la flexibilite du contrôle de la température. De plus, la combustion catalytique donne la possibilité d'utiliser le procédé dans des atmosphères explosives, la possibilité d'optimiser les échanges thermiques par une modification appropriée de la géométrie du lit et le chauffage par contact direct dans les industries agro-alimentaires (atomisation du café, étuvage de la farine, tourraillage du malt, atomisation des produits laitiers, etc...). La combustion peut se faire soit en lit fixe, soit en lit fluidisé.

2.2.1 Combustion en lit fixe

Lorsque la réaction est effectuée dans un réacteur adiabatique, la chaleur de combustion ne peut être évacuée du réacteur que par les gaz de combustion. Cette évacuation est très souvent insuffisante d'où le développement des points chauds dans le lit qui accélèrent le vieillissement du catalyseur et qui peuvent provoquer un emballement du réacteur. La chaleur peut être aussi évacuée du lit en intégrant au réacteur un échangeur de chaleur, ce dernier peut être aussi placé en aval du réacteur. L'une ou l'autre de ces configurations n'élimine pas forcément le problème de gradients de température et de points chauds dans le lit. Les modifications généralement apportées sont le recyclage des fumées (abaissement de la température), la dilution du catalyseur par des billes inertes de support et l'utilisation du lit fluidisé. Les panneaux radiants catalytiques utilisant la combustion du méthane fonctionnent en lit fixe [16].

2.2.2 Combustion en lit fluidisé

Les brûleurs à lit fluidisé peuvent être classés en deux groupes: les brûleurs atmosphériques ($AFBC$) et les brûleurs pressurisés ($PFBC$) [14]. Les brûleurs atmosphériques sont soit adiabatiques (pour les combustibles à faible pouvoir calorifique), soit refroidis (pour les combustibles à haut potentiel énergétique). Le lit fluidisé présente beaucoup d'avantages par rapport au lit fixe en ce qui concerne les transferts de chaleur entre le gaz et les particules et entre le lit et les éléments internes d'évacuation

de chaleur. De plus, les points chauds n'apparaissent pas grâce au mélange rapide des particules solides [17], le lit étant alors isotherme. La coalescence des bulles donne lieu à un rapide échange de matière entre le gaz et l'émulsion [18]. Le lit fluidisé peut être de plus utilisé pour des opérations à grande échelle. Son contrôle est beaucoup plus souple grâce à la fluidisabilité des particules et au réglage aisé des débits de gaz. Plusieurs difficultés sont cependant liées à son utilisation. On doit mentionner l'érosion des éléments internes et des parois du lit par les particules solides, l'attrition mécanique et thermique des particules, l'entraînement et l'emportement des fines particules, et le court–circuit du gaz. Cette dernière difficulté provoque une baisse de conversion et la non maîtrise de la phénoménologie de l'écoulement des gaz qui se réflète par une grande déviation par rapport à l'écoulement piston. En somme, les court-circuits sont responsables des conversions plus faibles observées dans les lits fluidisés [17] et par conséquent pour un même niveau de conversion, le lit fluidisé requiert plus de catalyseur qu'un lit fixe. Malgré ces inconvénients, les nouvelles technologies gazières destinées à générer de grandes puissances (production de gaz chauds, génération de vapeur, etc...) exigent que l'on mette à profit les avantages du lit fluidisé quitte à apporter des modifications appropriées pour minimiser ses failles.

2.2.3 Catalyseurs de combustion

Les catalyseurs se présentent généralement sous deux configurations différentes: les catalyseurs supportés et les catalyseurs non supportés. Les catalyseurs supportés

ont deux phases différentes; le support (poreux ou non) et la phase active (métaux, oxydes ou alliages). Le rôle du support est d'assurer la plus grande surface spécifique possible au catalyseur et de stabiliser les centres actifs. Les supports les plus utilisés sont, dans le cas de la combustion catalytique, les fibres d'alumine gamma qui présentent une surface spécifique de l'ordre de 150 m^2/g [19]. Les supports non poreux ont une surface spécifique beaucoup plus petite. La phase active est constituée de métaux nobles (Pd, Pt, Ir, Rh), de métaux de transition (Cu, Co, Mn, Ni, etc...) ou de leurs alliages [20]. Les promoteurs qui peuvent être inclus dans la préparation des catalyseurs supportés sont utilisés pour minimiser les effets des poisons, du frittage thermique et pour stimuler l'activité du catalyseur. Les oxydes de terres rares sont généralement utilisés comme promoteurs [21]. En général, l'activité des catalyseurs supportés dépend de la structure cristalline de l'élément actif, du promoteur utilisé, de la nature du support, de la méthode d'imprégnation de l'élément actif et de la méthode de réduction comme l'indique les résultats obtenus sur le Pd/Al_2O_3 et le Pt/Al_2O_3 [19]. Le palladium et le platine restent les éléments actifs les plus efficaces pour l'oxydation du méthane [22]. L'activité des catalyseurs au palladium peut être d'ailleurs plus de 300 fois celle des catalyseurs à base de platine [19]. Les oxydes tels que Co_3O_4, NiO, Cr_2O_3, MnO_2, CuO peuvent être utilisés pour la phase active pour des applications à températures élevées [21].

Les catalyseurs non supportés utilisés pour la combustion du méthane sont les oxydes mixtes métalliques pouvant présenter différentes structures cristallines; spinels

($CuCr_2O_4$), scheelite ($Bi_2O_3 \cdot 3MoO_3$) ou pérovskites ($La_{1-x}Sr_xMnO_3, 0 < x < 0.6$) [20]. Les raisons de leur activité sont très complexes à cause de la multiplicité des sites actifs, des cations et d'anions polyvalents, des défauts de structures, et des espèces adsorbées. Ils présentent par rapport aux catalyseurs supportés l'avantage d'une très grande stabilité thermique, de pouvoir se présenter sous une seule phase et d'être disponibles à bon marché. Par ailleurs, les données obtenues sur plusieurs d'entre eux [20] montrent que leur surface spécifique est appréciable ($LaMnO_3$: 28 m^2/g), $La_{0.75}Sr_{0.25}MnO_3$: 22 m^2/g, $La_{0.5}MnO_3$: 39 m^2/g). L'étude sur ces catalyseurs est encore exploratoire mais ils semblent beaucoup plus adaptés aux exigences des nouvelles technologies de combustion que les catalyseurs à base de métaux précieux qui en plus d'être très chers sont loin d'être très stables [7].

Une étude comparative de 28 catalyseurs supportés et non supportés pour la combustion du méthane [20] a montré que les catalyseurs à base de palladium sont de loin les plus actifs suivis par les catalyseurs à base de platine. Dans cette liste, le Co_3O_4 est le plus actif des catalyseurs non supportés et son activité est d'ailleurs comparable à celle des catalyseurs à base de platine. Cette activité décroît lorsque le Co_3O_4 est déposé sur un support. L'activité des métaux et des oxydes correspondants décroît dans l'ordre suivant [24]: $Pd, Pt, Cr, Mn, Cu, Ce, Co, Fe, Ni$ et Ag.

2.2.4 Mécanismes et cinétique réactionnels

Le méthane est parmi les hydrocarbures légers le plus difficile à oxyder [23]. Il exige des températures de combustion très élevées par rapport aux hydrocarbures supérieurs [22]. L'oxydation du méthane a fait l'objet de plusieurs travaux [16, 19, 20, 22, 29]. L'oxydation catalytique a particulierement été menée sur les catalyseurs au Pd et au Pt pour leur activité intéressante [16, 19, 20, 27, 29, 22, 24] et plus récemment sur les oxydes mixtes métalliques de type pérovskites [20]. Cependant, le mécanisme réactionnel est loin d'être connu. L'équation globale de la réaction est donnée par:

$$CH_4 + 2O_2 \longrightarrow CO_2 + 2H_2O$$

En fonction de la concentration d'oxygène adsorbé, deux chemins ont été proposés pour expliquer le mécanisme [20]. *Cullis* et al. [28] ont par contre proposé un mécanisme consistant à la déshydrogénation du méthane puis à l'oxydation de l'oxyde de méthyl adsorbé pour donner du CO_2 et l'oxydation de l'hydrogène adsorbé pour donner de l'eau. Malgré l'incertitude sur le chemin cinétique réel, plusieurs modèles mécanistes ont été proposés [19, 23, 24, 27] qui considèrent la réaction de surface comme étant l'étape limitante. *Mezaki* et *Watson* [27] ont postulé que la réaction se passait entre le méthane en phase gaseuse et l'oxygène adsorbé alors que *Ahuja* et *Mathur* [23], *Sicardi* et al. [19] ont considéré la réaction entre deux molécules adsorbées d'oxygène et une molécule adsorbée de méthane. Tous ont reporté une bonne corrélation avec leurs données expérimentales. Les modèles de puissance de la forme:

$$r_{CH_4} = k[CH_4]^{\alpha}[O_2]^{\beta} \tag{2.1}$$

ont aussi été reportés avec des énergies d'activations correspondantes [19, 20, 24, 28]. Les essais sur trois catalyseurs à base de Pt, Ni, Ir ont montré que les produits de combustion ordinaires (H_2O *et* CO_2) ne sont obtenus que lorsque la combustion est stoechiométrique ou en présence d'un excès d'oxygène, la combustion générant plutôt du CO et de l'hydrogène en défaut d'oxygène entre 600 et 800 K sur ces catalyseurs [20]. Par contre, sur les oxydes mixtes ($CuCr_2O_4$ *et* $Bi_2O_3 \cdot 3MoO_3$), le CO_2 et l'eau ont été obtenus au cours de la combustion en défaut d'oxygène. Par ailleurs, seule la déshydrogénation du méthane a été observée sur ces catalyseurs en l'absence totale d'oxygène. Les tests de sensibilité aux poisons ont montré que le nickel n'est pas un bon catalyseur pour la combustion de méthane contenant des traces de soufre [20].

2.3 Modèles de lit fluidisé

Les lits de particules percolés par un gaz présentent différents régimes hydrodynamiques allant du lit fixe au transport pneumatique en passant par la fluidisation particulaire, le régime de bullage, le régime de pistonnage dans le cas d'un lit de faible diamètre, le régime turbulent et la fluidisation rapide. Cette séquence étant obtenue au fur et à mesure que la vitesse du gaz augmente dans le lit. Les critères de limitation de ces régimes et les propriétés qu'ils présentent pouvant influencer la

performance des lits fluidisés considérés comme réacteur catalytique sont présentés par *Grace* [40]. Il importe pour la modélisation de tels réacteurs de déterminer le régime hydrodynamique de leur opération. Dans ce texte nous présentons les modèles du régime de bullage. De plus, étant donné la complexité de l'hydrodynamique des lits fluidisés et la confusion qui prévaut dans l'approche mathématique du phénomène de fluidisation, nous nous limitons juste aux principaux piliers théoriques qui sont à la base de l'approche actuelle de modélisation. Les efforts pour modéliser les lits fluidisés ont été jusqu'à présent axés sur l'aspect déterministe [18, 30, 37] et sur l'aspect stochastique [38, 39] avec une propension accrue vers les modèles déterministes. Les modèles déterministes qui, bien que loin d'apporter des éclaircissements inéquivoques sur le système, restent les plus élaborés. Ces modèles qui nous intéressent plus particulièrement considèrent le lit fluidisé comme étant un système biphasique constitué d'une phase bulle et d'une phase émulsion entre lesquelles s'effectue un échange de matière le long du lit. Ils peuvent être classés en modèles biphasiques simples et en modèles de bullage. Les premiers considérant la phase bulle comme un système continu et les deuxièmes la considérant comme un ensemble discret de bulles. La bulle est considérée comme une calotte sphérique pouvant être soit simple, soit entourée d'une couche de nuage et d'un sillage, ou entourée seulement d'une couche de nuage. Les particules solides se trouvent dans la phase émulsion mais on suppose qu'une fraction peut se retrouver aussi dans les bulles [30] voire même, dans les nuages et dans les sillages [17]. Le gaz de fluidisation se répartit entre les différentes phases

du système (bulle ou bulle + nuage et émulsion). Généralement, le bilan sur le gaz se fait en considérant seulement le gaz de la phase bulle et le gaz interstitiel (émulsion). Le gaz interstitiel est considéré soit comme parfaitement mélangé, soit comme étant en écoulement piston avec ou sans dispersion axiale en mouvement ascendant ou descendant.

Une récente simulation des données expérimentales [41] obtenues avec un réacteur industriel produisant l'anhydride phthalique à partir du naphtalène à montré une bonne prédiction de la conversion globale avec trois modèles: *Kato* et *Wen* [42], *Kunii* et *Levenspiel* [17], et *Grace* [30]. Le modèle de *Kunii* et *Levenspiel* est basé sur les hypothèses suivantes:

– Chaque bulle juste au dessus du distributeur entraîne du solide pour former son sillage. Ce solide est entraîné à la vitesse du gaz U_b et est continuellement remplacé par le solide frais de l'émulsion. A la surface du lit le solide du sillage rejoint l'émulsion et redescend dans le lit avec la vitesse U_s.

– La vitesse du gaz dans l'émulsion U_e est fonction de la vitesse de la bulle aux conditions minimales de fluidization U_f et de la vitesse U_s des particules en mouvement descendant.

$$U_e = U_f - U_s \tag{2.2}$$

$$U_f = U_{mf}/\epsilon_{mf} \tag{2.3}$$

– Seuls les lits avec des bulles à grande vitesse ($U_b/U_f > 5$) et des nuages de faible épaisseur sont considérés.

– Pour les diamètres de bulles uniformes, les particules descendant dans les nuages sont entraînées dans le sillage et y sont fluidisées par les gaz y circulant. Elles y sont parfaitement mélangées et en ressortent avec la même vitesse que celle avec laquelle elles l'ont pénétré.

– Au cours de son passage dans le lit, la bulle écarte l'émulsion et les particules voisines pénètrent son nuage et sont entraînées dans le sillage où elles sont parfaitement mélangées. Ceci donne lieu à un mélange latéral.

Dans le développement de ce modèle, la variation de la concentration des réactifs avec la hauteur du lit, dans le nuage, dans le sillage et dans l'émulsion a été négligée. *Fryer* et *Potter* [43], par contre, ont tenu compte de cette variation dans leur modèle tout en considérant le mouvement descendant du gaz dans l'émulsion.

Le modèle de *Grace* [30] est une simplification améliorée du modèle de *Kunii* et *Levenspiel* et une approximation du modèle de *Fryer* et *Potter*. Il est fondé sur les hypothèses suivantes:

–Les bulles engouffrent une fraction de particules α_1 au cours de leur montée dans le lit.

– La phase bulle ne comporte pas de nuage ou de sillage.

– Il n'y a pas écoulement de gaz dans la phase émulsion.

– La phase bulle est en écoulement piston sans dispersion axiale.

La prédiction de la conversion pour une réaction irréversible du premier ordre par ce modèle est donnée par l'équation 2.4.

$$1 - \mathrm{X} = \exp\left(-\frac{-\mathrm{N_r}\left[\mathrm{N}_\alpha[\alpha_1\epsilon_\mathrm{b} + (1-\epsilon_\mathrm{b})(1-\epsilon_\mathrm{mf})] + \mathrm{N_r}\alpha_1\epsilon_\mathrm{b}(1-\epsilon_\mathrm{b})(1-\epsilon_\mathrm{mf})\right]}{\mathrm{N}_\alpha + \mathrm{N_r}(1-\epsilon_\mathrm{b})(1-\epsilon_\mathrm{mf})}\right) \quad (2.4)$$

$$N_\alpha = k_{12}aH/U \quad (2.5)$$

$$N_r = k_rH/U \quad (2.6)$$

Il est à noter qu'on peut tenir compte du mouvement descendant du gaz et des particules dans la phase émulsion soit par l'introduction de la dispersion axiale dans l'écoulement piston, soit en assimilant le lit à une série de réacteurs mélangés soit en considérant une phase parfaitement mélangée [40].

2.4 Prédiction des paramètres hydrodynamiques

Le diamètre des bulles est une donnée cruciale des modèles de lit fluidisé car le débit de gaz traversant le lit en dépend et, par conséquent, la conversion des réactifs. Plusieurs corrélations sont données dans la littérature pour les distributeurs à plaques poreuses et perforées mais les plus utilisées sont celles de *Mori* et *Wen* [31], *Rowe* et *Partidge* [32], *Darton* et *al.* [33], et *Werther* [34]. La Figure 2.1 montre la prédiction de la puissance de combustion calculée à partir de l'équation 2.7 et de la conversion du méthane prédite à l'aide de l'équation 2.4 avec ces différents modèles utilisant les

données cinétiques de *Sicardi* et *al.* [19].

$$Pu = F_{CH_4} X \Delta H(T) \tag{2.7}$$

Sur la Figure 2.1, avec le modèle de *Mori*, la puissance de combustion présente un optimum autour d'un rapport vitesse superficielle de gaz sur vitesse superficielle du gaz aux conditions minimales de fluidisation de $R_u = 9$, alors que ceux de *Werther*, *Rowe* et *Darton* ont un comportement différent. La même étude sur un catalyseur beaucoup plus actif montre un comportement presque identique de tous les modèles (Figure 2.2). Ceci montre clairement que l'optimum de puissance observé précédemment n'est qu'un artefact du modèle utilisé. Les modèles de *Darton* et de *Werther* présentent un comportement régulier et presque similaire en fonction de la taille des particules, de la vitesse superficielle du gaz U et du nombre d'unité de réaction. Une récente étude comparative [44] des modèles pour la prédiction de la taille des bulles montre que le modèle de *Darton* et al. [33] est le plus adéquat. Nous utiliserons dans le design du générateur de chaleur pour la prédiction de la vitesse des bulles qui est généralement calculée à partir de l'équation 2.8:

$$U_b = U - U_{mf} + 0.71(gd_b)^{1/2} \tag{2.8}$$

La Figure 2.3 montre le rapport R_{ut} de la vitesse terminale de chute des particules U_t de densité 2.5 de taille comprise entre 30 μm et 650 μm sur leur vitesse minimale de fluidisation U_{mf} à plusieurs températures. U_t est calculée à partir des relations

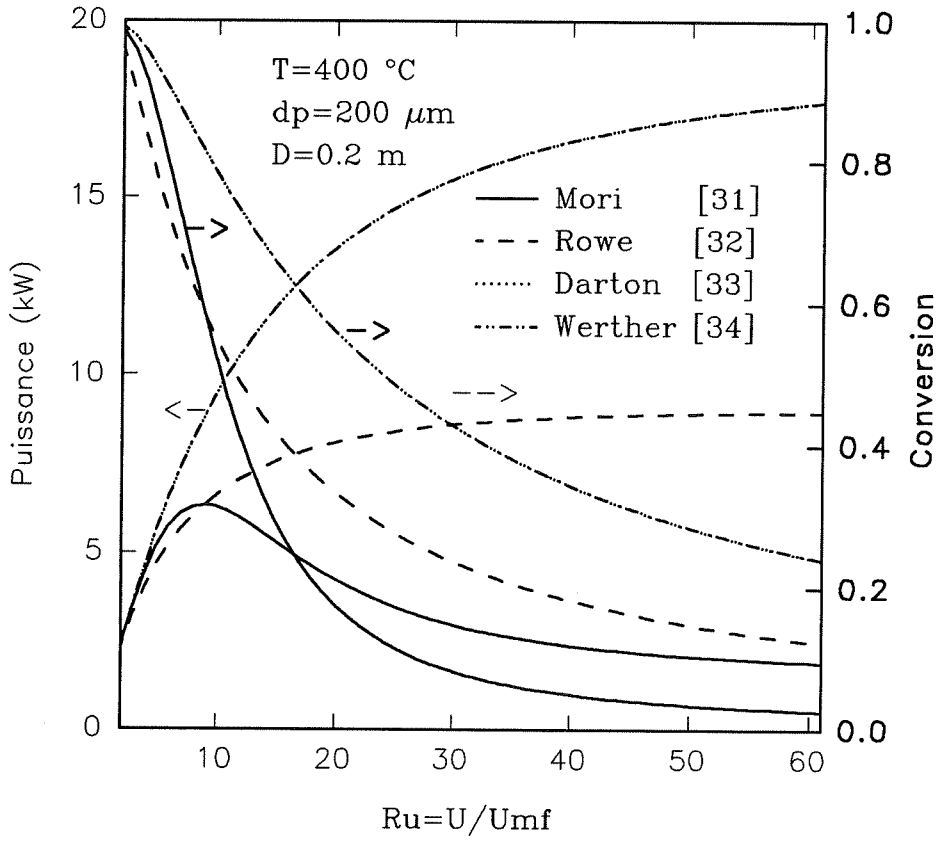

Figure 2.1. Puissance de combustion et conversion du méthane (*Pt* 0.25%)

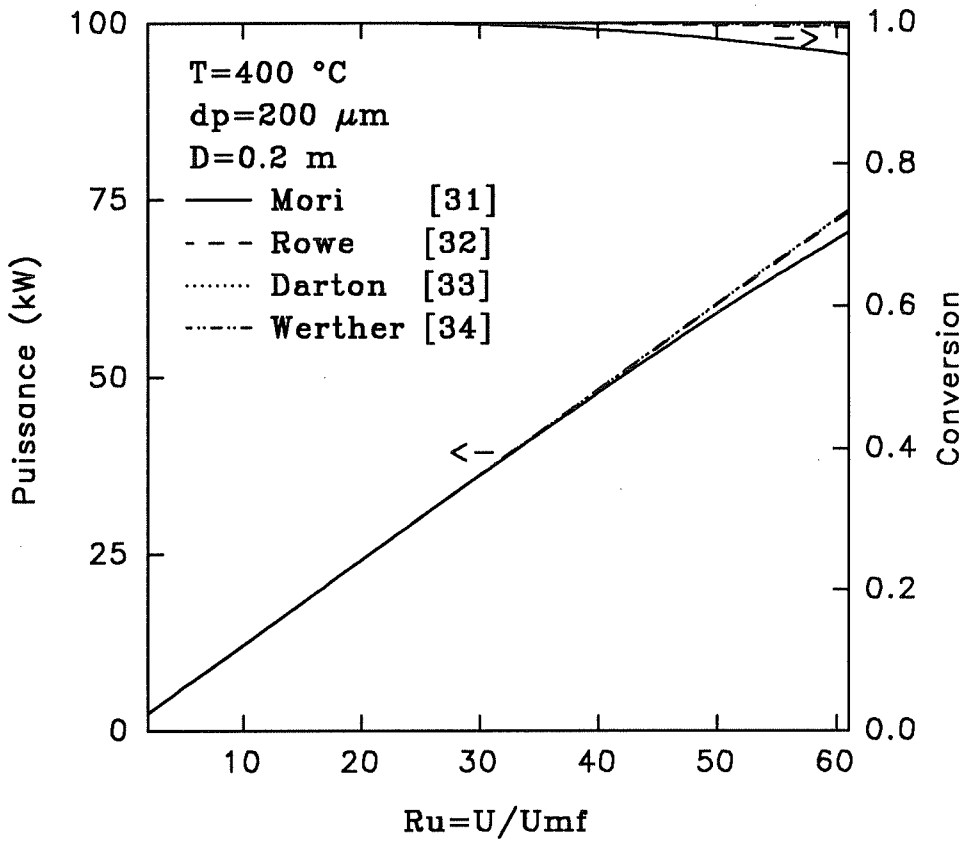

Figure 2.2. Puissance de combustion et conversion du méthane (Pd 0.21%)

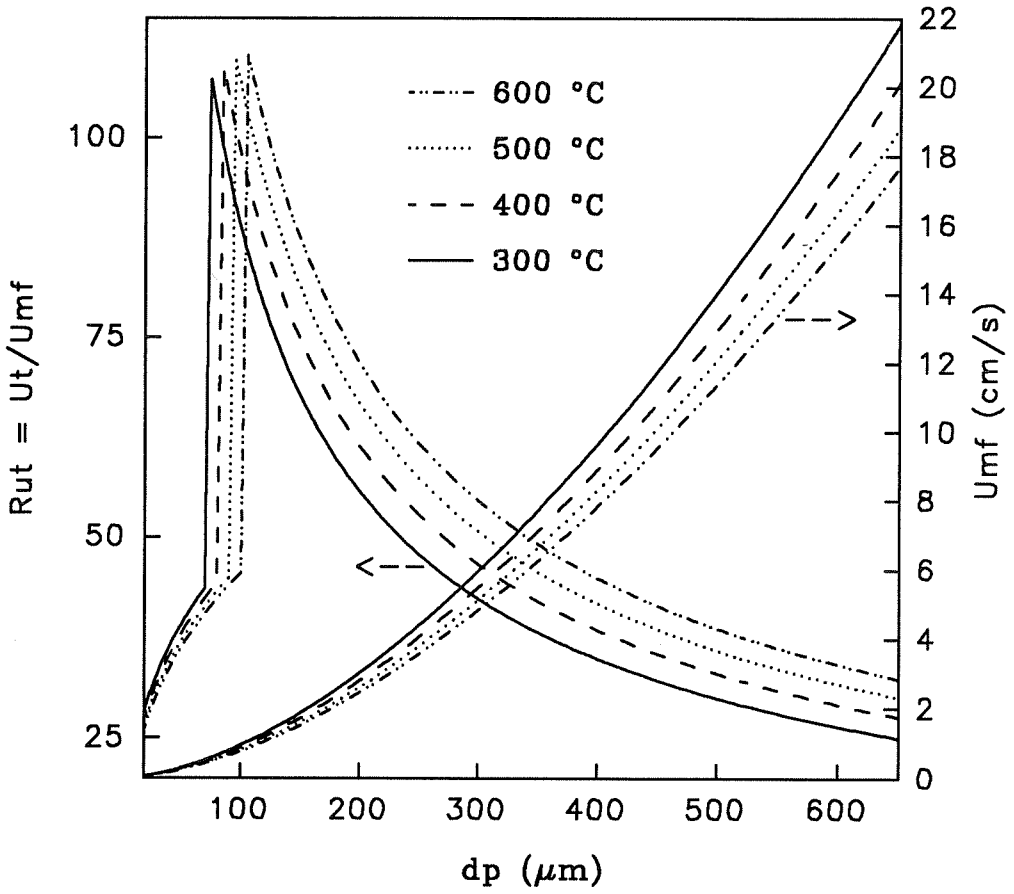

Figure 2.3. Vitesse terminale et vitesse minimale de fluidisation en fonction de la taille des particules

données par *Kunii* et *Levenspiel* [17] et U_{mf} à partir de l'équation 2.9 [40].

$$Re_{mf} = (27.2^2 + 0.0408Ar)^{1/2} - 27.2 \tag{2.9}$$

où:

$$Ar = \frac{\rho(\rho_p - \rho)gd_p^3}{\mu^2} \; et \; U_{mf} = \frac{\mu Re_{mf}}{\rho d_p} \tag{2.10}$$

On constate que pour des particules de diamètre supérieur à 100 μm il y a plus de flexibilité à utiliser les petites particules que les grosses car avec des rapports R_{ut} élevés on peut opérer à des rapports U/U_{mf} élevés. Cependant, l'utilisation des particules de diamètre inférieur à 100 μm est contraignante parce que le rapport R_{ut} devient faible et reste beaucoup plus faible lorsque la température augmente. Ceci est dû à l'accroissement de la viscosité du gaz avec la température[45] et par conséquent à l'accroissement de la force de *Stokes* sur une particule en chute libre dans le gaz de fluidisation. Nous prendrons R_{ut} comme la borne supérieure de l'axe R_u au cours de l'optimisation. Mais il est à noter que le régime turbulent se situe bien au delà de la vitesse terminale [49].

2.5 Optimisation et contraintes

Un code de calcul dont un algorithme simplifié est présenté à la Figure 2.4, a été développé pour obtenir, pour une puissance et une conversion, le diamètre minimal du réacteur et les valeurs optimales de la température d'opération, de la taille des

particules et de la vitesse superficielle du gaz. L'optimisation est soumise à plusieurs contraintes:

–Limites sur la température. Etant donné la production des radicaux de méthane à des températures supérieures à $800°C$[7], la température critique d'opération (Tc) est prise égale à $700°C$. Cette température marque la borne supérieure de l'axe des températures, la borne inférieure étant limitée par la température d'allumage du catalyseur qui est généralement autour de $300°C$ pour les catalyseurs au palladium et autour de $400°C$ pour les catalyseurs au platine[22].

–Contrainte sur le rapport hauteur-diamètre du lit R_{HD}. Pour des lits à éléments internes, ce rapport n'a qu'un effet négligeable sur la conversion. Cependant, un lit très peu profond favorise le court–circuit du gaz et par conséquent la baisse de la conversion. Pour des lits bouillonnant libres un grand R_{HD} favorise la formation de grosses bulles et par conséquent le court–circuit du gaz. Le rapport recommandé est de $R_{HD} = 1$ [17].

–Contraintes cinétiques. Le critère de $Weisz–Prater$ C_{wp}[46] qui est le rapport entre la vitesse de réaction observée et la vitesse de diffusion du réactif dans le catalyseur permet de s'assurer que la combustion a lieu en régime cinétique ($C_{wp} << 1$) et non en régime diffusionnel ($C_{wp} >> 1$). Ce critère étant fonction de la taille des particules et de l'activité du catalyseur, il limite aussi le diamètre des particules à utiliser pour des conditions d'opération données. Nous retiendrons la valeur 0.5 pour rester en régime cinétique.

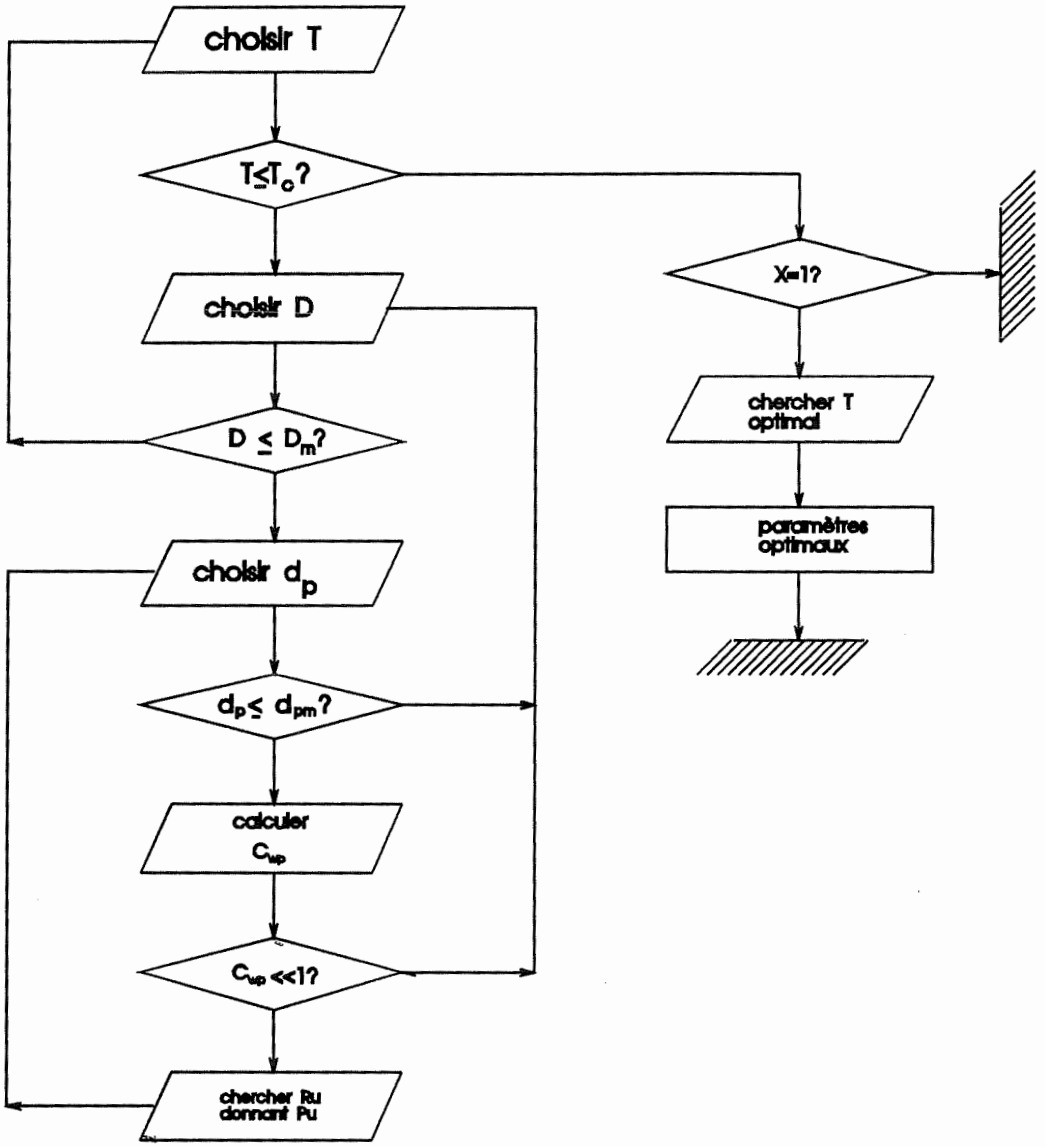

Figure 2.4. Algorithme simplifié d'un générateur de chaleur

–Contraintes sur la conversion. Les imbrûlés de méthane représentent une perte financière et une menace pour l'environnement; par conséquent, la conversion doit être de 100% lors de la combustion. Il est à noter sur la Figure 2.4 que X est un vecteur de conversions. Chaque élément de ce vecteur correspond à l'isopuissance Pu à une température donnée. La Figure 2.5 présente le comportement de l'algorithme de la Figure 2.4 pour un générateur de chaleur de puissance Pu=50 kW à 400°C. L'optimisation se fait de la façon suivante:

Pour un diamètre D donné du lit, le diamètre d_p des particules est fixé et l'axe des R_u balayé jusqu'à l'obtention de la puissance désirée (isopoint (R_u, d_p)). En incrémentant d_p et en répétant la procédure, l'isopuissance Pu (vecteur d'isopoints) est générée et le profil de conversion correspondant aussi (courbes à droite du graphe) jusqu'à ce qu'on soit limité par la contrainte cinétique. A ce stade, le diamètre du lit est incrémenté et toute la procédure recommence. On remarque sur la Figure 2.5 qu'à chaque isopoint (R_u, d_p) de l'isopuissance Pu=50 kW correspond une conversion représentée par le point (d_p, X) qui n'est pas forcément de 100%. Plus on augmente le diamètre du lit, plus les isopuissances se déplacent vers la gauche (faibles R_u) et les profils de conversion vers la droite (tendant vers 100%). Ainsi, à chaque élément de température sur l'axe T tous les paramètres correspondant à l'isopuissance Pu avec 100% de conversion sont répérés, à savoir la masse du catalyseur W, le diamètre du lit, le diamètre des particules et le rapport de vitesses R_u comme indiqué sur la Figure 2.6. Sur cette figure, la masse du catalyseur est donnée en fonction de la taille

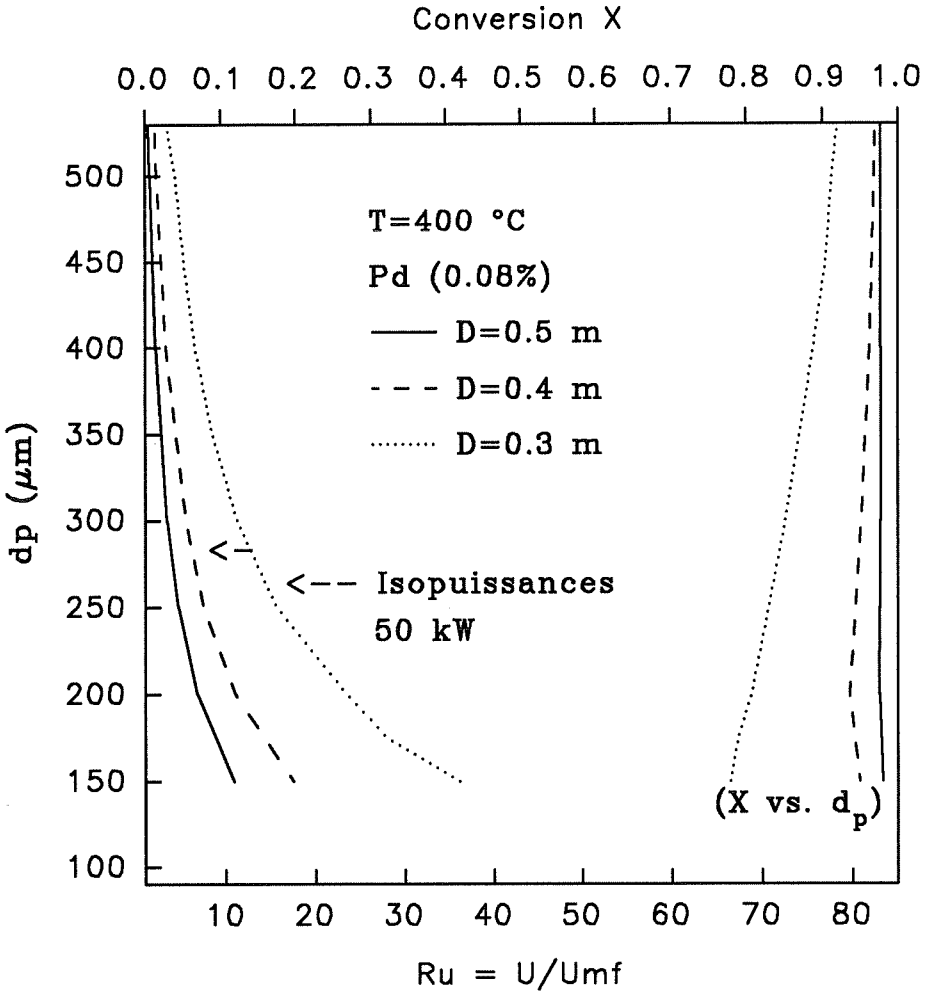

Figure 2.5. Isopuissance 50 kW et conversion du méthane

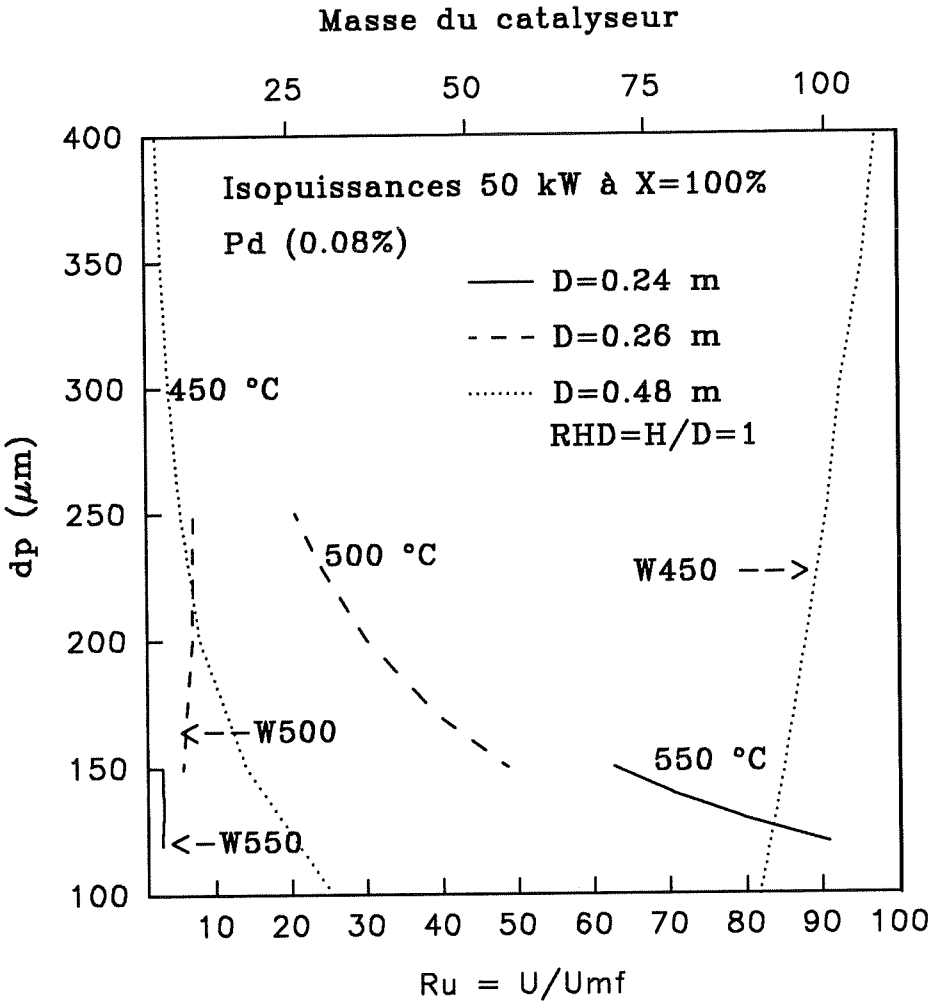

Figure 2.6. Isopuissance 50 kW et masse du catalyseur pour une conversion maximale du méthane sur $Pd(0.08\%)$

des particules d_p alors que le diamètre des particules pour lesquels la puissance désirée ($50\ kW$) est réalisée pour une conversion de méthane de 100% est donné en fonction du rapport R_u. Les différents points (R_u, d_p) forment l'isopuissance $50\ kW$. A chaque température correspond un diamètre du lit, une masse dénotée par W indicée par la température correspondante et une isopuissance $50\ kW$. L'optimisation sur l'axe T consiste à choisir l'isopuissance pour laquelle le diamètre du lit est minimal et à cette isopuissance correspondent les paramètres optimaux.

2.6 Résultats

Procédant comme indiqué précédemment, nous obtenons pour le catalyseur au palladium de *Sicardi*[19] et pour une puissance requise de $50\ kW$ (Figure 2.6) un diamètre du lit de $0.24\ m$ à $550°C$ pour une masse de catalyseur de $7\ kg$ avec la taille des particules comprise entre $110 - 140\ \mu m$ et le rapport R_u compris entre 70–91 comme indiqué dans la Table 5.1. Il est à noter ici que plus la température augmente plus on est limité par la taille des particules (critère de *Weisz–Prater*). Considérant un autre catalyseur cette fois–ci au platine [19] (Figure 2.7), on aboutit pour la même puissance à un diamètre de $0.35\ m$ à $550°C$. La différence est due à la plus faible activité du catalyseur. Il est à remarquer qu'au delà de $550°C$, le diamètre requis pour réaliser la même puissance et une conversion de 100% augmente dû au fait qu'on est obligé de fonctionner avec des particules plus petites pour être en régime cinétique,

Table 2.1. Paramètres optimaux de conception du générateur de chaleur

Pu	(kW)	50	500
D	(m)	0.24	0.56
T	$(°C)$	550	500
Ru		91-70	64.8-44.6
d_p	(μm)	120-140	200-250
W	(kg)	7-7.15	101-102
E_s	(kg/s)	9.5×10^{-3}	0.341
U_{mf}	(m/s)	1.076×10^{-2}	2.6×10^{-2}
U	(m/s)	0.979	1.685
d_b	(m)	5.3×10^{-2}	0.112
U_b	(m/s)	1.48	2.404
U_t	(m/s)	1.05	1.736
ϵ_{mf}		0.45	0.43

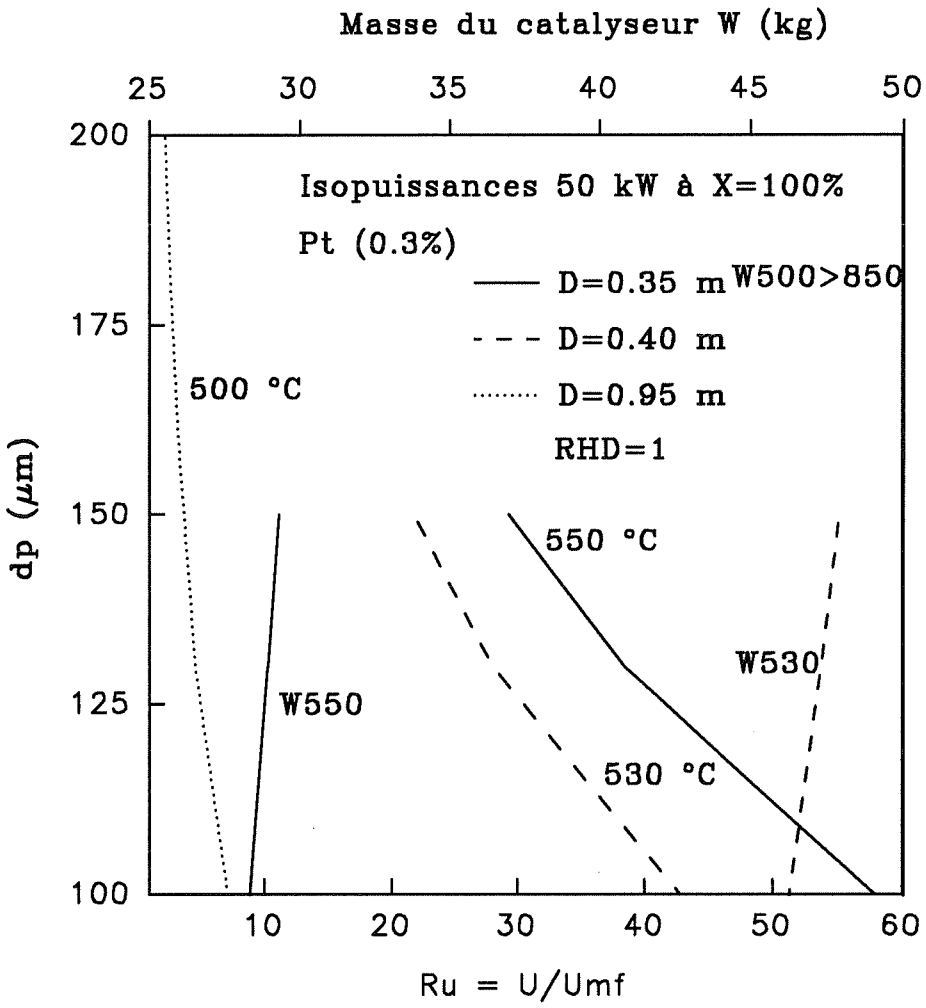

Figure 2.7. Isopuissance 50 kW et masse du catalyseur pour une conversion maximale du méthane sur $Pt(0.3\%)$

ce qui exige beaucoup plus de catalyseur (grande hauteur du lit). Ce phénomène est beaucoup plus visible sur la Figure 2.8 avec l'isopuissance 500 kW. A 550°C par exemple le diamètre requis pour avoir 100% de conversion est de 0.7 m alors qu'à 500°C il est de 0.56 m. Dans la Table 5.1, l'emportement minimal (taux à la saturation) E_s est calculé à $d_p = 140\ \mu m$ pour 50 kW et $d_p = 200\ \mu m$ pour 500 kW avec la corrélation de $Zenz$ et $Weil$[47] et la porosité aux conditions minimales de fluidisation ϵ_{mf} par la corrélation de $Broadhurst$ et $Becker$[48].

Les dimensions du réacteur paraissent très attrayantes pour les niveaux de puissance requis mais l'emportement des particules est élevé à ces conditions d'opération et les paramètres hydrodynamiques du lit suggèrent beaucoup plus un régime turbulent. Il est à noter que la taille des particules a été supposée uniforme pendant l'optimisation. Dans la pratique, on a plutôt une distribution de particules dans le lit puisqu'on a besoin de particules fines pour améliorer la fluidisation. Ce qui veut dire que l'emportement des particules sera beaucoup plus élevé que ce qui est prédit dans la Table 5.1.

2.7 Conclusion

Un algorithme d'optimisation permettant de dimensionner un générateur de chaleur pour la combustion propre du méthane a été testé avec les paramètres tirés de la littérature. Bien qu'ayant utilisé pour la simulation un distributeur à plaques poreuses

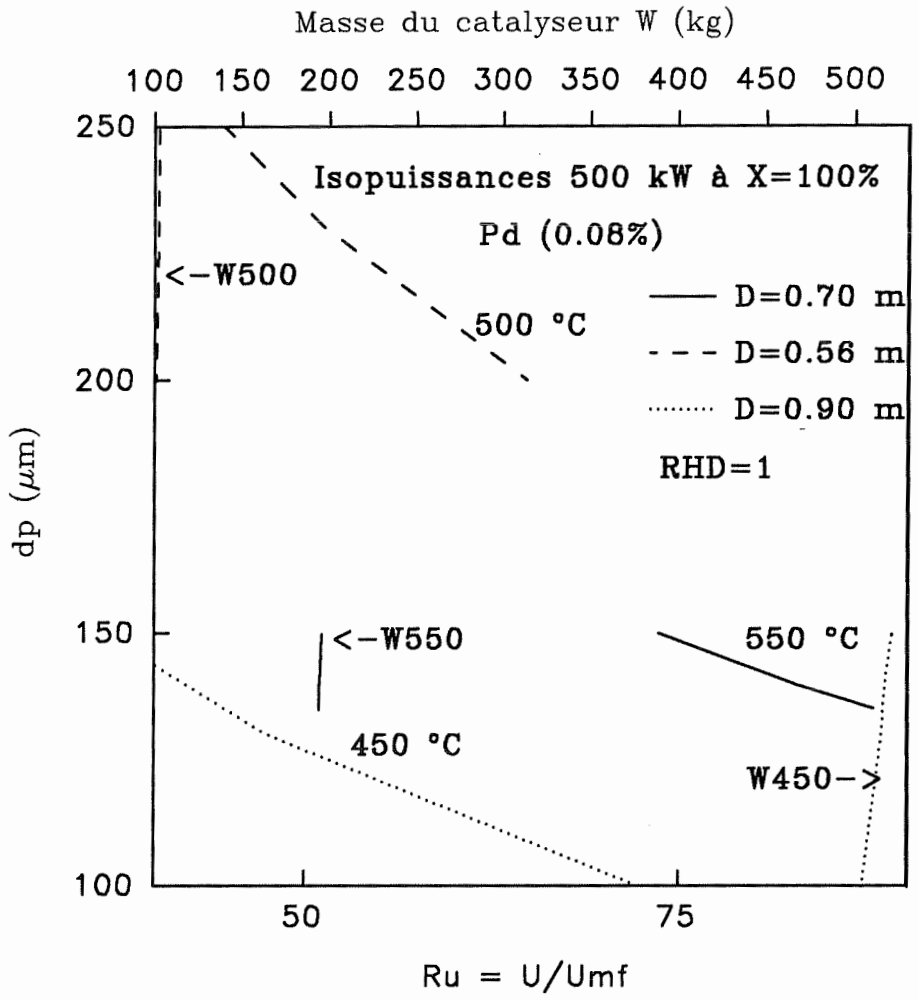

Figure 2.8. Isopuissance 500 kW et masse du catalyseur pour une conversion maximale du méthane

généralement réservé aux réacteurs de laboratoire, les dimensions optimales du lit obtenues sont assez petites pour pouvoir justifier ce choix. Cependant, malgré la petitesse du lit, l'emportement des particules parait élevé aux conditions optimales. Pour contrecarrer ce problème, il suffit d'augmenter le diamètre du réacteur dans la zone de désengagement dans des proportions économiquement acceptables. Par ailleurs, l'activité du catalyseur s'est avéré être un paramètre crucial du design. Ce fait montre bien l'intérêt qu'on a à mettre au point de nouveaux catalyseurs de combustion bon marché, stables (thermiquement et mécaniquement) et très actifs (faible température d'allumage) pour la promotion de cette nouvelle technologie gazière basée sur la combustion en lit fluidisée.

Remerciements

Nous tenons à remercier la compagnie Gaz Métropolitain, Inc. qui, grâce à sa subvention de recherche, nous a permis d'aborder ce sujet et de poursuivre les travaux en cours.

2.8 References

[1] Yaverbaum, L.H. (1979). Nitrogen Oxides-Control and Removal. Notes Data Corporation N.J.

[2] Perthuis, E. (1989). Revue des techniques de réduction des émissions d'oxydes d'azote au niveau des brûleurs. Rev.Gen.Therm., 28, 374.

[3] Audibert, F. (1989). Cinétique de la conversion de NO en NO_2 dans les lignes de prélèvement vers les analyseurs. Rev.Gen.Therm., 28, 459.

[4] Perret, R. (1989). Mesure des oxydes d'azote. Rev.Gen.Therm., 28, 454.

[5] Lievoux, P.; Locanetto, P., et Bury, F. (1989). Etude d'un brûleur bas Nox pour chaudière industrielle. Rev.Gen.Therm., 28, 379.

[6] De Soete, G.G. (1989). Mécanisme de formation et de destruction des oxydes d'azote dans la combustion. Rev.Gen.Therm., 28, 353.

[7] Veg. Gasinstitut rapport m.t. 89v12 (1989). Dispositif de Combustion catalytique en lit fluidisé pour la génération de vapeur.

[8] Leygonie, R. (1989). Effets des oxydes d'azote sur la santé humaine et sur le milieu naturel. Rev.Gen.Therm., 28, 343.

[9] Williams, C.L.H. (1988). Nitrosation. Cambridge University Press, N.Y.

[10] De Soete, G.G. (1989). Les oxydes d'azote, Introduction. Rev.Gen.Therm., 28, 339.

[11] Molière, M.; Colas, M.; Freimark, M. (1989). Des émulsions eau/fuel pour réduire les émissions de NOx de turbines à gaz. Rev.Gen.Therm., 28, 428.

[12] De Reydellet, A. (1989). Les mesures de réduction des émissions d'oxydes d'azote en aval du foyer. Rev.Gen.Therm., 28, 453.

[13] Martin, G. (1989). Les émissions d'oxydes d'azote dans les Chaudières à lit fluidisé circulant. Rev.Gen.Therm., 28, 415.

[14] Friedrich, F.D. (1980). Fluidized-bed Combustion–An Emerging Technology. Energy Research Laboratories Report, CANMET, Energy, Mines and Ressources Canada, Ottawa.

[15] Salfati, D.J., van Der Wal, W. (1989). Développement de nouveaux appareils utilisant la combustion catalytique du gaz naturel. Congrès A.T.G., Lyon.

[16] Trim, D.L., and Lam, C. (1980). The Combustion of Methane on Platinum–Alumina fibre catalysts–II, Design and Testing of a Convective–Diffusive Type Catalytic Combustor. Chem.Eng.Sci., 35, 1731.

[17] Kunii, O., and Levenspiel, O. (1969). Fluidization Engineering. Krieger, Huntington, N.Y.

[18] Pereira, J.; Chandrasekharan, K., and Calderbank, P.H. (1981). A Revised Model for Predicting the Performance of a Fluidized–Bed Catalytic Reactor. Chem.Eng.Sci., 36, 239.

[19] Sicardi, S., Specchia, V., and Ferrero, F. (1982). Kinetics of Combustion of Methane with Different Catalysts. Chimica Industriale, 3, 217.

[20] Wise, H., and Quinlan, M. (1986). Elementary Processes in the Catalytic Combustion of Methane. Gas Research Institute Report, Chicago Il.

[21] Jones, D.J, et Salfati, S. (1989). Combustion catalytique et gaz naturel. Rev.Gen.Therm., 28, 401.

[22] Anderson, R.B.; Stein, K.C.; Feenan, J.J., and Hofer, L.J.E. (1961). Catalytic Oxidation of Methane. Ind.Eng.Chem., 53, 809.

[23] Ahuja, O.P., and Mathur, G.P. (1967). Kinetics of Catalytic Oxydation of Methane: Application of Initial Rate Technique for Mechanism Determination. Can.J.Chem.Eng., 45, 367.

[24] Trim, D.L., and Lam, C. (1980). The Combustion of Methane on Platinum–Alumina fibre catalysts–I, Kinetics and Mechanism. Chem.Eng.Sci., 35, 1405.

[25] Norrish, R.G.W. (1948). Role des aldéhydes dans l'oxydation des hydrocarbures. Colloques internationaux, CNRS.

[26] Eltenton, G.C. (1948). Détection des produits intermédiaires des réactions par spectroscopie de masse. Colloques internationaux, CNRS.

[27] Mezaki, R., and Watson, C.C. (1966). Catalytic Oxidation of Methane I&EC Process Design and Development, 5, 63.

[28] Cullis, C.F.; Keene, D.E, and Trimm, D.L. (1971). Pulse Flow Reactor Studies of Methane Oxidation over Palladium Catalysts. Trans.Faraday Soc., 67, 864.

[29] Firth, J.G., and Holland, H.B. (1969). Catalytic Oxidation of Methane Over Noble Metals. Trans.Faraday Soc., 65, 1121.

[30] Grace, J.R. (1984). Generalized Models for Isothermal Fluidized bed reactors. Chap. 13 in "Recent Advances in the Engineering Analysis of Chemically Reacting Systems". Edited by Doraiswamy L.K. New Dehli, Wiley Eastern.

[31] Mori, S., and Wen, C.Y. (1975). Estimation of Bubble Diameter in Gaseous Fluidized Beds. AICHE J., 21, 190.

[32] Rowe, P.N., and Partridge, B.A. (1965). Trans.Instn.Chem.Engrs., 43, T157.

[33] Darton, R.C.; Lanauze, R.D.; Dandson, J.F., and Harrison, D. (1977). Bubble Growth Due to Coalescence in Fluidized Beds. Trans.IChemE, 55, 274.

[34] Werther, J. (1978). Scale–up of Fluidized Bed Reactors. Ger.Chem.Eng., 1, 243.

[35] Geldart, D. (1973). Types of Gas Fluidization. Powder Technol., 7, 285.

[36] Grace, J.R. (1982). Fluidized Bed Hydrodynamics. Chap. 8.1 in "Handbook of Multiphase Systems". Edited by Hetsroni, G. Hemisphere Publishing, Washington.

[37] Bolthrunis, C.O. May (1989). An Industrial Perspective on Fluid Bed Reactor Models. Chem.Eng.Prog., 51.

[38] Krambeck, F.J.; Katz, S., and Shinnar, R. (1969). A Stochastic Model for Fluidized Beds. Chem.Eng.Sci., 24, 1497.

[39] Krambeck, F.J.; Katz, S., and Shinnar, R. (1967). A Stochastic Mixing Models for Chemical Reactors. I&EC Fundamentals, 6, 276.

[40] Grace, J.R. (1986). Fluidized Beds as Chemical Reactors. Chap. 11 in "Gas Fluidization Technology". Edited by Geldart, D. Wiley, London, 285.

[41] Johnson, J.E., Grace, J.R., Graham, J.J. (1987). Fluidized–Bed Reactor Model Verification on a Reactor of Industrial Scale. AICHE J., 33, 619.

[42] Kato, K. and Wen, C.Y. (1969). Bubble Assemblage Model for Fluidized Catalytic Reactors. Chem.Eng.Sci., 24, 1351.

[43] Fryer, C. and Potter, O.E. (1972). Bubble Size Variation in Two–phase Models of Fluidized Bed Reactors. Powder Technol., 6, 317.

[44] Baron, T., Briens, C.L., Galtier, P. and Bergougnou, M.A. (1990). Verification of Models and Correlations for Bubble Properties in Fluidized Beds. 45, 2227.

[45] Bird, R.B; Stewart, W.E, and Lightfoot, E.N. (1960). Transport Phenomena. John Wiley & Sons, Inc.

[46] Fogler, H.S. (1986). Elements of Chemical Reaction Engineering. Prentice–Hall, Englewood Cliffs, N.J.

[47] Zenz, F.A., and Weil, N.A. (1958). A Theoretical–Empirical Approach to the Mechanism of Particle Entrainment from Fluidized Beds. AICHE J., 4, 472.

[48] Broadhurst, T.E., and Becker, H.A. (1975). Onset of Fluidization and Slugging in Beds of Uniform Particles. AICHE J., 21, 238.

[49] Yerushalmi, J., and Avidan, A. (1985). High–Velocity Fluidization. Chap. 7 in "Fluidization". Edited by Davidson, J.F., Clift, R., and Harrison, D. (1985). Academic Press.

CHAPTER 3

CATALYTIC COMBUSTION OF NATURAL GAS IN A TURBULENT FLUIDIZED BED REACTOR

M. Foka, J. Chaouki*, C. Guy & D. Klvana

Proc. 12th Int. Conf. on Fluid Bed Combustion. ASME, may 9–13, vol 1, 179–184

(1993)

*To whom correspondence should be addressed

Abstract

Air pollution has altered many traditional practices in the design and operation of combustion equipment. Fluidized–bed catalytic combustion presents real advantages compared to conventional combustion systems and to fixed bed catalytic combustors. Turbulent Fluidized Bed Catalytic Combustors ($TFB2C$) appear to be the ideal combustors for the generation of low temperature (less than $650°C$) hot air that can be used in food processing. Their performance can be predicted by coupling the hydrodynamic model describing the flow behavior of gas through the bed and the kinetics of combustion of the fed gas. An algorithm for the optimal design of $TFB2C$ predicts reasonable bed diameters compared to conventional combustion beds.

3.1 Introduction

The greenhouse effect, the thinning of the stratospheric ozone layer, acid rains, and the oxidic smogs represent nowadays a real threat to human survival in our biosphere. For many years, gases emanating from human or natural activities have been known to participate directly or indirectly to atmospheric photochemical reactions responsible for these harmful phenomena. At the forefront of this list are nitrogen oxides (NOx) from human sources (automobiles, stationary combustion sources, moving engines, industrial activities, agricultural activities, etc...) and from natural sources (storms, biological activities in the soil, etc...). This family of nitrogen oxides is composed of seven oxides [1] among which are: nitrogen monoxide (NO), nitrogen dioxide (NO_2) and nitrous oxide (N_2O). In direct drying processing, NOx form carcinogenic compounds with foodstuff [2]. N_2O is known for its contribution to the greenhouse effect [3] and the reduction of the stratospheric ozone layer [4]. NO predominates in combustion chambers (90–95%) [1, 5] and is formed by three different mechanisms: Thermal NO mechanism, Fuel NO mechanism, and Prompt NO mechanism. Thermal NO is generated by chemical combination of molecular nitrogen and oxygen present in the combustion air; Fuel NO is formed by oxidation of the organic nitrogen present in the fuel (fossil and solid fuels) at moderate temperatures; and Prompt NO is formed from the hydrocarbonated radicals present in the combustion chamber and the nitrogen present in the combustion air [6]. At temperatures less

than $800°C$, it is not likely that methane radicals are produced [7] and the combustion of natural gas at temperatures below $800°C$ can be considered to be clean. In conventional combustors the flame temperature is usually above $1200°C$ with an intense generation of NOx. Many techniques have been devised to reduce these compounds: the primary techniques for in situ reduction [5, 8], the secondary techniques applied downstream of the combustor to convert NOx into harmless compounds [9]. The catalytic combustion of nitrogen–free fuels does not produce NOx at low temperatures. This combustion can be performed in a fixed bed reactor but the rise in the bed temperature leads to the formation of hot–spots, the deactivation of the catalyst and the homogeneous phase combustion with production of thermal NOx if the reactor is not insulated. The fluidized bed on the contrary operates isothermally and can handle high throughputs in the turbulent regime. The purposes of this paper are (1) to determine the kinetics of combustion of methane on an appropriate catalyst in an integral tubular reactor, (2) to characterize the hydrodynamics of a turbulent fluidized bed catalytic combustor, (3) to couple the kinetics and the hydrodynamics to predict the performance of the $TFB2C$.

3.2 Combustion Catalysts

Combustion catalysts are either supported or nonsupported. Supported catalysts present two phases: the support (porous or nonporous) and the active element (met-

als, oxides, metal alloys). The support provides the catalyst with a high specific surface area and help stabilize the active sites. Gamma alumina are the most used supports with specific surface areas of the order of 150 m^2/g [10]. Nonporous supports have smaller specific surface areas. The active phase is usually made of noble metals (Pd, Pt, Ir, Rh), transition metals ($Cu, Co, Mn, Ni, etc...$), or of their alloys [11]. Promoters are usually included in the preparation of supported catalysts to minimize the effects of poisons, thermal sintering and to stimulate their activity. Rare earth oxides are the most used promoters [12]. The activity of supported catalysts depends upon the crystal structure of the active element and the nature of the support. Furthermore, the promoter used in the preparation and the methods of impregnation and reduction, are also very important as indicated by the results of Sicardi [10] on Pt and Pd supported alumina catalysts. Palladium and platinum remain the most active element for the combustion of methane [13]. The activity of palladium catalysts may be as high as 300 times the activity of platinum catalysts [10]. Oxides such as Co_3O_4, NiO, Cr_2O_3, MnO_2, CuO can be used as active sites for high temperature applications [12]. Alumina supports are known to sinter at high temperatures and noble metal catalysts are not only expensive but unstable at temperatures above $600°C$ [7] Nonsupported catalysts used for the combustion of methane are mixed oxides of different crystal structures: Inverse 2,3 Spinel ($CuCr_2O_4$), Scheelite ($Bi_2O_3 \cdot 3Mo \cdot O_3$) and Perovskite ($La_{1-x}Sr_xMnO_3$, $0 < x < 0.6$) [11]. Their activity may be accounted for by the multiplicity of active sites, polyvalent cations, anions, adsorbed species

and lattice vacancies. They offer several advantages compared to supported catalysts: they exhibit thermal stability, are available at low costs and oxidize sulfur compounds without loss of activity [11]. Therefore, they seem to be the most appropriate catalysts for the combustion of natural gas in which sulfur compounds are used as odorants. We are dealing in parallel with the development of a perovskite type combustion catalyst for fluidized beds and the design criteria for an atmospheric $TFB2C$. The kinetic study presented below is for a platinum catalyst that we are presently using to forward the design of the fluidized bed reactor. At the same time, some work is being performed to improve the activity and the fluidizability of the perovskite type catalyst. No primary results are presented on the latter catalyst.

3.3 Combustion of Methane on a Pt/Al_2O_3 Catalyst

3.3.1 Catalyst Properties

An industrial reforming catalyst referenced PSA ($Pt - Sn/Al_2O_3$) with a very low platinum content (0.2%) and doped with tin was ground and the particle distribution shown in Figure 3.1 was obtained. The mean particle diameter was evaluated to be 182 μm . The fluidizability was studied in a transparent glass column and the pressure drop through the bed recorded with a $FCO14$–Micromanometer. The pressure drop

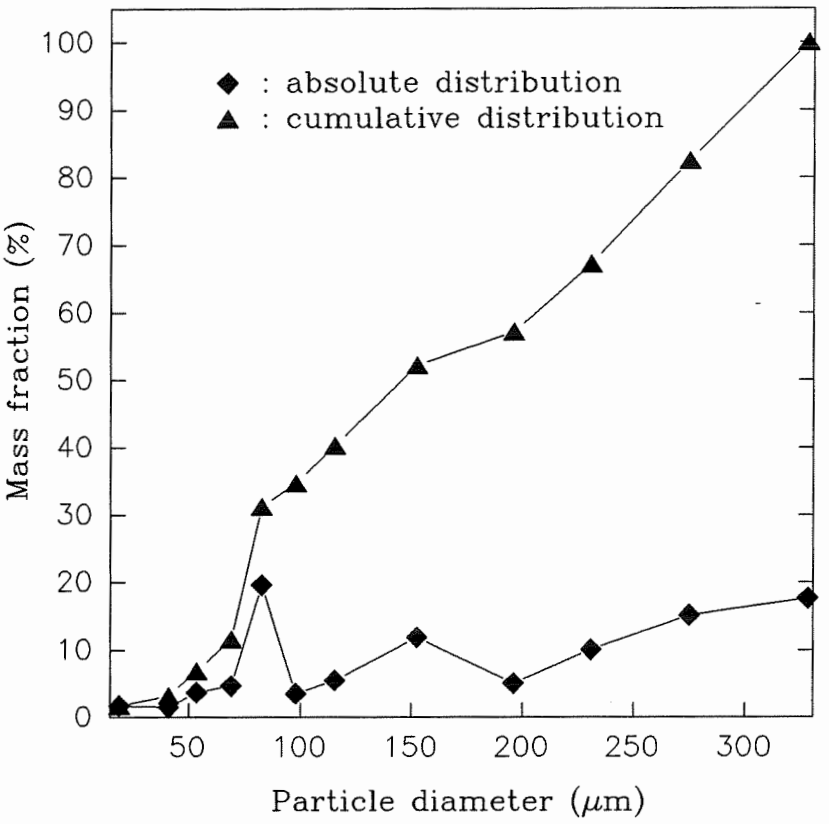

Figure 3.1. Particle size distribution of PSA catalyst

readings obtained by increasing and decreasing the gas velocity gave a minimum fluidization velocity of 0.03 m/s (U_{mf}) which is of the order of magnitude of the prediction by the correlations found in the literature.

3.3.2 Experimental Equipment and Technique

The study was carried out in an integral tubular flow reactor of 7 mm in diameter with a conventional setup for kinetic studies. In order to avoid hot–spots and maintain a constant temperature in the bed, the catalyst was diluted with nonporous alumina. 1 g of catalyst was used for all the experiments. The reactor was placed in an electrically controlled oven. The total pressure in the reactor was kept atmospheric and the temperature range of $400 - 600°C$ was covered. The design equation of the plug flow reactor is given by:

$$\frac{W}{(F_{CH4})_0} = \eta = \int_0^X \frac{dX}{R_{CH4}} \tag{3.1}$$

where W is the mass of the catalyst, X the conversion of methane, R_{CH4} its rate of disappearance and $(F_{CH4})_0$ its inlet molar flow rate to the reactor. The conventional procedure to determine the reaction rate R_{CH4} is to vary η at a fixed temperature, register the conversion and take the derivative of X versus η. The methane mole fraction was kept constant at 4.2% and the total flow rate was varied in the range of 0.09–0.3 L/min at different temperatures. The conversion of methane was monitored with a gas chromatograph.

3.3.3 Results and Analysis

The experimental data are ploted in Figure 3.2 at various temperatures. The plain lines are the prediction by the model:

$$X = A[1 - \exp(-B\eta)] \tag{3.2}$$

fitted to experimental data with the method of Marquardt [14]. The constants A and B are shown in Table 3.1 and the reaction rate is given by:

$$R_{CH4} = \frac{dX}{d\eta} = AB\exp(-B\eta) \tag{3.3}$$

Wiesz–Prater criterion [15] was used to check internal diffusion control and *Mears* criterion [15] for external diffusion control at all temperatures. No diffusion control was found at these operating conditions. The following kinetic model:

$$R_{CH4} = k_0 \exp(-\frac{E}{RT})P_{CH4} \tag{3.4}$$

where k_0 is the preexponential factor, E the activation energy, T the temperature and P_{CH4} the partial pressure of methane was found to fit our experimental data best with an activation energy of 28 $kcal/mole$ and a preexponential factor of 3200 $mol/g/s/atm$. Figure 3.3 shows the comparison between experimental and predicted data. The activation energy is of the order of magnitude reported in the literature [10].

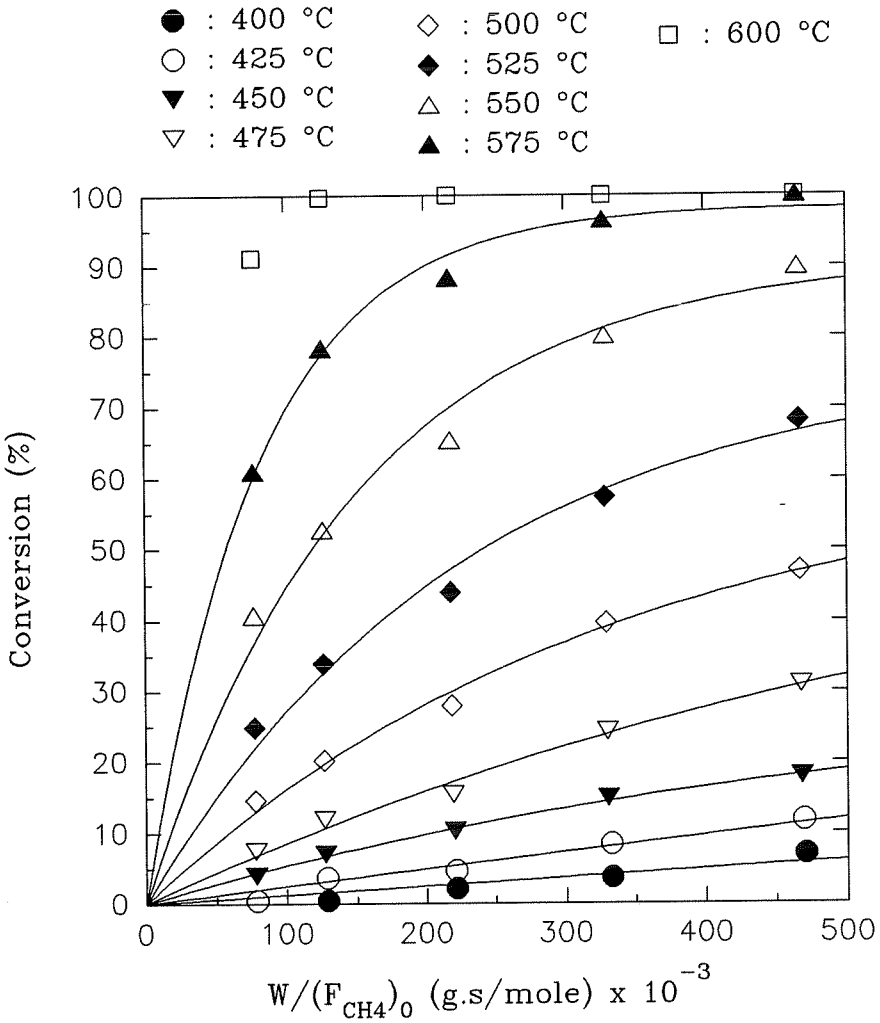

Figure 3.2. Conversion of methane vs. η

Table 3.1. Constants A and B in Equation 3.2

Temperature (°C)	A	B
400	$6.361 \times 10^{3} \pm 1.69 \times 10^{-6}$	$1.929 \times 10^{-7} \pm 5.150 \times 10^{-9}$
425	$1.485 \times 10^{2} \pm 8.41 \times 10^{-2}$	$1.686 \times 10^{-6} \pm 1.217 \times 10^{-7}$
450	$2.951 \times 10^{1} \pm 3.423$	$2.034 \times 10^{-6} \pm 3.414 \times 10^{-7}$
475	$5.899 \times 10^{1} \pm 1.696$	$1.576 \times 10^{-6} \pm 6.053 \times 10^{-7}$
500	$6.156 \times 10^{1} \pm 5.974$	$3.055 \times 10^{-6} \pm 5.038 \times 10^{-7}$
525	$7.642 \times 10^{1} \pm 6.007$	$4.396 \times 10^{-6} \pm 7.040 \times 10^{-7}$
550	$9.127 \times 10^{1} \pm 4.673$	$6.691 \times 10^{-6} \pm 8.830 \times 10^{-7}$
575	$9.836 \times 10^{1} \pm 1.673$	$1.230 \times 10^{-5} \pm 7.695 \times 10^{-7}$
600	not calculated	not calculated

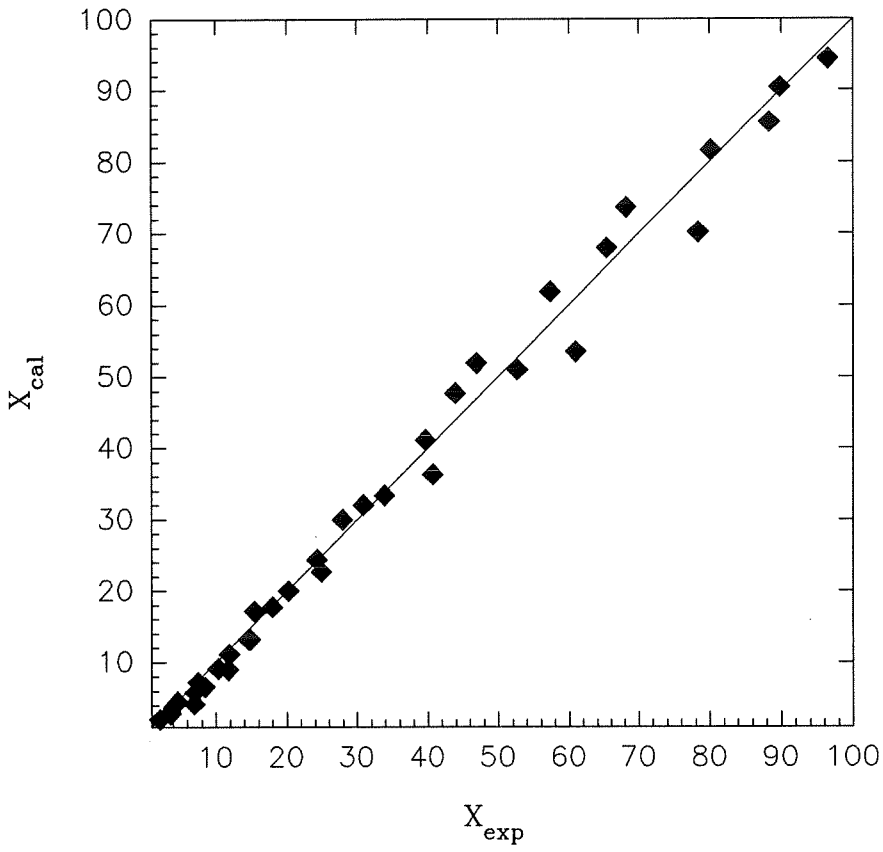

Figure 3.3. Calculated vs. experimental conversion

3.4 Fluidized Bed Hydrodynamics and Modeling

3.4.1 Fluidization Regimes

Successful commercial processes involving fluidized beds have been extensively reported in the literature [16, 17, 18]. They have included solid wastes treatment, solid drying, catalytic cracking of hydrocarbons and combustion of a wide variety of fuels. We focus here on the hydrodynamics of fluid beds used as catalytic reactors. When gas is fed at the bottom of a column filled with solid particles, they are levitated and set in motion when the friction force of the gas becomes greater than the apparent bed weight. As the gas flow rate is increased, various hydrodynamic regimes are observed: the bubbling regime, the slug flow (small diameter and deep beds), the turbulent regime, and the fast fluidization regime [18]. The performance of a fluidized bed catalytic combustor is directly related to the hydrodynamic regime at which it operates especially when the reaction is fast. Therefore, the limits and the characteristics of the different flow regimes are key elements to the modeling and the design of such reactors. Bubbling beds have been extensively studied by academics. The bubbling regime is characterized by a gross gas bypassing (large bubbles) and therefore a poor gas–solid contact, high gas backmixing, and a low throughput. This regime is not suitable for reactions requiring a high conversion. However, it is well known that most commercial processes operate in the turbulent regime. The turbulent bed has a homogeneous appearance with small bubbles and a good gas–solid

contact [18, 26]. This regime offers the advantage of a good heat transfer, small gas backmixing and bypassing and is suitable for high conversion reactions. In contrast, it suffers the major drawback of a significant particle entrainment. The transition velocities between the different flow regimes depend upon the gas–solid system, the reactor geometry and the operating conditions. The turbulent regime has been characterized in the literature by two velocities: U_c and U_k [19, 20, 21, 22, 23, 24]. U_c has been characterized as the velocity where the pressure fluctuations peak (large bubbles) and U_k the velocity at which they level off after a gradual decrease from U_c due to the breaking up of large bubbles into smaller ones. However, a recent study has shown that U_k is an artifact of the experimental method and that the turbulent regime is only characterized by U_c [25].

3.4.2 Modeling of Fluidized Beds

The modeling effort has been largely devoted in the literature to the bubbling bed using group A or B particles of the classification of *Geldart* [27]. The basic bubbling bed model considers the bed as composed of two phases: a discontinuous phase (dilute phase) made up of gas bubbles and the continuous phase (dense phase or emulsion) between which exists a mass tranfer along the bed. These models are well categorized and presented by *Grace* [28]. The hydrodynamics of bubbling beds differs from that of turbulent beds. The conversion of chemical reactions is less in bubbling beds due to a poor gas–solid contact. Therefore, the correlations used for bubbling beds are

not appropriate to describe the behavior of turbulent beds. The design of commercial reactors tend to ignore the two–phase theory in favor of bubble suppression using baffles and an appropriate fraction of fines ($< 40\ mm$) [17, 26, 29]. Considering the homogeneous appearance of turbulent beds, *van Swaaij* [30] and *Wen* [31] used a piston flow model to describe the hydrodynamics of their reactor. However, it is clear from the results of *Grace* [18] that the conversion is far from being predicted by the plug flow model in the turbulent regime. *Avidan* [26] successfully modeled and scaled up the Mobil Methanol–To–Gasoline (MTG) process using a piston flow model with axial gas dispersion. The exit concentration predicted by this model for a first order reaction is given by:

$$\frac{C}{C_0} = 1 - X = \frac{4q\exp(\frac{Pe}{2})}{P} \tag{3.5}$$

where:

$$P = (1+q)^2\exp(\frac{qPe}{2}) - (1-q)^2\exp(-\frac{qPe}{2}) \tag{3.6}$$

$$q = \sqrt{1+\frac{4k\theta}{Pe}} \tag{3.7}$$

Pe is the Peclet number, k the first order reaction rate constant, θ the mean gas residence time, C the exit concentration and C_0 the inlet concentration.

3.4.3 Gas Mixing

There is no correlation in the literature that can be used to predict the Peclet number which characterizes the axial gas mixing of turbulent fluidized beds. A small pilot

scale $TFB2C$ of 100 mm I.D. and 1 m tall was used for tracer experiments. ^{41}Ar produced in a $Slowpoke$ nuclear reactor by irradiation of ^{40}Ar with thermal neutrons was used as tracer. This radionucleide decays with a short half–life of 1.83 h emitting β^- particles and a characteristic $\gamma - ray(99.2\%)$ of 1.283 MeV that can be detected even in a thick-walled steel pipe [32]. Four scintillation detectors placed along the reactor with a distance of 0.26 m between them were connected to an $ORTEC$ amplification system linked to a multichannel analyzer supported by a $486IBM$ compatible. ^{40}Ar samples of 7 ml were irradiated for 40 minutes and injected into the reactor plenum. The equations for one–dimensional dispersion are:

$$\frac{\partial C}{\partial t} = D_g \frac{\partial C^2}{\partial y^2} - u\frac{\partial C}{\partial y} \tag{3.8}$$

$$C = \frac{c(t)}{\int_0^\infty c(t)dt} \tag{3.9}$$

where D_g is the effective axial gas dispersion coefficient, u the interstitial velocity, y the axial distance, t the time and $c(t)$ the tracer concentration at time t. The Peclet number is defined as:

$$Pe = \frac{1}{N_D} = \frac{uL}{D_g} \tag{3.10}$$

where N_D is called the number of dispersion, and L the distance between two detectors. In terms of the apparent axial dispersion coefficient D_{ax}, the previous equation becomes:

$$Pe = \frac{1}{N_D} = \frac{UL}{D_{ax}} \tag{3.11}$$

where U is the empty column velocity. The Peclet number can be determined by the method of moments [15] or by the method of the transfer function in the real time domain [33]. The latter method has been shown to be more accurate [33]. The number of dispersion N_D and the mean residence time θ are predicted by matching the response curve of the exit detector (subscript 2) to the theoretical response given by:

$$C_{2calc}(t) = \int_0^t C_{1exp}(t) f(t-\varphi) d\varphi \tag{3.12}$$

using the transfer function $f(t)$ and the objective function ψ given below:

$$f(t) = \frac{1}{2\theta\sqrt{\pi N_D \left(\frac{t}{\theta}\right)^3}} \exp\left(-\frac{\left(1-\frac{t}{\theta}\right)^2}{4N_D\frac{t}{\theta}}\right) \tag{3.13}$$

$$\psi = \sqrt{\frac{\int_{t_1}^{t_2} \left(C_{2exp}(t) - C_{2calc}(t)\right)^2 dt}{\int_{t_1}^{t_2} \left(C_{2exp}(t)\right)^2 dt}} \tag{3.14}$$

Two types of particles were used for the study: Fluid Cracking Catalyst (FCC) and sand. Since the attenuation of $\gamma - rays$ is significantly different between a space filled with particles and a particle–free space, the experiment required a lot of solids in the reactor in order to record the first two responses to be compared by the method of the transfer function. Therefore, the PSA catalyst could not be used for the study because the quantity available was small. However, the Archimedes numbers of the FCC particles used for the study and the PSA catalyst were close and the dispersion parameters obtained from the FCC gas mixing study can then be used

for experiments involving the PSA catalyst. The axial gas dispersion coefficients determined by the method of the transfer function are presented in Figure 3.4 for FCC and in Figure 3.5 for sand (70 $mesh$). It is obvious from the curves that the axial dispersion coefficient goes through a maximum as the velocity increases. These maximum velocities correspond to the transition velocity U_c determined by various techniques in our laboratory [25]. Peclet numbers are summarized in table Table 3.2.

3.5 Simulation of a $TFB2C$

Coupling the kinetics of combustion of methane with the plug flow hydrodynamic model with axial dispersion (equat. 3.5, 3.6, 3.7) and using the Peclet from tracer experiments, the conversion of methane is predicted in a small 100 mm I.D. pilot scale $TFB2C$. The Peclet number from the FCC experiment is used in the simulation. In the turbulent regime, a Peclet number of 5 is then used and the number of reaction units N_r is changed by varying the catalyst inventory. Figure 3.6 shows the sensitivity of the prediction with respect to the Peclet number and the limits of conversion predicted by the plug flow and the perfect mixing flow models. The predicted conversion with the axial dispersion plug flow model is quite close to the data reported by Grace [18] in the turbulent regime for the first order decomposition of ozone with a FCC catalyst in a 102 mm I.D. reactor. However, the graph shows that the maximum number of reaction unit that can be achieved in our reactor is

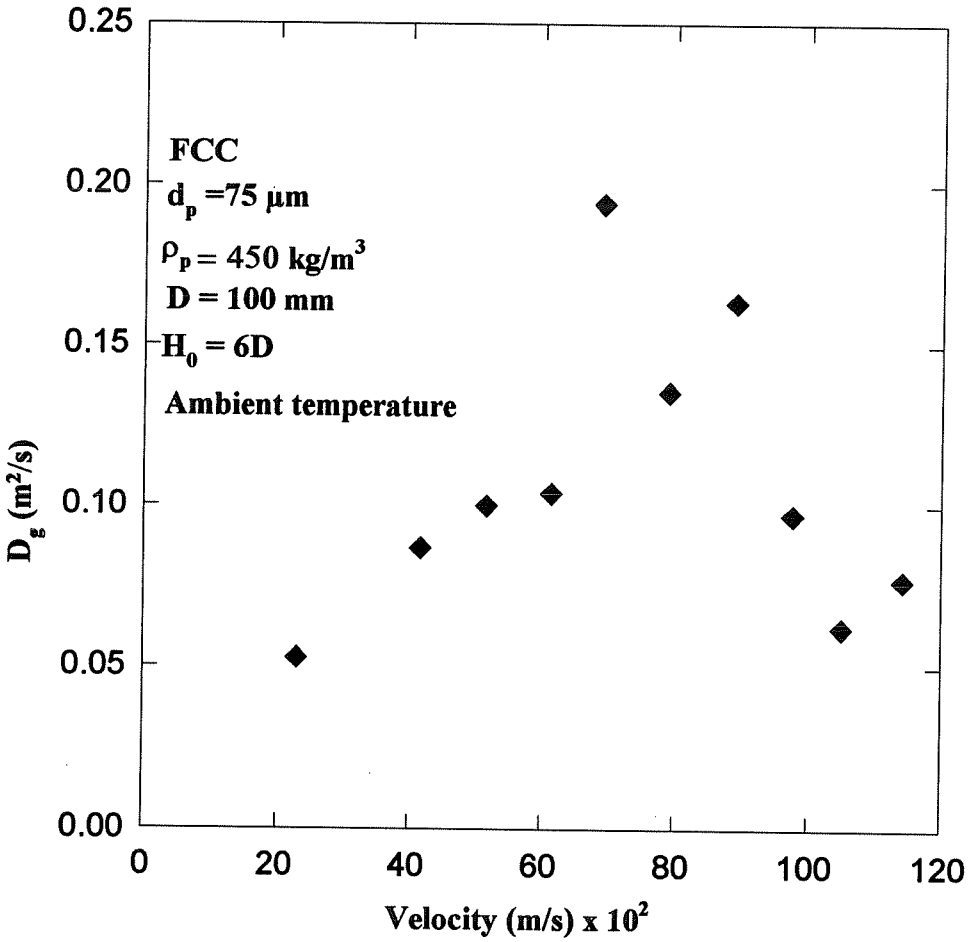

Figure 3.4. Axial dispersion coefficient vs. velocity, FCC particles

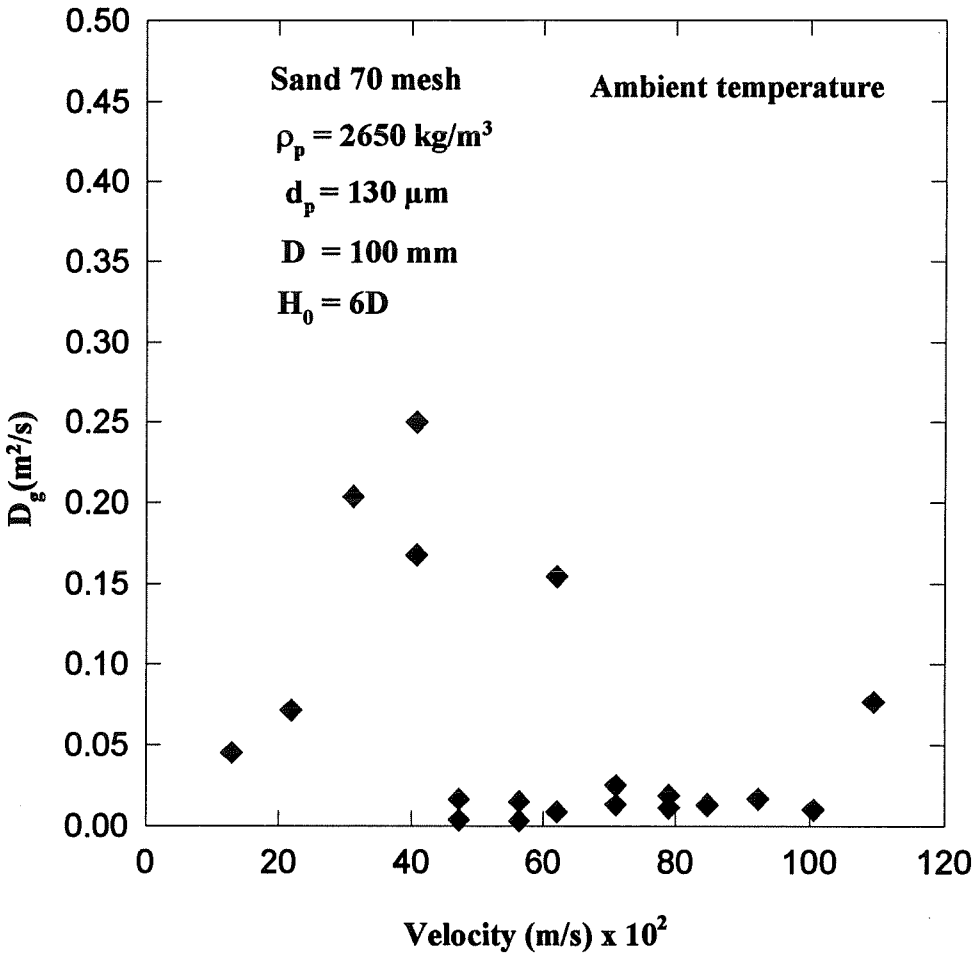

Figure 3.5. Axial dispersion coefficient vs. velocity, Sand particles

Table 3.2. Axial Peclet number. FCC particles and sand (70 $mesh$)

Velocity (m/s)	*Axial Peclet–FCC*	*Velocity (m/s)*	*Axial Peclet–Sand*
0.230	1.32	0.128	1.584
0.417	2.64	0.218	1.42
0.516	2.64	0.311	0.71
0.614	1.61	0.407	1.75
0.691	2.02	0.471	16.5
0.792	2.02	0.563	18
0.892	1.84	0.620	35.
0.977	4.43	0.710	29
1.051	6.78	0.79	28
1.142	6.1	0.848	36
		1.006	54

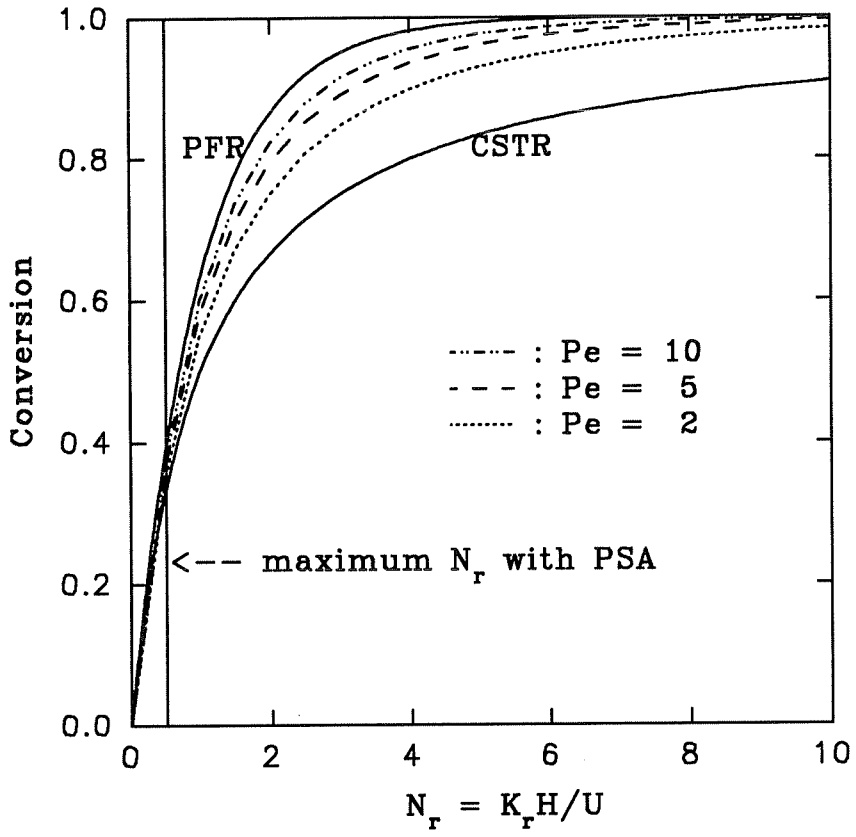

Figure 3.6. Prediction of methane conversion in a $TFB2C$ at different number of reaction units

0.5 and corresponds to a conversion less than 40%. Using a more active catalyst it can be shown [34] that the bed diameter of a 50 kW $TFB2C$ can be of the order of 0.25 m and the diameter of a 500 kW $TFB2C$ of the order of 0.5 m.

3.6 Conclusion

The catalytic combustion of natural gas for heat generation purposes is an advantageous alternative to the conventional gas combustion; the reaction exhibits no flammability limits and an efficient combustion can be performed with a wide range of gas–to–air ratios and without generating NOx. Gas mixing data has been shown to be a valuable tool for the delineation and the characterization of the different flow regimes of fluidized beds. The PSA catalyst is not active enough for turbulent bed use. With very active catalysts, the dimensions of $TFB2C$ are reasonable with respect to the conventional combustors.

Acknowledgement

The financial support of Gaz Métropolitain, Inc. to pursue research in fluidization is gratefully acknowledged.

3.7 References

[1] Yaverbaum, L.H. (1979). Nitrogen Oxides-Control and Removal. Notes Data Corporation N.J.

[2] Williams, C.L.H. (1988). Nitrosation. Cambridge University Press, N.Y.

[3] Leygonie, R. (1989). Effets des oxydes d'azote sur la sant humaine et sur le milieu naturel. Rev.Gen.Therm., 28, 343.

[4] De Soete, G.G. (1989). Les oxydes d'azote. Rev.Gen.Therm., 28, 339.

[5] Perthuis, E. (1989). Revue des techniques de réduction des émissions d'oxydes d'azote au niveau des brûleurs. Rev.Gen.Therm., 28, 374.

[6] De Soete, G.G. (1989). Mécanisme de formation et de destruction des oxydes d'azote dans la combustion. Rev.Gen.Therm., 28, 353.

[7] Veg. Gasinstitut rapport m.t. 89v12 (1989). Dispositif de Combustion catalytique en lit fluidisé pour la génération de vapeur.

[8] Molière, M.; Colas, M.; Freimark, M. (1989). Des émulsions eau/fuel pour réduire les émissions de NOx de turbines à gaz. Rev.Gen.Therm., 28, 428.

[9] De Reydellet, A. (1989). Les mesures de réduction des émissions d'oxydes d'azote en aval du foyer. Rev.Gen.Therm., 28, 453.

[10] Sicardi, S., Specchia, V., and Ferrero, F. (1982). Kinetics of Combustion of Methane with Different Catalysts. Chimica Industriale, 3, 217.

[11] Wise, H., and Quinlan, M. (1986). Elementary Processes in the Catalytic Combustion of Methane. Gas Research Institute Report, Chicago Il.

[12] Jones, D.J. et Salfati, S. (1989). Combustion catalytique et gaz naturel. Rev.Gen.Therm., 28, 401.

[13] Anderson, R.B., Stein, K.C., Feeman, J.J. and Hofer, L.J.E. (1961). Catalytic oxidation of methane. Ind.Eng.Chem., 53, 809.

[14] Marquardt, D.W. (1963). J.Soc.Ind.Appl.Math., 11, (2), 431.

[15] Fogler, S. (1991). Elements of Chemical Reaction Engineering. Prentice hall.

[16] Squires, A.M., Kwauk, M. and Avidan, A. (1985). Fluid Beds: At Last, Challenging two Entrenched Practices. Science, 230, 1329.

[17] Avidan, A. (1982). Turbulent Fluid Bed Reactors Using fine Powder Catalysts. A.I.Ch.E.– CIES Mtg Beijing.

[18] Grace, J.R. (1990). High Velocity Fluidized Bed Reactors. Chem.Eng.Sci., 45, (8), 1953.

[19] Yerushalmi, J. and Kankurt, N.T. (1979). Further Studies of the Regimes of Fluidization. Powder Technol., 24, 187.

[20] Grace, J.R. (1986). Fluidized Beds as Chemical Reactors. Chap. 11 in "Gas Fluidization Technology". Edited by Geldart, D. Wiley, London, 285.

[21] Cai, P., Yin, Y., Yu, Z.Q. and Qi, P.Y. (1987). In "Proceedings of the International Symposium on Multiphse–Flows". Hangzhou, China, 221.

[22] Cai, P., Chen, S.P., Jin, Y. and Wang, Z.W. (1989). Effect of Operating Temperature on the Transition from Bubbling to Turbulent Fluidization. A.I.Ch.E Symp.Ser., 37.

[23] Sun, G. and Chen, (1989). In "Fluidization VI". Edited by Grace, J.R., Shemilt, L.W. and Bergougnou, M.A. Engineering Foundation, 33.

[24] Mori, S., Hashimoto, O., Haruta, T. and Yamada, I. (1989). In "Fluidization VI". Edited by Grace, J.R., Shemilt, L.W, and Bergougnou, M.A. Engineering Foundation, 49.

[25] Chehbouni, A., Chaouki, J., Guy, C. and Klvana, D. (1992). Characterization of the Flow Transition Between Bubbling and Turbulent Fluidization, A.I.Ch.E.J., submitted.

[26] Avidan, A. and Edwards, M. (1986). Modeling and Scale up of Mobil's Fluid–bed MTG Process. In "Fluidization V". Edited by Ostergoard, K. and Sorenson, A. Engineering Foundation, N.Y., 457.

[27] Geldart, D. (1973). Types of Gas Fluidization. Powder technol., 7, 285.

[28] Grace, J.R. (1986). Fluid Beds as Chemical Reactors. In "Gas Fluidization Technol.". Edited by Geldart, D. Wiley Chichester, U.K.

[29] Bergougnou, M.A. and Kunii, D. (1979). Design Aspects and Research Needs for Commercial Fluidized Bed Reactors. Presented at the NSF Fluidization Workshop, RPI, N.Y.

[30] van Swaaij, W.P.M. (1978). The Design of Gas-solids Fluid Bed and Related Reactors. ACS Symp. Ser., 72, 193.

[31] Wen, C.Y. (1984). Flow regimes and Flow models for fluidized Bed Reactors. In "Recent Advances in the Engineering Analysis of Chemically Reacting Systems". Edited by Doraisamy, L.K. Wiley Eastern, New Dehli, 256.

[32] Kolar, Z., Thyn, J., Martens, W., Boelens, G. and Korving, A. (1987). The Measurement of Gas Residence Time Distribution in a Pressurized Fluidized–bed Combustor using ^{41}Ar as Radiotracer. App.Radiat.Isot., 38, (2), 123–127. Int.J.radiat.Appl.Instrum. part A.

[33] Wakao, N. and Kaguei, S. (1982). Heat and Mass Transfer in Packed Beds. Gordon and Breach Science Publishers.

[34] M. Foka, Chaouki, J., Guy, G. and Klvana, D. (1991). Dimensionnement optimal d'un générateur de chaleur sans NOx. Rev.Gen.Therm., 352, 225.

CHAPTER 4

NATURAL GAS COMBUSTION IN A CATALYTIC TURBULENT FLUIDIZED BED

M. Foka, J. Chaouki*, C. Guy & D. Klvana

Chem. and Engng Sci. (accepted)

*To whom correspondence should be addressed

Abstract

Catalytic fluidized bed combustion of natural gas is shown to be an emerging technology capable of meeting all environmental constraints as far as nitrogen oxides and carbon monoxide are concerned. This technology uses powder catalysts in the turbulent flow regime where the gas–solid contact is optimal so as to maintain a high combustion efficiency. In fact, the catalytic combustion carried out in both the bubbling and the turbulent regimes at $450 - 500°C$ shows that the turbulent regime is more favorable. A single phase plug flow model with axial dispersion is shown to fit satisfactorily the data obtained at $500°C$ where the combustion efficiency is very good. A self–sustained combustion was achieved with a mixture of 4% methane at around $500°C$ with a complete conversion of methane and a zero emission of NOx and CO.

Keywords

NOx, Turbulent fluidized bed catalytic combustor, self–sustained catalytic combustion, fluid bed hydrodynamics.

4.1 Introduction

The nitrogen oxides contribution to air pollution is well established and very stringent regulations have been imposed on their emissions in various industrial nations. They participate in the greenhouse effect, the reduction of the stratospheric ozone layer, the oxidic smogs, the acid rains etc... In direct drying processes, nitrogen oxides (NOx) are known to form carcinogenic compounds in foodstuffs. Thermal NOx are generated in conventional natural gas combustors where the flame temperature is usually above $1200°C$. At temperatures below $800°C$, no NOx are formed. The combustion of natural gas at such temperatures can be considered clean but is impossible in the homogeneous phase at low fuel concentrations. Low–temperature catalytic combustion of natural gas can be performed in a fixed bed reactor. However, the rise in the bed temperature usually leads to the formation of hot–spots, the deactivation of the catalyst and even causes homogeneous phase combustion. Furthermore, for very low gas concentrations, the autothermicity of a fixed bed is difficult to achieve because of the "creeping phenomenon" in the reaction zone which consists of the movement of the reaction front with time towards the outlet of the reactor.

Flow reversal fixed bed (*Chaouki* et *al.*, 1994) and fluidized bed reactors are more appropriate for the combustion of natural gas which requires complete conversion. The periodic change in the flow direction of the reaction feed in flow reversal

reactors counters the "creeping phenomenon" by maintaining the heat front within the catalytic bed and a stable self–sustained combustion can be achieved. The control of the rate of combustion is flexible with fluidized beds and the reaction can be carried out beyond the flammability limits. Moreover, fluidized beds operate isothermally and do not develop hot-spots.

Various hydrodynamic regimes are observed in fluidized beds but the turbulent regime appears to be the most suitable for a complete combustion of natural gas. Turbulent fluidized beds have an overall homogeneous appearance and high conversions are achieved due to a more intimate gas–solid contact (*Chehbouni*, 1993). The success of the catalytic fluidized bed combustion of natural gas also depends on the nature of the catalysts used; they are the battle horse of this emerging combustion technology. They must be robust and effective. A complete combustion of methane, the main component of natural gas, can be achieved only in the presence of active catalysts to produce only water and carbon dioxide. Oxide–supported platinum and palladium catalysts have so far proved to be of excellent activity for this reaction.

The performance of Turbulent Fluidized Bed Catalytic Combustors ($TFB2C$) can be predicted by coupling the hydrodynamic model describing the flow behavior of gas through the bed and the kinetics of combustion of the fed fuel. The scale–up of such combustors is not straightforward and it is crucial to fully characterize the gas hydrodynamics.

The aim of the present work is (1) to carry out the combustion of methane in a

$TFB2C$, and (2) to combine the kinetics and the hydrodynamics data to model the reactor behavior.

4.2 Catalyst Characterization

4.2.1 Physical properties

An industrial catalyst from $PROCATALYSE$ Pd/Al_2O_3 (0.2 wt % in palladium) of 2–4 mm diameter referenced as $PC263$ was ground and sieved in a mechanical agitator. The cumulative weight fractions are presented in figure Figure 4.1. The mean particle diameter calculated by the formula

$$d_p = \frac{1}{\sum(X_i/d_{pi})} \tag{4.1}$$

was 196 μm. The minimum fluidization void fraction ϵ_{mf} was 0.48 and the bulk density 570 kg/m^3. A pure aluminum oxide of 105 μm in mean diameter and of 3970 kg/m^3 density from *Aldrich Chemical Company* was also used in the hydrodynamic studies.

4.2.2 Transition velocities

Since the emergence of the art of fluidization in the twenties, tremendous efforts have been deployed in the modeling of the fluidized bed on the bench and pilot scales for scale–up or for learning purposes. An excellent history of fluidization technology up

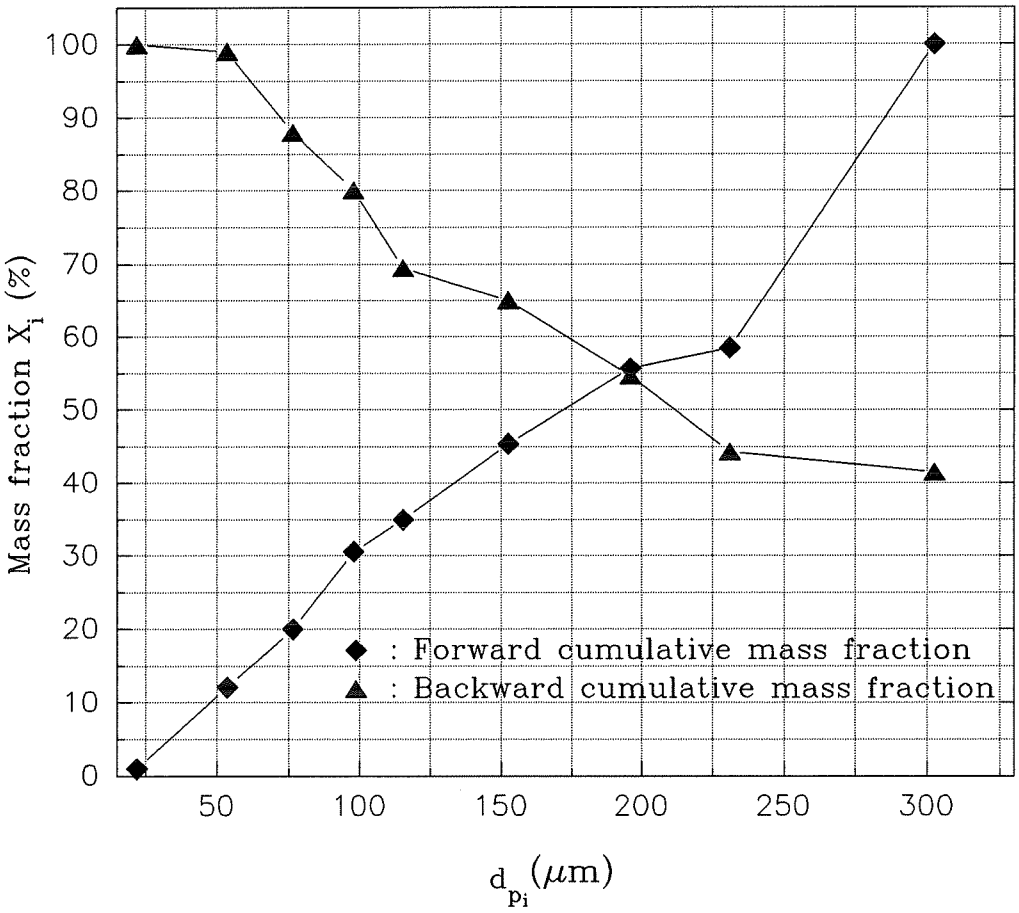

Figure 4.1. Determination of the mean particle diameter

until 1985 is presented by *Squires* et *al.* (1985). Historical highlights and industrial applications of fluid bed technology are also presented by *Kunii* and *Levenspiel* (1991).

The bubbling bed is observed after the minimum fluidization velocity (U_{mf}) is reached and is characterized by the passage of gas bubbles through the bed of particles. As the gas velocity increases the bubble coalescence leads in some systems to a bubble size of the order of the column diameter and the regime is known as the slug flow regime. The turbulent regime appears when the rate of bubble splitting exceeds the rate of bubble coalescence and the bubble diameter becomes very small as the system proceeds into a full scale turbulent regime. The transition from bubbling or slugging to turbulent fluidization has been extensively studied in the literature and has been characterized by two velocities (U_c, U_k) (*Kehoe* and *Davidson*, 1971; *Grace*, 1986; *Mori* et *al.* , 1989) determined with pressure transducers, capacitance probes, or by visual means. The transition from the turbulent fluidized bed to the circulating fluidized bed is characterized by the velocity U_{tr} (*Jiang* and *Fan*, 1991; *Horio* et *al.*, 1992). A comprehensive study of the state of the art is presented by *Chehbouni* et *al.* (1994a,1994b) and rules out the existence of U_k. The turbulent fluidization regime is characterized by pressure fluctuations of low amplitude and of high frequencies (*Lanneau*, 1960; *Kehoe* and *Davidson*, 1971), and of bubbles of small diameter with a high relative density (percentage of particles). At the prevailing velocities, the entrainment of particles is substantial and external reverse

flow cyclones are required. The formation of particle aggregates with a higher density than individual particles limits the elutriation of fines which remain in the freebaord (*Bolthrunis*, 1989; *Yerushalmi* and *Avidan*, 1985) and the bed surface is not well defined as in the bubbling bed regime. The pressure effect is similar to that of velocity in the sense that the bed is more uniform at high pressures than at low pressures (*Cai* et *al.*, 1989). Gas backmixing which may be detrimental to high conversion and selectivity in bubbling beds is low in turbulent beds.

The minimum fluidization velocity of the catalyst was studied in a glass column of 50 mm ID by monitoring the pressure drop through the bed with a $FCO14$–micromanometer and was estimated to be 0.043 m/s. The pilot scale $TFB2C$ presented in Figure 4.2 was used to characterize the transition velocity (U_c). It has a diameter of 100 mm and is 1.6 m tall including the disengaging section. Two probes connected to a differential pressure transducer were located 50 mm above the porous distributor for the first probe and the second was located 2D above the first one. Pressure fluctuations in the bed were monitored with a $P.C$ connected to an acquisition interface at a rate of 50 readings per second and were analyzed in terms of the standard deviation. The reverse flow cyclone was highly efficient for the particles used. Nevertheless, a bag filter was placed on the exit line after the cyclone for security. Experiments were carried out with both pure alumina and the $PC263$ catalyst at ambient temperature and with alumina at 500°C over a wide range of superficial gas velocities. Above 1 m/s particle entrainment and elutriation were

substantial and particle recirculation from the cyclone was detected by the change in temperature in the recirculation pipe.

The experimental and predicted values of U_c and U_{tr} are presented in Table 4.1. At $500°C$, U_c is 5–10% higher than at ambient temperature. Most works on transition velocities (U_c, U_{tr}) have been done only at ambient temperature. One of the rare exceptions is the work of *Cai* et *al.* (1989) where the temperature and pressure effects on transition to turbulent fluidization were investigated. Their results show a decrease in the amplitude of pressure fluctuations and an increase in U_c at high temperatures, this is similar to what is observed in our experiments.

4.2.3 Kinetic Evaluation of the $PC263$ Catalyst

The kinetic study was carried out in a tubular fixed bed reactor with a gas mixture containing 3% of methane and is detailed elsewhere (*Chaouki* et *al.*, 1994). The ignition temperature was around $275°C$. Since the study used an excess of air, the rate of combustion in terms of the concentration of methane was expressed as

$$R_{CH_4} = K_0 \exp\left(-\frac{E_\theta}{T}\right) C_{CH_4} \tag{4.2}$$

where K_0 is the preexponential factor evaluated to be $(2 \pm 1.6 \times 10^{-5}) \times 10^8$ and E_θ the activation energy to be $(11.1 \pm 5 \times 10^{-3})$ kK.

Table 4.1. Experimental and predicted transition velocities

Particle	$U_c(m/s)$		U_{tr} (m/s)
	$25°C$	$500°C$	$25°C$
Aluminum	0.97	1.05	–
oxide	1.05 *Chehbouni*[1993]	1.18 *Cai et al.* [1989]	2.4 *Chehbouni*[1993]
PC263	1.	–	–
catalyst	0.89 *Cai et al.* [1989]	1.07 *Cai et al.* [1989]	–
	1.13 *Chehbouni*[1993]	–	2.6 *Chehbouni*[1993]

4.3 Fluid Bed Modeling and Design

4.3.1 Reactor models

The performance of fluid beds as chemical reactors is directly dependent upon the particle characteristics used and upon the regime of fluidization. Research on modeling fluidized bed processes in academia has put emphasis on bubbling flow regime with group B particles at the expense of high–velocity regimes with group A powders which are common practice in industry. Although the number of bubbling bed models is considerable in the literature, the progress in high–velocity, especially in turbulent fluidized bed modeling has remained very modest (*Grace*, 1990).

The two–phase theory of fluidization considers the fluid bed as a two–phase system consisting of a discontinuous phase (dilute phase) made up of bubbles and of a continuous phase (dense phase or emulsion phase) made up of a dense mixture of solid particles and air with mass transfer occurring between the two phases. Most bubbling bed models are based on this theory and others consider a third phase which is a cloud around the bubble. All these models can be classified only in two groups: the two–phase models and the bubbling bed models. The former consider the dilute phase as a continuous system and the latter consider it as a discrete set of bubbles whose diameters are the key parameter in these models. Most of these models are derived or simply summarized by *Kunii* and *Levenspiel* (1991) and *Grace* (1986). The sensitivity of bubbling bed models to the bubble diameter is very crucial as suggested

by the data presented by *Levenspiel* (1993) where the conversion in a chlorination process decreases from 95% to 32% as the bubble diameter increases. Bubbling bed models have been referred to as learning models, and the two–phase models that incorporate solid fractions, mixing parameters and interchange coefficients and which can be used for modeling and scale–up purposes as predictive models (*Avidan* and *Edwards*, 1986). Even though some of these models may predict high conversions of the order of those achieved in turbulent beds, their descriptions do not reflect the physical picture of the turbulent bed (*Avidan*, 1982).

The apparent homogeneity is the key to the success of commercial units operating in the turbulent regime. A simple plug flow model has been used to describe the turbulent bed hydrodynamics (*van Swaij*, 1978). However, despite the homogeneous appearance of the bed, the level of conversion is usually far from that of a plug flow reactor. *Avidan* (1982) and *Wen* (1984) suggest the use of axial dispersion to correct the discrepancy.

4.3.2 Gas Mixing Experiments

The axial dispersion coefficient D_g can be derived from RTD measurements. Gas *RTD* experiments usually involve a gas tracer that can be sampled and analyzed at different locations in the bed. This type of sampling can affect the bed hydrodynamics and the measured gas concentration at a given bed level may not be representative of the whole bed section.

The author's experiments consisted of using a radioactive nonadsorbing gas tracer (^{41}Ar) obtained by irradiation in a *Slowpoke* nuclear reactor of ^{40}Ar with thermal neutrons. A sample of 7 ml of argon was injected into the reactor plenum and the signal responses were detected at different points above the distributor by $NaI(Tl)$ detectors positioned outside the reactor. The ^{41}Ar decays with a half–life of 1.83 h and emits β^- particles and a characteristic $\gamma - ray$ (99.2%) of 1.283 Mev able to traverse a thick stainless steel wall without being affected. The photons arriving at the detector generate a signal that is amplified and sent through a multichannel analyzer to a personal computer. The first detector is positioned 250 mm above the porous distributor and the mean distance between two detectors is 260 mm. Only two detectors were used in these experiments. The method of analysis of the experimental results is presented elsewhere (*Foka* et *al.*, 1993). The experimental results obtained in the turbulent regime at various temperatures are shown in Table 4.2 in terms of the Peclet number,

$$Pe = \frac{uL}{D_g} \tag{4.3}$$

the axial dispersion coefficient, and the mean bed porosity estimated from the mean residence time. Two aspects of these results are very important: the values of the mean porosity which consistently fall within the range of values reported in the literature for turbulent beds (0.6–0.9) (*Grace*, 1990), and the values of the axial dispersion coefficient (of the order of 0.2 m^2/s) which remain low with respect to the

Table 4.2. Experimental gas Peclet number at high temperatures with the $PC263$ catalyst

$U(m/s)$	$T(°C)$	*Calculated Porosity*	Pe	$D_g(m^2/s)$
1.09	314	0.73	3.6	.11
1.07	305	0.82	2.4	.14
1.09	400	0.67	2	.21
1.09	402	0.88	1.6	.20
1.13	500	0.86	2.4	.14
1.24	494	0.77	3.6	.12

values reported in the bubbling bed (order of 0.6 m^2/s) (*Jinghai* and *Weinstein*, 1989).

4.4 Catalytic Combustion in the Fluidized Bed Reactor

4.4.1 Experimental Setup and Procedure

The experimental setup presented in Figure 4.2 was also equipped for the sampling and analysis of reaction products. Sampling probes were placed along the reactor centerline with their tips protected from particle clogging by Nupro filters in ceramic material. The reactor wall was made up of stainless steel $SS310$ able to withstand high temperatures. The probes were connected to the gas chromatograph by a 1 mm ID tube in stainless steel and the samples were withdrawn with a variable pressure vacuum system. Type-K thermocouples were also located along the centerline to monitor the temperature profile. The signal from the differential pressure transducer was used to control the level of particles in the reactor by monitoring pressure fluctuations every 30 seconds. The inlet gas was preheated by an electric resistance of 6 kW and a second resistance of 2.5 kW was directly placed around the reactor external wall within a jacket insulated with Kaowool ceramic fibers from *Thermal*

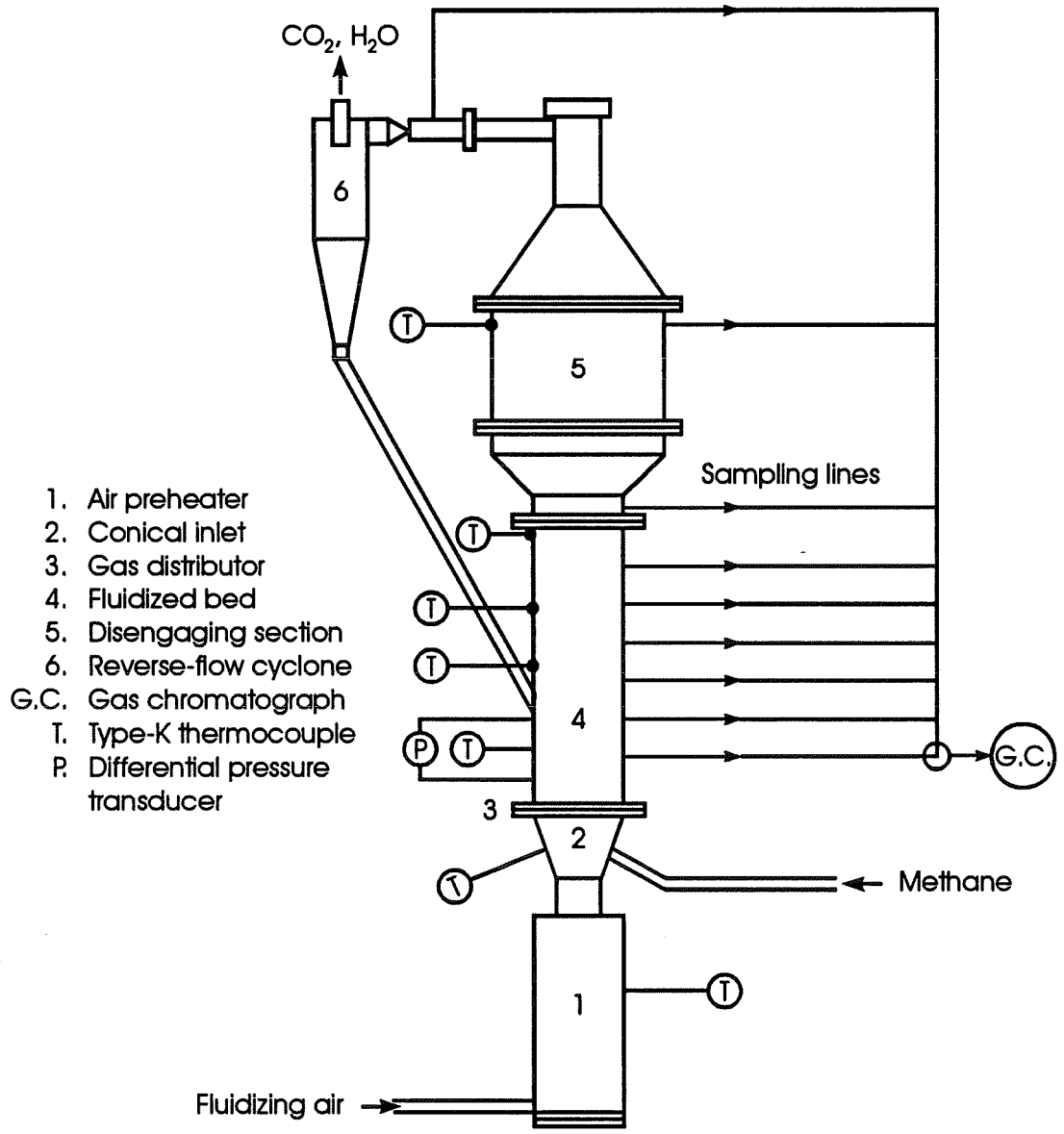

Figure 4.2. Schematic diagram of experimental Atmospheric Turbulent Fluidized Bed Combustor

Ceramics Corporation. A blower was used to cool the reactor by sending air through the jacket. The two resistances and the blower were controlled by a numerical PID controller through an acquisition board. The gas distributor with a porosity of 10 μm and made of Inconel 600 was a product of *Mott Metallurgical Corporation.* An initial bed height H_0 of 2D was used in all experiments. A gas mixture of 3% methane was premixed in the reactor plenum using steel filings and was used in a series of experiments at three different temperatures $(450, 475, 500°C)$ and at two velocities 0.77 m/s and 1.1 m/s, in the bubbling and turbulent regimes respectively. The bed temperature control was achieved within ± 2 to $\pm 4°C$ The bed temperature profile in the turbulent regime shows various small peaks which result from the recirculation of particles at lower temperature to the bed (Figure 4.3a). Figure 4.3b shows the axial temperature profile in the reactor in the turbulent regime. The expanded bed height can be approximated from this profile. The temperature drop between the bed and the exit is due to the fact that the disengaging section was not insulated. An example of the conversion profiles obtained from these experiments is shown in Figure 4.4.

4.4.2 Modeling the Turbulent Bed Experiments

Figure 4.5 shows the experimental data in the turbulent regime in terms of conversion versus the number of reaction units. It is obvious that the conversion is higher than in the bubbling regime (Figure 4.6) at the same number of reaction units. It is also

noted that the combustion efficiency is higher at 500°C than at lower temperatures. In order to model this reactor with a dispersive model, the number of reaction units (N_r) needs to be between 2.5 and 10 where the model is very sensitive. This model fits quite well the data obtained at 500°C in a wide range of number of reaction units with a Peclet number of 2 obtained by averaging the values shown in Table 4.2 between 400 and 500°C at 1.09–1.13 m/s. The data in both regimes and at various temperatures show that the combustion process which requires a high conversion needs to be carried out in the turbulent regime and can be modeled with a simple homogeneous phase dispersive model. It is important to note that the purpose of a real catalytic combustion of natural gas is to achieve a total conversion and for a given power and a desired temperature level, the mass of catalyst needed depends on the inlet composition. Therefore, the model for the process needs to be derived from data showing a high efficiency of combustion.

4.4.3 Self-sustained Combustion

In the bubbling regime, a mixture of 4% of methane was used and the conversion was 100% above 500°C. The system operated at 0.75–0.8 m/s and the maximum temperature was 540°C. No NOx and no carbon monoxide were recorded with a $LandCombus$ device (sensitivity 1ppm). All the readings were between 0 and 1ppm. At these conditions 2.9 kW were produced by the reaction and were able to sustain the reacting system. The ratio of the power required to raise the temperature of the

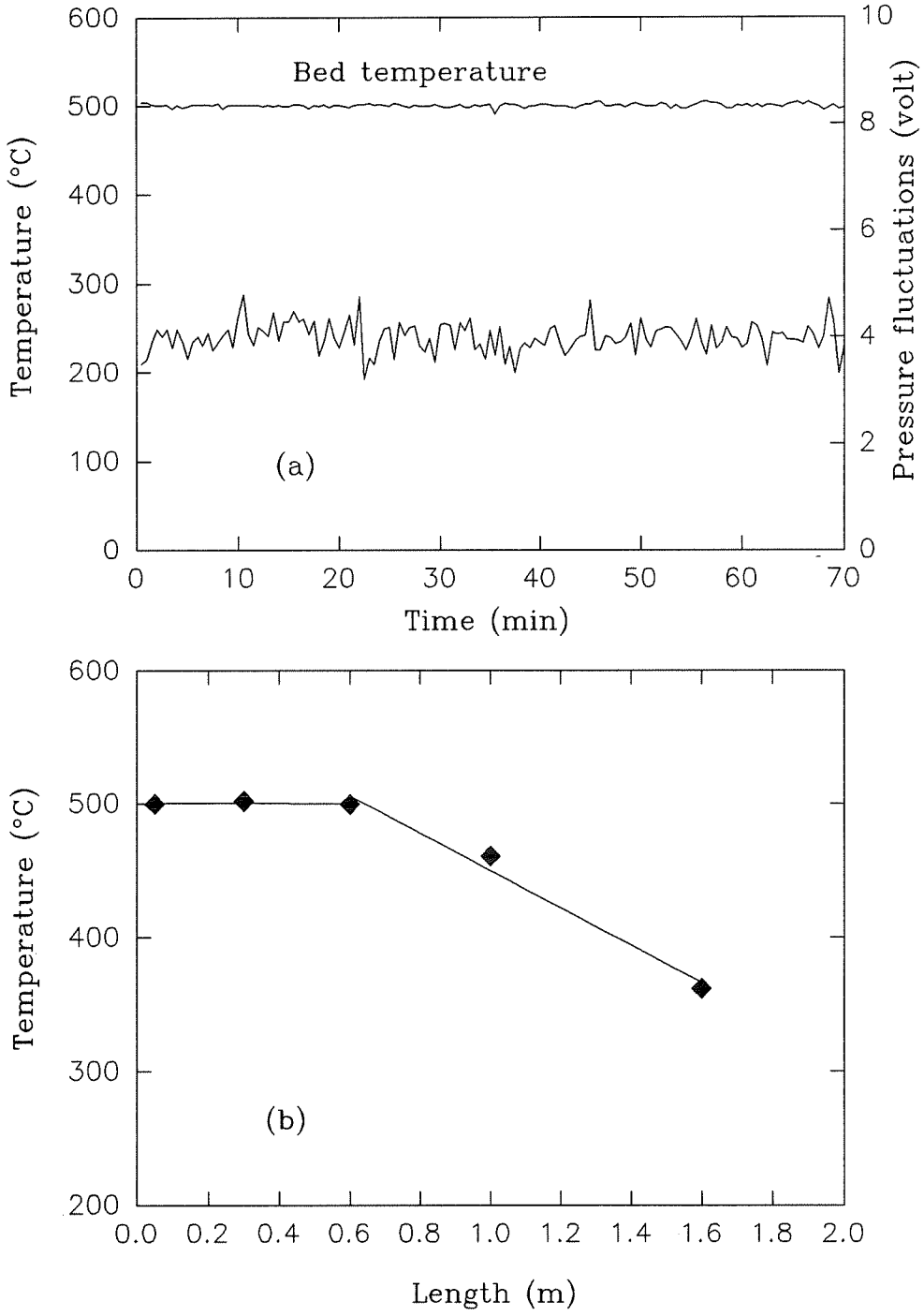

Figure 4.3. Temperature control and temperarure axial profile in the turbulent flow regime at 500°C

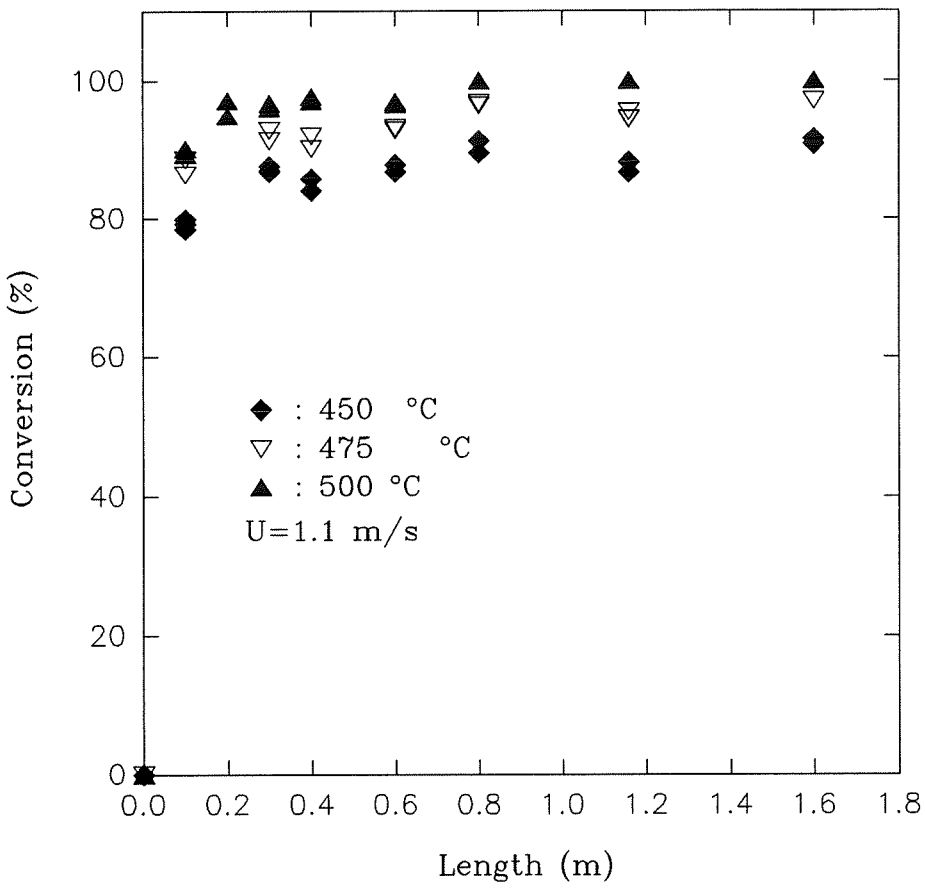

Figure 4.4. Methane conversion profile in the turbulent flow regime at various temperatures

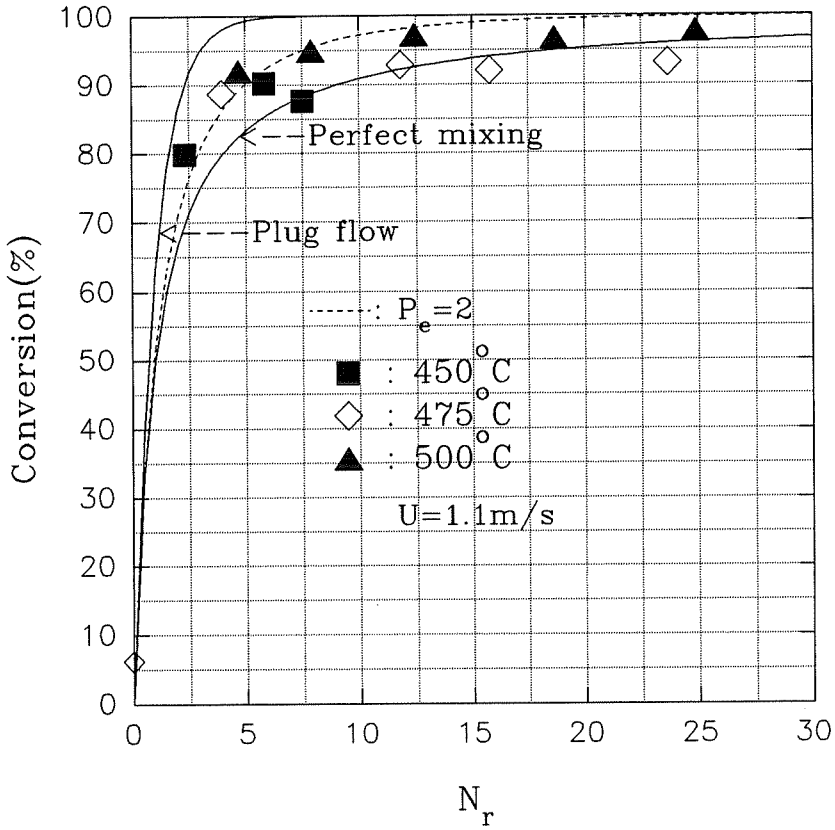

Figure 4.5. Predicted and observed methane conversion in the turbulent flow regime for high reaction rates

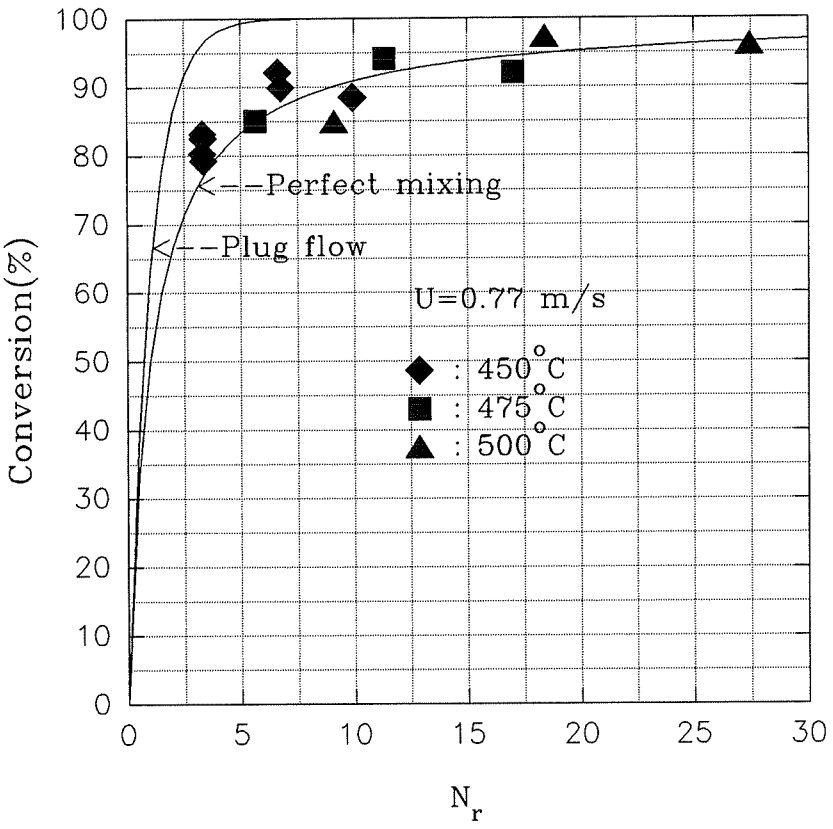

Figure 4.6. Predicted and observed methane conversion in the bubbling flow regime for high reaction rates

gas mixture to the power generated by the reaction was 0.077 in the bubbling bed and 0.074 in the turbulent bed. A temperature buildup occurred in the reactor with time. This suggests that a catalytic combustion commercial process operating in this regime will need a control system based on the gas flow rate instead of an external power source as we implemented for the kinetic study.

In the turbulent regime a power of 4.6 kW was generated and no pollutants (NOx or CO) were recorded. The system was operated at 1.1 to 1.2 m/s using a mixture of 4% of methane. The bed temperature profile showed sporadic peaks as the elutriated particles were recycled back into the reactor. This profile was more irregular than the one obtained in the bubbling regime where no particles were elutriated from the disengaging section.

It is clear from these experiments that in the turbulent regime the power generated by the reaction is higher than in the bubbling regime at a lower temperature.

4.5 Conclusion

A new combustion process was implemented using a turbulent fluidized bed technology. The transition velocity of the industrial catalyst used was determined in a pilot scale $TFB2C$ by monitoring pressure fluctuations in the bed with a differential pressure transducer at ambient temperature and at $500°C$. Gas mixing was studied with a radioactive tracer monitored with two $NaI(Tl)$ scintillation detec-

tors positioned outside the reactor, below the bed surface and hooked to a PC. A dispersive plug flow model was used in the turbulent regime to fit the data. The catalytic combustion of methane was carried out with a mixture of air and methane and the methane–to–air ratio was 3% for the kinetic study and 4% for self–sustained experiments. The conversion of methane was obtained by probe sampling and GC analysis. The pressure in the bed was atmospheric and the temperature was varied from 450 to 500°C. The conversion was predicted using a plug flow model with axial dispersion at 500°C where the reaction efficiency was high.

The parameters obtained in this study were used to estimate the optimal operating conditions and the bed diameter of a combustor that could generate 50 kW. Typically, with an inlet mixture containing 5% of methane, an initial bed height of 2D, and when the gas velocity is 1.5 m/s, a minimum bed diameter of 240 mm is required at a temperature of 500°C to achieve a complete combustion.

Acknowledgement

The financial support of Gaz Métropolitain, Inc. to pursue research in fluidization is gratefully acknowledged.

4.6 References

Avidan, A. (1982). Turbulent Fluid Bed Reactors Using Fine Powder Catalysts. A.I.Ch.E-CIESC Mtg Beijing, 411–423.

Avidan, A. and Edwards, M. (1986). In "Fluidization V". Modeling and Scale–up of Mobil's Fluid-bed MTG Process. Edited by Ostergoard, K. and Sorenson, A. Engineering Foundation, New York. 456–464.

Bolthrunis, C.O., May (1989). An Industrial Perspective on Fluid Bed Reactor Models. Chem. Engng Progr., 51–54.

Cai, P., Chen, S.P., Jin, Y. and Wang, Z.W. (1989). Effect of Operating Temperature on the Transition From bubbling to Turbulent Fluidization. A.I.Ch.E Symp.Ser., 37–43.

Chaouki, J. Guy, C., Sapunzhiev, C., Kusohorsky, D. and Klvana, D. (1994). Combustion of Methane in a Cyclic Catalytic Reactor. ACS Symp. meeting, 13–18 March, San Diego.

Chehbouni, A. (1993). Frontières et structures du lit fluidisé turbulent. Ph.D. thesis, Ecole Polytechnique, Montréal.

Chehbouni, A. Chaouki, J. Guy, C. and Klvana, D. (1994a). Characterization of the Flow Transition Between Bubbling and Turbulent Fluidization. IEC J., (accepted).

Chehbouni, A., Chaouki, J., Guy, C. and Klvana, D. (1994b). Effets de differents paramètres sur les vitesses de transition de la fluidisation en régime turbulent. Can.J.Chem.Engng, (accepted).

Foka, M., Chaouki, J., Guy, C. and Klvana, D. (1993). Catalytic Combustion of Natural Gas in a Turbulent Fluidized Bed Reactor. 12th Inter.Confer. on Fluidized Bed Combustion, 9–13 May, San Diego, ASME, **1**, 179–184.

Grace, J.R. (1986). Chap. 11 in "Gas Fluidization Technology". Fluidized Beds as Chemical Reactors. Edited by Geldart, D. Wiley, London. 285.

Grace, J.R. (1990). High Velocity Fluidized Bed Reactors. Chem.Engng Sci., 45, 1953.

Horio, M., Ishii, H. and Nishimuro, M. (1992). On the Nature of Turbulent and Fast Fluidized Beds. Powder Technol., 70, 229.

Jiang, P.J. and Fan, L.S. (1991). Regime Transition in Gas–Solids Circulating Fluidized Beds. AIChE Meeting, Los Angeles, Paper #101e.

Jinghai, Li, and Weinstein, H. (1989). Experimental Comparison of Gas Backmixing in Fluidized Beds Across the Regime Spectrum. Chem.Engng Sci., 44, 1697.

Kehoe, P.W.K. and Davidson, J.F. (1971). Continuously Slugging Fluidized Beds. Inst.Chem.Engng Symp.Ser., 33, 97.

Kunii, D. and Levenspiel, O. (1991). Fluidization Engineering, second edition. Butterworth– Heinemann, New York.

Lanneau, K.P., 1960, *Gas–solids Contacting in Fluidized bed.* Trans.Inst.Chem.Eng, 38, 125.

Levenspiel, O. (1993). Anomaly Hunters. Trans.IChemE, 71, Part **A**. 629–636.

Mori, S., Hashimoto, O., Haruta, T. and Yamada, I. (1989). Fundamentals of Turbulent Fluidized Catalytic Reactor. Edited by Grace, J.R., Shemilt, L.W. and Bergougnou, M.A. Engineering Foundation, New York, 49.

Squires, A.M., Kwauk, M., Avidan, A. (1985). Fluid beds: At last challenging two entrenched practices. Science, 230, 1329.

van Swaij, V.P.M. (1987). The Design of Gas–solids Fluid Bed and Related Reactors. ACS Symp.Ser., 72, 193.

Wen, C.Y. (1984). Flow regimes and Flow models for Fluidized Bed Reactors. In "Recent Advances in the Engineering Analysis of Chemically Reacting Systems". Edited by Doraisamy, L.K. Wiley Eastern, New Dehli, 256.

Yerushalmi, J. and Avidan, A. (1985). High–velocity Fluidization. Chap. 7 in "Fluidization". Edited by Davidson, J.F., Clift, R. and Harrison, D. Academic Press, London, 226.

CHAPTER 5

GAS PHASE HYDRODYNAMICS OF A GAS-SOLID FLUIDIZED BED

M. Foka, J. Chaouki*, C. Guy & D. Klvana

Can. J. of Chem. Engng (submitted)

*To whom correspondence should be addressed

Abstract

Transient gas mixing tests in a gas–solid fluidized bed are analyzed with a dispersive plug flow model from the bubbling to the turbulent regime, and with the two–phase model of *van Deemter*. It is shown that dispersion fluctuations can also be used besides pressure fluctuations or capacitance probes to characterize the transition between the bubbling or the slugging regime and the turbulent regime. Furthermore, the gas Peclet number in the turbulent regime is correlated in terms of the operating parameters, the geometric characteristics and the particles properties as:

$$Pe = 7.10^{-2} Ar^{0.32} \delta^{-0.4}$$

The cross–flow mass transfer coefficient α_{12} of the two–phase model of *van Deemter* in the bubbling and the turbulent regimes is correlated in terms of the height of a transfer unit as:

$$\frac{U}{\alpha_{12}} = 0.613 Sc^{-0.37}$$

The parameters from both correlations are coupled with the kinetics of an industrial catalyst to model the performance of a catalytic combustor.

Keywords: Gas mixing, hydrodynamics, axial gas dispersion fluctuations

5.1 Introduction

The performance of gas–solid fluidized beds used as chemical reactors is strongly dependent on the prevailing flow regime in the bed. Gas mixing has been extensively studied in the literature especially in the bubbling regime (*Handlos* et *al.*, 1957; de *Groot*, 1967; de *Vries* et *al.*, 1972; *van Deemter*, 1980; *Li* and *Weinstein*, 1989, etc...). Gas mixing parameters can be used to model and scale–up fluidized bed processes (*Avidan*, 1986). However, a few experiments have been reported in the turbulent fluidization regime (*Li* and *Wu*, 1990) and no reliable correlations exist in the literature for the prediction of mixing parameters. This is in part due to the lack of standardization of the measurement procedure and of the method of analysis of residence time distribution (*RTD*) data. *Li* and *Weinstein* (1989) and other workers have shown a strong radial gradient in tracer concentration during gas backmixing experiments. This fact throws doubt about the measurement method consisting of sampling the tracer at one or two points in the bed and considering the derived parameters as representing the reality of the entire bed section. Moreover, a pseudo–steady state diffusion equation has been used to estimate the gas dispersion (*Cankurt* and *Yerushalmi*, 1978; *Li* and *Weinstein*, 1989), but may be misleading in analyzing a dynamic system. There is some evidence in the literature that the dispersion in fluidized beds may vary while operating at almost the same conditions (*van Deemter*, 1980; *Foka* et *al.*, 1993). It is well known that the dispersion of gas

in a fluidized bed is due to the gas velocity distribution. Since this distribution is chaotic by nature, the spread in RTD experiments must be expected to be chaotic. Furthermore, it has been shown recently that a fluidized bed is a deterministic chaotic system (*Daw* et *al.*, 1990; *Schouten* and *van den Bleek*, 1991). This suggests that the fluctuations of the dispersion are not random but deterministic and can still be a useful tool for the characterization of a fluidized bed system.

The purpose of this study was (1) to estimate the global dispersion parameters between two sections of the bed at different experimental conditions without disturbing the hydrodynamics during the measurements, (2) to correlate the Peclet number data in the turbulent regime where most commercial plants operate and the mass–transfer data in the bubbling and the turbulent regimes, (3) to use the hydrodynamics information to model a combustion reaction.

5.2 Experimental Equipment and Procedure

Two small pilot scale reactors of 100 mm and 200 mm I.D. were used for tracer experiments. ^{41}Ar produced in a *Slowpoke* nuclear reactor by irradiation of ^{40}Ar with thermal neutrons was used as tracer. This radionucleide decays with a short half–life of 1.83 h emitting β^- particles and a characteristic γ–ray (99.2%) of 1.283 MeV that can be detected even in a thick–walled steel pipe (*Kolar* et *al.*, 1987). Two scintillation detectors placed along the reactor and separated by a distance of

0.26 m were connected to an $ORTEC$ amplification system linked to a multichannel analyzer supported by a 486 IBM compatible. They were shielded with thick lead bricks to minimize background radiation. ^{40}Ar samples of 7 ml were irradiated for 40 minutes and injected into the reactor plenum. The first detector was 0.15 m above the distributor. Three types of particles were used: Fluid Cracking Catalyst (FCC, d_p=75 μm, ρ_p=1450 kg/m^3), sand particles (d_p=130 μm, ρ_p=2650 kg/m^3) and an industrial catalyst ($PC263$, d_p=196 μm, ρ_b=570 kg/m^3). The concentration of gas at the entrance and exit planes were recorded, thus eliminating the error introduced by sampling non radioactive tracers at one or two points in the bed. Since the attenuation of γ–rays is significantly different between a space filled with particles and a particle–free space, the precaution was taken to keep the two detectors below the bed surface. Injections were repeated up to 21 times at the same experimental conditions. Two typical distribution curves for sand particles are shown in Figure 5.1 in the bubbling and the turbulent regimes. They suggest the existence of a large mean dispersion coefficient and a large fluctuation in the bubbling regime as well as a small mean dispersion coefficient and less fluctuation in the turbulent regime. Therefore, two consecutive tracer injections at the same conditions can give completely different dispersion coefficient values in the bubbling regime which is not the case in the turbulent regime where the spread in the data is less pronounced. The counting rate g of γ rays is proportional to the tracer concentration. The dead time is the time elapsed between the moment an incident γ ray strikes a detector and the moment

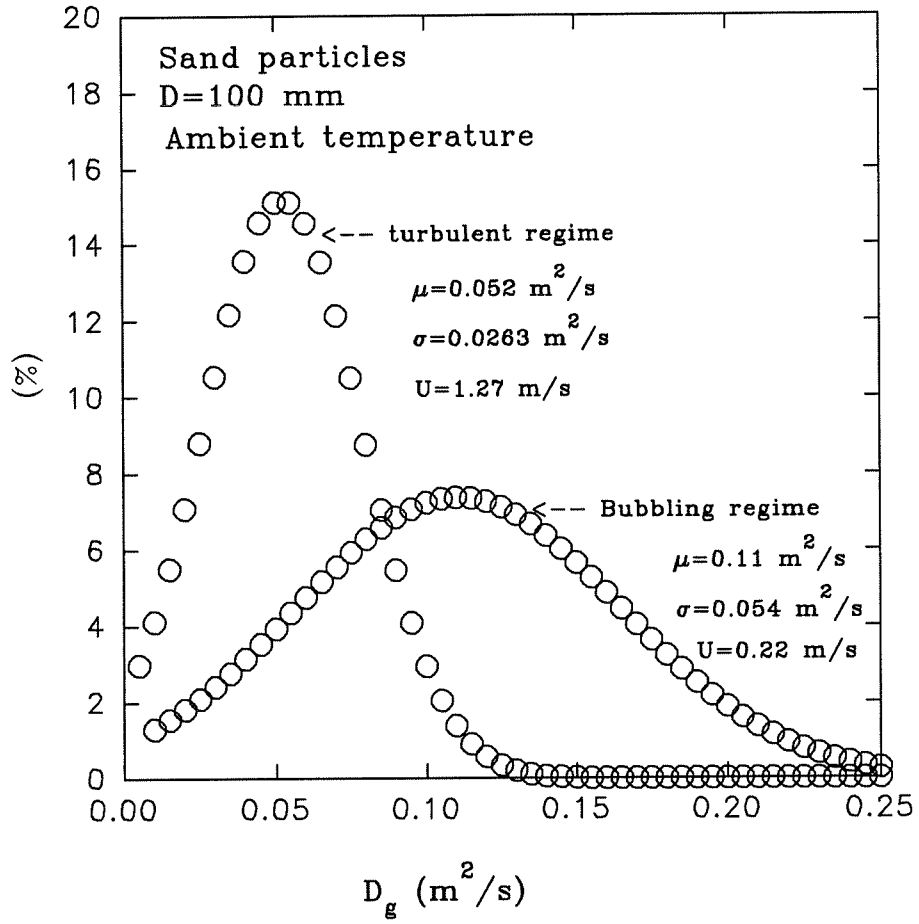

Figure 5.1. Gaussian distribution of the gas mean dispersion in the bubbling and turbulent regimes. Sand particles

the voltage pulse generated is recorded so that the next photon can be counted. At high counting rates, the loss of particles due to the dead time is very important. The gross counting rate g is the observed number of γ photons per unit time. The true counting rate g_c is obtained by correcting the observed counting rate g as follows:

$$g_c = \frac{g}{1 - g\vartheta} \tag{5.1}$$

where where ϑ the detector dead time. ϑ was estimated experimentally by the "two–source" method described by *Tsoulfanidis* (1983) to be 3.45 μs for the two detectors.

Pressure fluctuation experiments were carried out with a differential pressure transducer in order to determine the regimes of fluidization. The capacitance probe was also used in the larger bed to determine the porosity of FCC particles simultaneously with the RTD measurements. A comprehensive study of pressure fluctuations and of the capacitance probe use in fluidized beds has been reported by *Chehbouni et al.* (1994a,1994b).

5.3 Dispersive Model

5.3.1 Method of analysis

A one–dimensional dispersion equation was used to characterize the gas mixing pattern in the flow regime spectrum ranging from the bubbling regime to the turbulent

regime. The dispersion equation is given by

$$\frac{\partial C}{\partial t} = D_g \frac{\partial C^2}{\partial x^2} - u\frac{\partial C}{\partial x} \tag{5.2}$$

$$C = \frac{c(t)}{\int_0^\infty c(t)dt} \tag{5.3}$$

where D_g is the effective axial gas dispersion coefficient, u the interstitial velocity, x the axial distance, t the time and $c(t)$ the tracer concentration at time t.

The Peclet number was determined by the method of the transfer function in the real time domain (*Wakao*, 1982) by matching the response curve of the exit detector (subscript 2) to the theoretical response given by

$$C_{2calc}(t) = \int_0^t C_{1exp}(t) f(t-\varphi) d\varphi \tag{5.4}$$

using the transfer function transfert $f(t)$ and the objective function ψ given below:

$$f(t) = \frac{1}{2\tau\sqrt{\pi N_D \left(\frac{t}{\tau}\right)^3}} \exp\left(-\frac{\left(1-\frac{t}{\tau}\right)^2}{4N_D\frac{t}{\tau}}\right) \tag{5.5}$$

$$\psi = \sqrt{\frac{\int_{t_1}^{t_2} \left(C_{2exp}(t) - C_{2calc}(t)\right)^2 dt}{\int_{t_1}^{t_2} \left(C_{2exp}(t)\right)^2 dt}} \tag{5.6}$$

5.3.2 Results and Discussion

A typical fit of the exit tracer concentration profile to the prediction of the above model is shown in Figure 5.2. In light of pressure fluctuations data, the RTD measurements were carried out up to about the transport velocity. Figure 5.3 shows

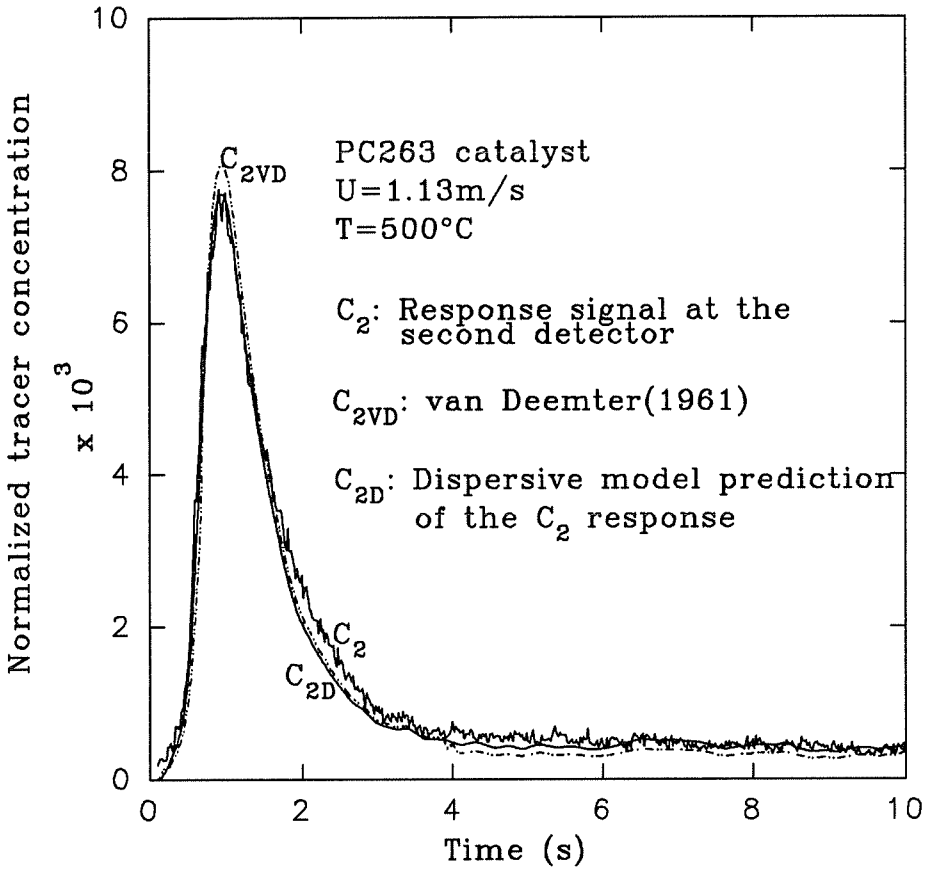

Figure 5.2. Typical calculated and experimental exit responses

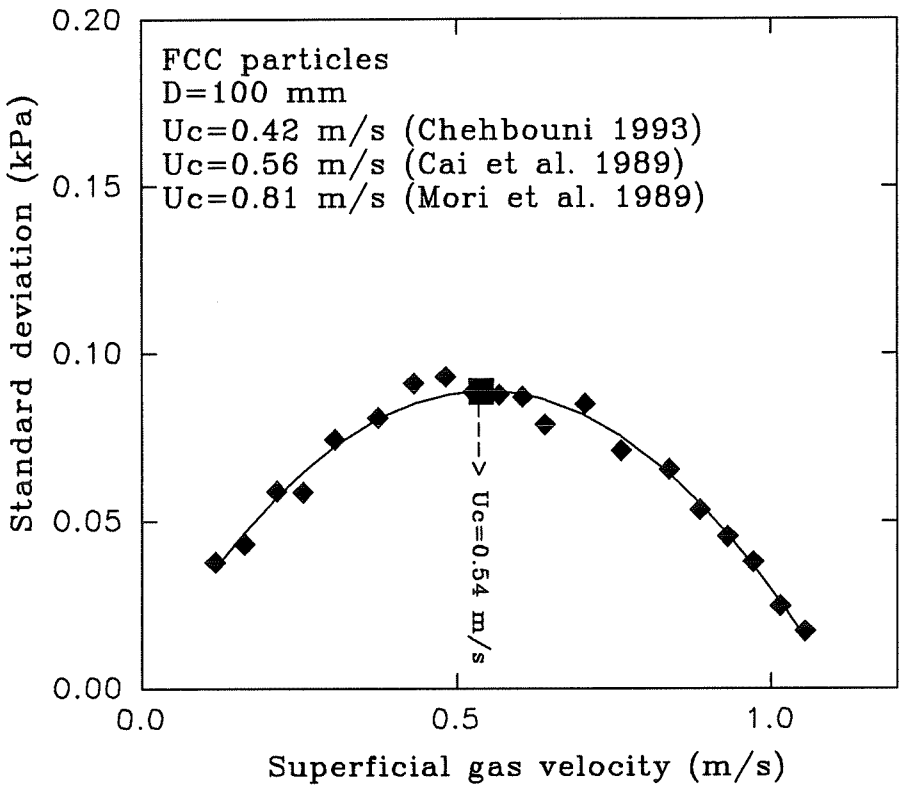

Figure 5.3. Standard deviation of differential pressure fluctuations versus superficial gas velocity. *FCC* particles

the transition velocities U_c in the 100 mm I.D. bed obtained from pressure fluctuations data for the FCC particles. Figure 5.4a shows the mean values of the dispersion in a bed of FCC particles from 8 repeated experiments at each velocity. It is clear that the dispersion increases and passes through a maximum at 0.53 m/s which corresponds to the transition velocity U_c determined from pressure fluctuations. This is a clear indication that the stability of the system has changed and that a new regime prevails beyond 0.53 m/s. The transition velocity is quite in agreement with the results of Cai et $al.$ (1989) obtained from pressure fluctuation measurements. Identical experiments were carried out with in the 200 mm $I.D.$ bed and the results are shown in Figure 5.4b. The value of U_c observed is of the order of magnitude of the prediction from reported correlations (see Table 5.1). A limited number of experiments designed to monitor simultaneously the bed porosity using a capacitance probe and the mixing experiments were carried out in this reactor in the turbulent regime and the trend in the data compared quite well with the data of Li and Wu (1990) obtained for FCC particles in a 90 mm $I.D.$ reactor i.e the dispersion coefficient decreases with porosity in the turbulent regime.

Many other experiments were carried out at different operating conditions with the three particles described above and at temperatures up to 600 $^{\circ}C$ in the turbulent regime. The dimensionless governing parameters in the fluidized bed can be derived from the mass and momentum balances (*Glicksman*, 1984) and are Ar, Re, d_p/H, $\delta = d_p/D$, and ρ/ρ_s. The results were correlated in terms of the Peclet given by

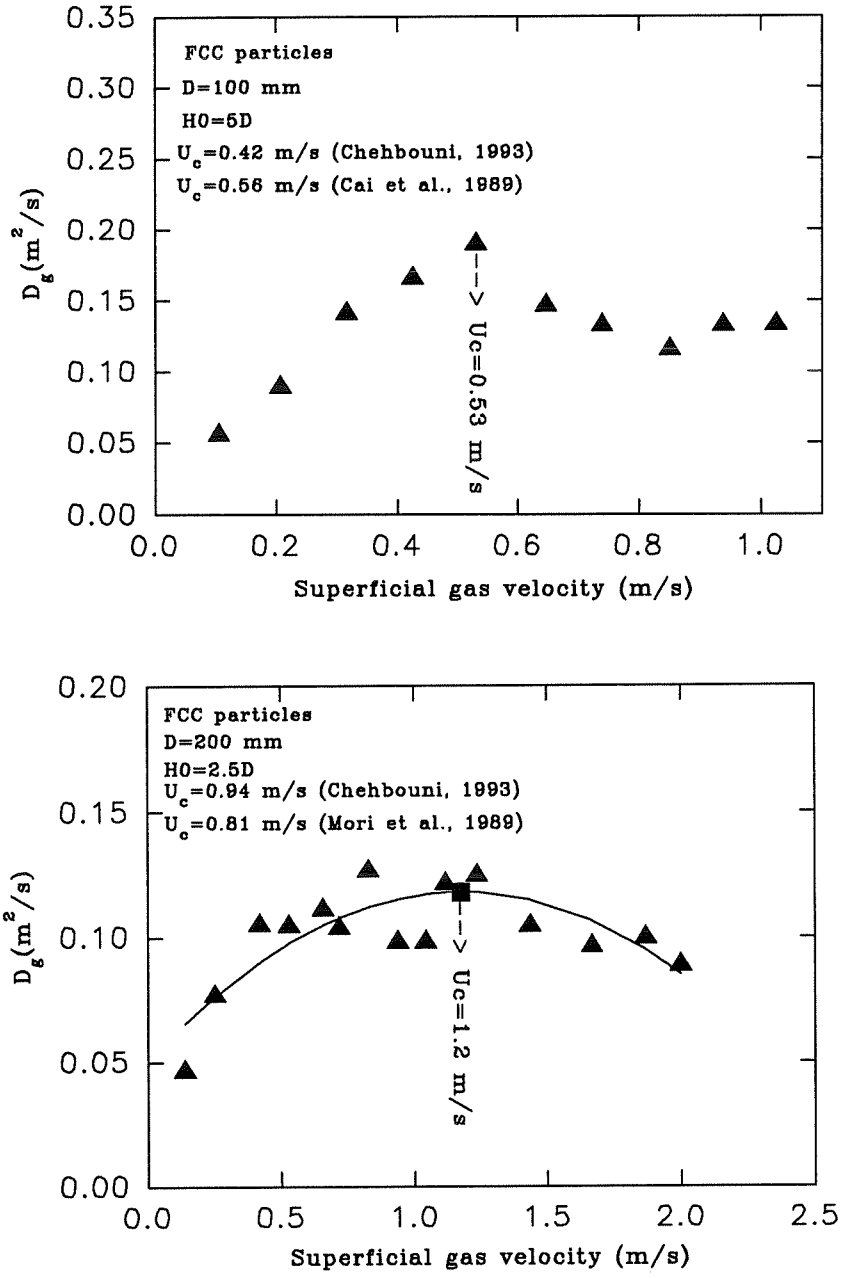

Figure 5.4. Gas dispersion coefficient versus superficial gas velocity. *FCC* particles in 100 *mm* & 200 *mm* I.D. beds

Table 5.1. Comparison of the U_c from gas RTD with the prediction of reported correlations

	d_p (μm)	ρ_p (kg/m^3)	D (mm)	U_c (m/s)	*Experimental technique*
Cai et al. (1989)	75	1450	100	0.56	PF
(Correlation)	130	2650		0.75	
Mori et al. (1989)	75	1450	100	0.81	PF
(Correlation)	130	2650		1.35	
Chehbouni (1993)	75	1450	100	0.42	PF, CP
(Correlation)	130	2650		0.90	
This work	75	1450	100	0.53	RTD
	75	1450		0.54	PF
	130	2650		1.02	RTD
	130	2650		1.08	PF
Cai et al. (1989)	75	1450	200	0.54	PF
(Correlation)	130	2650		0.71	
Mori et al. (1989)	75	1450	200	0.81	PF
(Correlation)	130	2650		1.35	
Chehbouni (1993)	75	1450	200	0.94	PF, CP
(Correlation)	130	2650		1.43	
This work	75	1450	200	1.20	RTD
	130	2650		1.7	RTD

PF: Pressure fluctuation

CP: Capacitance probe

RTD: Residence time distribution

Equation 5.7. The Peclet number does not vary much in the turbulent regime. This feature has also been reported with gas–solid packed beds and with liquid–solid packed beds and fluidized beds (*Wen* and *Fan*, 1975).

$$Pe = 7.10^{-2} Ar^{0.32} \delta^{-0.4} \tag{5.7}$$

Agreement between the correlation and the data is shown in Figure 5.5 where our data are reasonably well predicted by the correlation. Equation 5.7 suggests that the Peclet number ($1 \leq Pe \leq 8$) increases with the Archimedes number ($2 \leq Ar \leq 216$) but decreases with the particle to bed diameter ratio ($510 \leq 1/\delta \leq 2667$). The range of Pe agrees well with the data of *Li* and *Wu* (1990).

The estimated porosity from the mean residence time agrees well with the correlation of *Cai* et *al.* (1992) for sand particles (Figure 5.6a) in a wide range of velocities. *Chehbouni* (1993) used the modified correlation of Richardson and Zaki to model capacitance probe data in a 82 mm *I.D.* bed with two parameters ($U_t^* = 4\ m/s$, $n = 6.4$) for sand particles. The prediction with these parameters are also shown in Figure 5.6a and is not as good as with the correlation of *Cai* et *al.* (1992). Figure 5.6b shows the data obtained over the *FCC* particles. The correlation of *Cai* et *al.* (1992) totally overpredicts the mean bed porosity. The modified Richardson and Zaki correlation is used in the bubbling regime with U_t^*=28 m/s as reported by *Chehbouni* (1993) but the coefficient n=5.5 is half the value he used for his data. In the turbulent regime the parameters used (U_t^* =2 m/s,$n = 2$) are both lower than

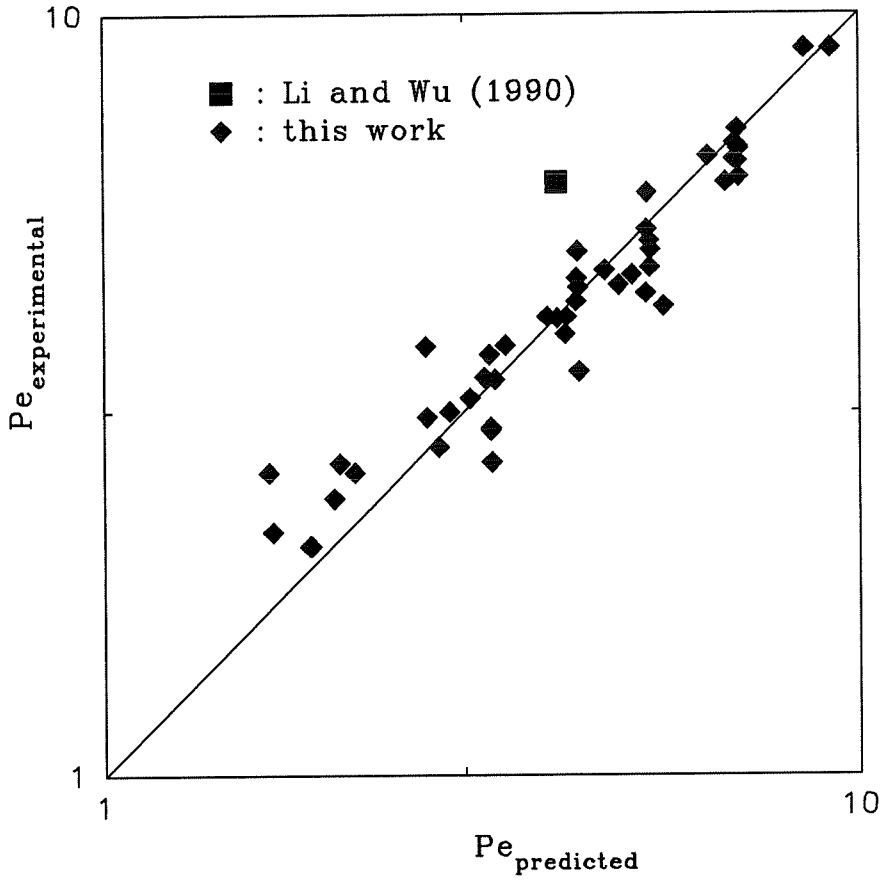

Figure 5.5. Peclet number from the dispersive model compared with the prediction from the correlation

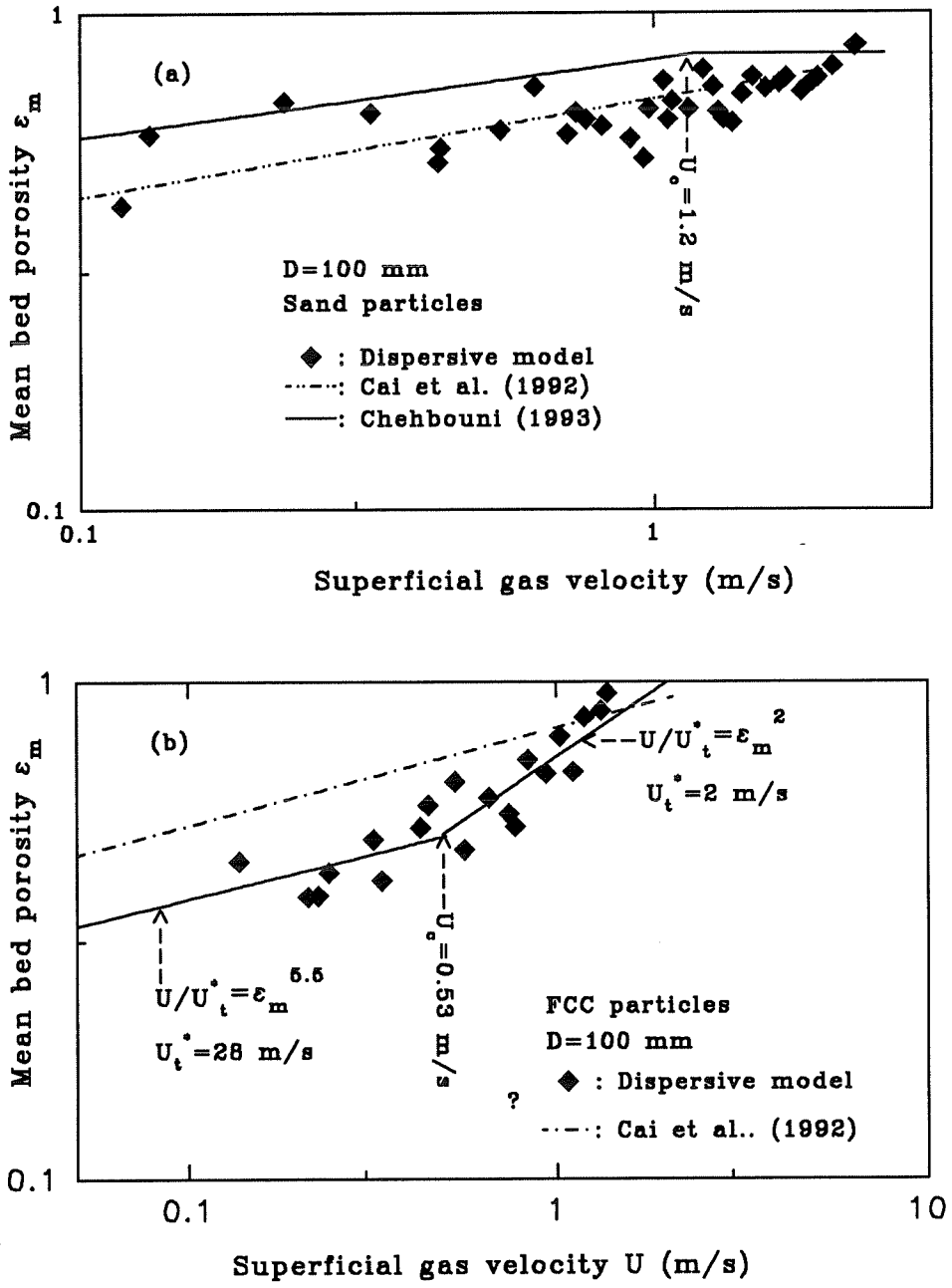

Figure 5.6. Estimated bed porosity from the mean residence time and from correlations

the values he used for these particles (U_t^* =4 m/s,n = 6.4). Eventhough the onset of turbulence is not quite self–evident from the porosity data derived from the RTD as from the reported capacitance probe data (*Chehbouni* et *al.*, 1994a,1994b), the magnitude of the two data sets are quite comparable in a wide range of velocities.

The two–phase model has been widely used in the bubbling bed regime to model the reactor performance (*Werther* ,1980; *Bauer et al.*, 1981; *Kunii* and *Levenspiel*, 1990). The parameters of the two–phase model of *van Deemter* are estimated in the next section using the same mixing data as above in the bubbling and the turbulent regimes. The advantage of this model is that it has only two parameters (*Villermaux*, 1993).

5.4 Two–Phase Model

5.4.1 Model derivation

Figure 5.7a shows the schematic diagram of the general two–phase model in which the gas fed to the reactor flows through the dilute and the emulsion phases. The mass balance applicable to each phase is given by

$$\frac{\partial C_i}{\partial t} + u_i \frac{\partial C_i}{\partial x} - D_{gi} \frac{\partial^2 C_i}{\partial x^2} + k_m a \frac{A_{gd}}{A_{gi}} (C_i - C_j) - R_i = 0 \tag{5.8}$$

where

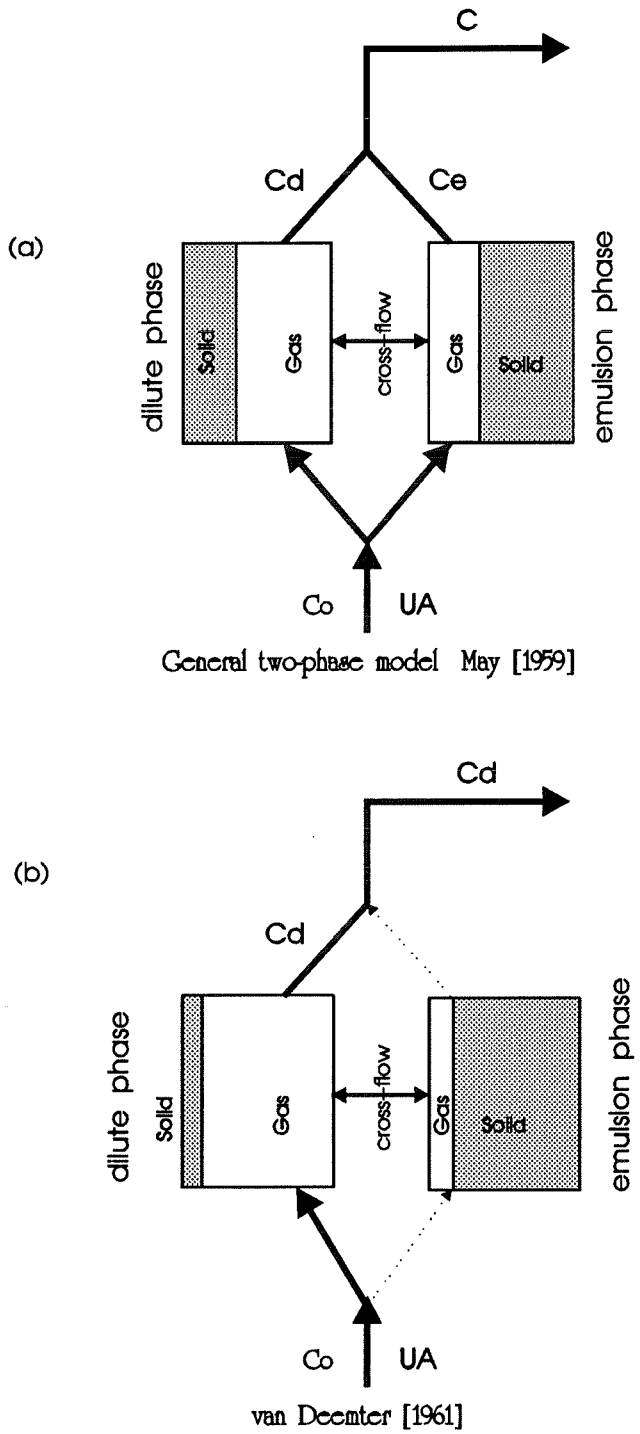

Figure 5.7. Schematic diagrams of two–phase models

a = transfer surface between the phases

A_{gi} = area cross–section occupied by the gas of phase i

A_{gd} = area cross–section occupied by the gas of the dilute phase

A_{ge} = area cross–section occupied by the gas of the emulsion phase

C_i = gas concentration in phase i

D_{gi} = gas axial dispersion of phase i

k_m = cross–flow mass transfer coefficient

R_i = rate of production in phase i

u_i = interstitial velocity of gas in phase i

The model of *van Deemter* presented in Figure 5.7b assumes a negligible fraction of solids in the dilute phase and a negligible fraction of gas flowing through the emulsion phase, and that the reaction takes place only in the emulsion phase. Equation 5.8 above reduces to

$$\frac{\partial C_d}{\partial t} + u_d \frac{\partial C_d}{\partial x} + \alpha_{12}(C_d - C_e) = 0 \tag{5.9}$$

$$\frac{\partial C_e}{\partial t} + \frac{\alpha_{12}}{\beta}(C_e - C_d) = D_{ge}\frac{\partial^2 C_e}{\partial x^2} + R_e \tag{5.10}$$

For a first order reaction $R_e = -k_r C_e$ the dimensionless form of Equations 5.9 and 5.10 are given by

$$\frac{\partial C_d}{\partial \tau} + \frac{\partial C_d}{\partial Z} + N_\alpha(C_d - C_e) = 0 \tag{5.11}$$

$$\beta\frac{\partial C_e}{\partial \tau} + N_\alpha(C_e - C_d) = \frac{1}{P_{ee}}\frac{\partial^2 C_e}{\partial Z^2} - N_r C_e \tag{5.12}$$

where

$$Z = \frac{x}{H}$$

$$\tau = \frac{u_d t}{H}$$

$$\beta = \frac{A_{ge}}{A_{gd}} = \frac{\epsilon_{em}}{\epsilon_{dm}}$$

$$N_\alpha = \alpha_{12}\frac{H}{u_d}$$

$$\alpha_{12} = k_m a$$

$$P_{ee} = \frac{u_d H}{\beta D_{ge}}$$

$$N_r = \beta\frac{k_r H}{u_d}$$

Two limiting cases of this model have been considered in the literature:

a). $P_{ee} \rightarrow \infty$ with a finite mass-transfer rate, Equations 5.11 and 5.12 reduce to

$$\frac{\partial C_d}{\partial \tau} + \frac{\partial C_d}{\partial Z} + N_\alpha(C_d - C_e) = 0 \tag{5.13}$$

$$\beta\frac{\partial C_e}{\partial \tau} + N_\alpha(C_e - C_d) + N_r C_e = 0 \tag{5.14}$$

At steady–state, Equations 5.13 and 5.14 give the reactant slip

$$\frac{C_d}{C_O} = \exp(-\frac{N_\alpha N_r}{N_\alpha + N_r}) \tag{5.15}$$

b). $N_\alpha \rightarrow \infty$ and $C_d = C_e$ Equations 5.11 and 5.12 reduce to a plug flow model with axial dispersion.

5.4.2 Parameter estimation

For the imperfect one–shot input, the method of the transfer function in the real time domain is more convenient for the prediction of the output response if the transfer

function in the Laplace domain can be easily inverted. The Laplace transform of the two–parameter model given by Equations 5.13 and 5.14 in the absence of reaction leads to the following equation

$$\frac{\partial C_d}{\partial Z} + W(p)C_d = 0 \tag{5.16}$$

where

$$W(p) = \frac{\beta p^2 + N_\alpha(1+\beta)}{\beta p + N_\alpha} \tag{5.17}$$

The transfer function is easily shown to be

$$G(p) = \exp(-W) \tag{5.18}$$

The inversion of Equation 5.18 is not straightforward by conventional methods. However, the inversion can be performed in terms of a Fourier series by expressing the measured input signal by a Fourier series as:

$$C_{1expt(t)} = \frac{a_{10}}{2} + \sum_{n=1}^{\infty}\left(a_{1n}\cos\frac{n\pi t}{\theta} + b_{1n}\sin\frac{n\pi t}{\theta}\right) \tag{5.19}$$

the measured output signal as:

$$C_{2expt(t)} = \frac{a_{20}}{2} + \sum_{n=1}^{\infty}\left(a_{2n}\cos\frac{n\pi t}{\theta} + b_{2n}\sin\frac{n\pi t}{\theta}\right) \tag{5.20}$$

the predicted output signal as:

$$C^{\star}_{2expt(t)} = \frac{a^{\star}_{20}}{2} + \sum_{n=1}^{\infty}\left(a^{\star}_{2n}\cos\frac{n\pi t}{\theta} + b^{\star}_{2n}\sin\frac{n\pi t}{\theta}\right) \tag{5.21}$$

and using the transfer function to evaluate the Fourier coefficients $a_n^\star$ and $b_n^\star$ as

$$a_{2n}^\star - ib_{2n}^\star = G(\frac{in\pi}{\theta})(a_{1n} - ib_{1n}) \tag{5.22}$$

The objective function used to fit the data of Equation 5.20 to the model of Equation 5.21 is shown (*Wakao*, 1982) to be

$$\Psi = \sqrt{\frac{2\left(\frac{a_{20}}{2} - \frac{a_{20}^\star}{2}\right)^2 + \sum_{n=1}^{\infty}((a_{2n} - a_{2n}^\star)^2 + (b_{2n} - b_{2n}^\star)^2)}{2(\frac{a_{20}}{2})^2 + \sum_{n=1}^{\infty}(a_{2n}^2 + b_{2n}^2)}} \tag{5.23}$$

The transfer function can be expressed as

$$G(\frac{in\pi}{\theta}) = exp(A_n + iB_n) \tag{5.24}$$

where

$$A_n = -\frac{N_\alpha\beta(\frac{n\pi}{\theta})}{N_\alpha^2 + (\frac{n\pi\beta}{\theta})^2} \tag{5.25}$$

$$B_n = -\frac{\left(\frac{n\pi}{\theta}\right)\left((1+\beta)N_\alpha^2 + (\frac{n\pi\beta}{\theta})^2\right)}{N_\alpha^2 + (\frac{n\pi\beta}{\theta})^2} \tag{5.26}$$

θ is a period of time long enough for the signal to vanish, and $a_n^\star$ and $b_n^\star$ can be expressed in terms of the input response coefficients as:

$$a_{2n}^\star = \exp A_n\,(a_{1n}\cos B_n + b_{1n}\sin B_n) \tag{5.27}$$

$$b_{2n}^\star = \exp A_n\,(b_{1n}\cos B_n - a_{1n}\sin B_n) \tag{5.28}$$

5.4.3 Results and discussion

The model parameters α_{12} and β are estimated for three different particles mentioned above in two beds, at various temperatures and gas velocities. The cross–flow mass transfer α_{12} is between 0.19 and 4.6 s^{-1} and is correlated in terms of the height of a transfer unit as shown in Equation 5.29 for both the bubbling and the turbulent regimes with a superficial gas velocity up to 2.6 m/s.

$$\frac{U}{\alpha_{12}} = 0.613 Sc^{-0.37} \ (in\ m) \tag{5.29}$$

Agreement between the correlation and the data is shown in Figure 5.8 and is quite satisfactory. The values of the mass transfer coefficient are in the range of values reported by *Werther* (1980) or calculated from the correlation of *van Swaij* (1978) which predicts the height of a transfer unit.

The parameter β was almost constant at about 0.08 for sand particles and 0.11 for the FCC and the $PC263$ catalyst. This is probably due to the fact that the area cross–section occupied by the gas of the dilute phase A_{gd} is almost constant since the model allows no particles in the dilute phase, and that the area cross–section occupied by the gas of the emulsion phase A_{ge} is also almost constant as the particles always occupy almost the totality of this phase. Furthermore, the mean bed voidage ϵ_m is the sum of the mean dilute phase voidage ϵ_{dm} and the mean emulsion phase voidage ϵ_{em} and β is the ratio of the mean emulsion phase voidage to the mean dilute phase voidage. As ϵ_m increases with velocity, $\epsilon_{dm} + \epsilon_{em}$ increases.

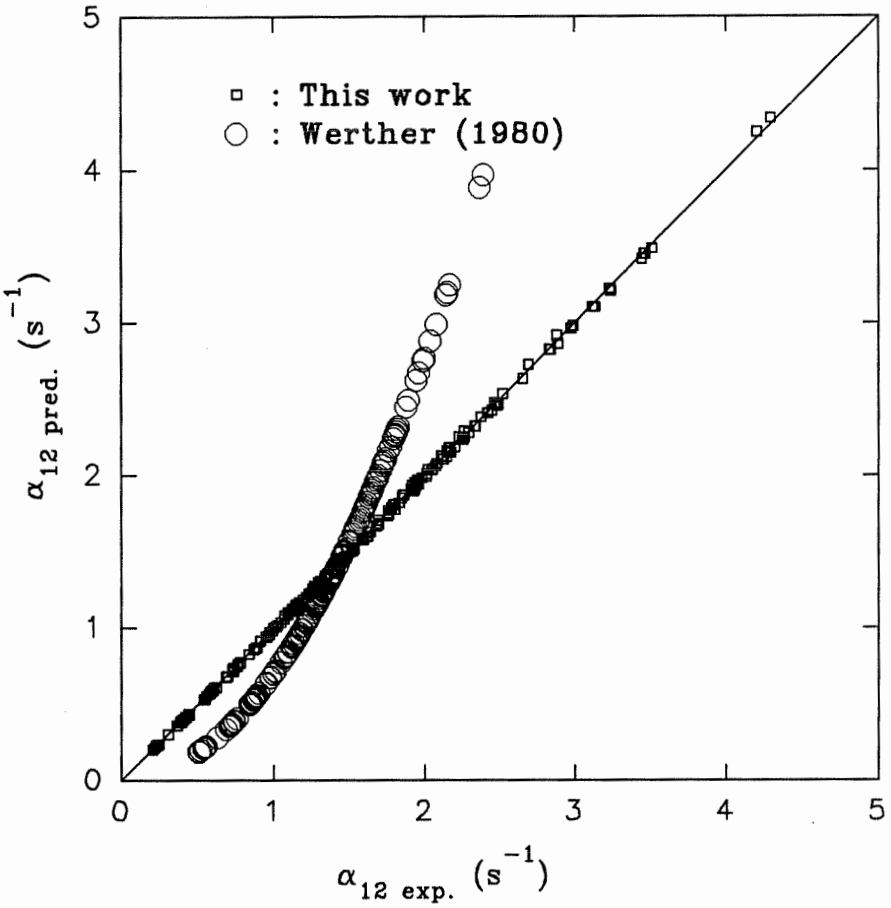

Figure 5.8. Cross–flow mass transfer coefficient from the model of *van Deemter* compared with the prediction from the height of a transfer unit correlation

If ϵ_{dm} and ϵ_{em} increase correlatively it is normal that β remains constant. One would be tempted to estimate ϵ_{dm} and ϵ_{em} from the above values of β but that would be misleading since they are very small. Their order of magnitude can be traced directly to one of the key assumptions of the model which neglects the flow of the gas through the emulsion phase and which is the main drawback of this model.

5.5 Prediction of the Reactor Performance

The kinetic data for the combustion of natural gas in a turbulent fluidized bed combustor (*Foka* et *al.*, 1994) are presented in Figure 5.9 along with the prediction of different models. The plug flow model obviously overpredicts the observed data. Eventhough the perfect mixing predicts reasonably well the data over a wide range of number of reaction units, it underestimates the data at N_r between 2 and 10 where the axial dispersion model gives a good prediction. The latter model slightly overpredicts the data only at high number of reaction units.

The two–phase model of *van Deemter* (1961) with $\alpha_{12} = 1.96\ s^{-1}$ obtained at the conditions of the reaction experiments with the $PC263$ catalyst shows a poor prediction of the conversion. This is normal since this model is valid only when the mass–transfer rate is not influenced by the reaction rate (*van Swaij* and *Zuiderweg*, 1973; *Werther*, 1980) i.e for $k_r < 1 - 2\ s^{-1}$ whereas the rate constant of the catalyst used here is of the order of $70\ s^{-1}$.

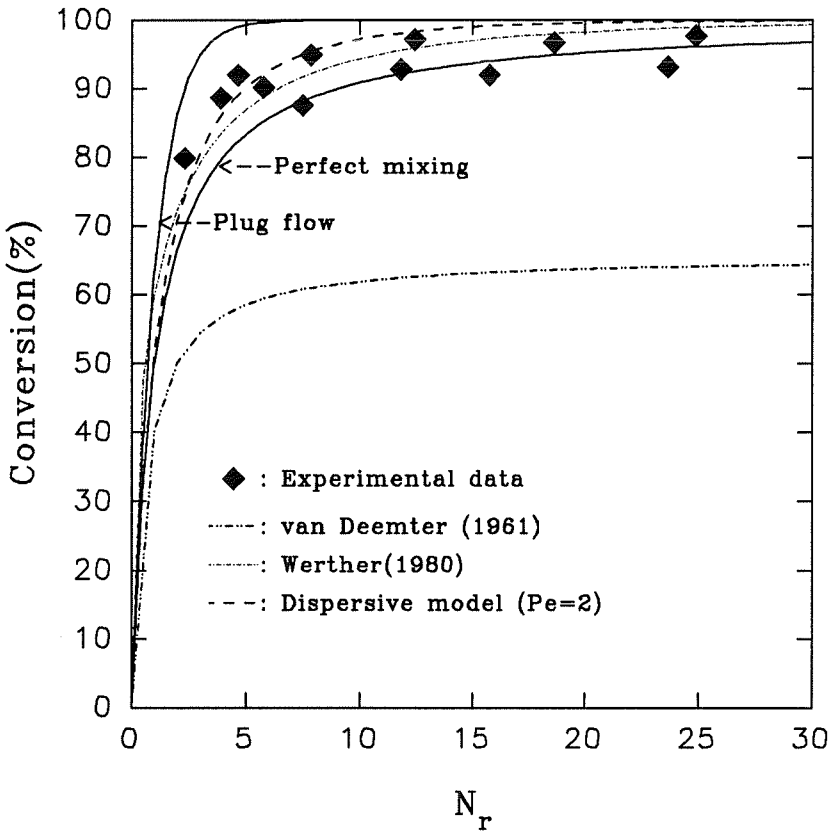

Figure 5.9. Experimental and predicted conversions of methane in the turbulent flow regime. $PC263$ catalyst

Under these conditions a chemical acceleration factor can be phenomenologically introduced. The most applicable two–phase model to industrial scale fluid bed reactors is the model of *Werther* (1980). It can be used here for the reasons evoked by *Pell* (1990):

- The ajustable parameters are based upon observations in fluid beds up to several meters in diameter.
- It recognizes the existence and importance of a maximum stable bubble size. This enables the impact of the fines to be incorporated into the model.
- The model takes into account the effects of bed diameter and bed height.
- Geldart group A and group B particles are recognized as being fundamentally different in behavior.

This model (see Equation 5.30) introduces the film theory

$$\frac{C}{C_0} = exp\left(-\left[\frac{(\frac{1}{\Phi}-1)Ha + tanh(Ha)}{(\frac{1}{\Phi}-1)Ha\ tanh(Ha)+1}\right] HaN_\alpha\right) \tag{5.30}$$

Ha $= \sqrt{k_r D_v}/k_m$

Φ $= \frac{aD_v}{k_m(1-\epsilon_b)}$

a = transfer surface between the phases ll

D_v = gas diffusivity

ϵ_b = bubble gas hold-up in the fluidized bed

k_m = cross-flow mass transfer coefficient

in the model of *van Deemter* (1961) and the correction factor appears in terms of the Hatta number Ha which is ratio of the maximum quantity of material chemically convertible in the film per unit time to the maximum quantity of material transported through the film per unit time. The value of k_m is typically 0.0159 m/s for group A particles and 0.0089 m/s for group B particles (*Werther*, 1980). $Ha \ll 1$ indicates that the conversion of the reactant in the film can be neglected in which case the two–phase model of *van Deemter* (1961) applies. At large Hatta numbers, a significant part of the reactant reacts within the film. The concentration gradient across the film is then magnified by the reaction and the mass transfer is amplified. When $Ha \geq 1$ the first term in Equation 5.30 is one whatever is the value of Φ and the equation reduces to

$$\frac{C}{C_0} = exp(-HaN_\alpha) \tag{5.31}$$

The Hatta number estimated from our experiments was above 1 and Equation 5.31 was used to model the reaction as shown in Figure 5.9. It is clear from this figure that this model can also satisfactorily predict our data in a wide range of the number of reaction units.

5.6 Conclusion

The gas flow behavior has been dynamically characterized by a one–dimensional pseudo–homogeneous dispersion model throughout the fluidization regime spectrum ranging from bubbling to turbulent fluidization and with a two–phase model. The assumption of a gas plug flow with axial dispersion in the bubbling regime may not be quite phenomenologically exact. However, it is quite clear from our data that the global dispersion coefficient can be used to predict the change in the flow regimes. In the turbulent regime this assumption is quite tenable since this regime is almost bubbleless and the gas can be assumed to move in plug flow through the system. The results in this regime also agree quite well with the data reported in the literature at high velocities and can be used to model the reactor performance.

The two–phase model of *van Deemter* is used to characterize the reactor hydrodynamics and the model parameters coupled with the kinetic data to predict the reactor performance. The dispersive model predicts better the experimental data with a number of Peclet of 2. However, a comparable prediction can also be obtained with the two–phase model of *Werther* (1980) which phenomenologically introduces the enhancement factor due to chemical reaction in the model of *van Deemter* (1961).

This work has demonstrated that besides pressure fluctuations and capacitance probe techniques, dispersion fluctuations can also be used to characterize a gas–solid fluidized bed hydrodynamics and that an appropriate two–phase model can be used

to model a turbulent fluidized bed performance.

Acknowledgement

The financial support of Gaz Métropolitain, Inc. to pursue research in fluidization is gratefully acknowledged.

5.7 References

Avidan, A. and Edwards, M. (1986). Modeling and Scale–up of Mobil's Fluid–bed MTG Process. In "Fluidization V". Edited by Ostergaard, K. and Sorenson, A. Engineering Foundation, New York, 457.

Bauer, W., Werther, J. and Emig, G. (1981). Influence of Gas Distributor Design on the Performance of Fluidized Bed Reactor. Ger.Chem. Engng, 4, 291–298.

Cai, P., Chen, S.P., Jin, Y. and Wang, Z.W. (1989). Effect of Operating Temperature on the Transition from Bubbling to Turbulent Fluidization. A.I.Ch.E Symp.Ser., 37.

Cankurt, N.T. and Yerushalmi, J. (1978). Gas mixing in High Velocity Fluidized Beds. In "Fluidization". Edited by Davidson, J.F., and Keairns, D.L. Cambridge Univ. Press.

Chehbouni, A. (1993). Frontières et structures du lit fluidisé turbulent. Ph.D. thesis, Ecole Polytechnique, Montréal.

Chehbouni, A. Chaouki, J., Guy, C. and Klvana, D. (1994a). Characterization of the Flow Transition Between Bubbling and Turbulent Fluidization. IEC J., (accepted).

Chehbouni, A. Chaouki, J., Guy, C. and Klvana, D. (1994b). Effets de différents

paramètres sur les vitesses de transition de la fluidisation en regime turbulent. Can.J.Chem.Engng, (accepted).

Daw, C.C., Lawkins, W.F., Downing, D.J. and Clapp, N.E. (1990). Chaotic characteristics of a complex gas-solids flow. Phys.Rev.A, 41, 1179–1181.

Foka, M., Chaouki, J., Guy, C. & Klvana, D. (1993). Catalytic Combustion of Natural Gas in a Turbulent Fluidized Bed Reactor. Proc.12th Inter.Conf. on Fluidized Bed Combustion, ASME, San Diego, 1, 179–184.

Foka, M., Chaouki, J., Guy, C. and Klvana, D. (1994). Natural Gas Combustion in a Turbulent Fluidized Bed Reactor. Chem.Engng Sci., (accepted).

Glicksman, L.R. (1984). Fluid Beds as Chemical Reactors. Chem.Engng Sci., 39, 1373–1379.

De Groot, J.H. (1967). Proc. Symposium on fluidization. Eindhover, 782.

Handlos, A.E., Kunstman, R.W., and Schissler, D.O. (1957). Ind.Engng Chem., 49, 25.

Kolar, Z., Thyn, J., Martens, W., Boelens, G. and Korving, A. (1987). The Measurement of Gas Residence Time Distribution in a Pressurized Fluidized-bed Combustor using ^{41}Ar as Radiotracer. Appl.Radiat.Isot., 38, 123–127. Int. J. radiat. Appl. Instrum. part A.

Kunii, D. and Levenspiel, O. (1990). Fluidized Reactor Models.Ind.Eng.Chem.Res., 29, 1226–1234.

Li, J. and Weinstein, H. (1989). An Experimental Comparison Of Gas Backmixing In Fluidized Beds Across the Regime Spectrum. Chem. Engng Sci., 44, 1697–1705.

Li, Y and Wu, P. (1990). A Study on Axial Gas Mixing in a Fast Fluidized Bed. Circulating Fluidized Bed Technology III, Proc. 3rd Inter. Conf. on Circulating Fluidized Beds. Edited by Basu, P., Horio, M. and Hasatani, M. Nagoya, Japan, 581.

Mori, S., O. Hashimoto, T. Haruta and Yamada, I. (1989). In "Fluidization VI". Edited by Grace, J.R., Shemilt, L.W. and Bergougnou, M.A. Engineering Foundation, 49.

May, W.G. (1959). Fluidized Bed Reactor Studies. Chem.Engng Progr.. 55, 49–56.

Pell, M. (1990). Gas Fluidization. In "Handbook of Powder Technology". Edited by Williams, J.C. and Allen, T. Elsevier, the Netherlands, 8.

Schouten, R.J.C. and van den Bleek, C.M. (1991). Chaotic behaviour in a hydrodynamic model of a fluidized bed reactor. Proc.11th Inter.Conf. on Fluidized Bed Combustion. ASME, New York, 1, 459–466.

Tsoulfanidis, N. (1983). Measurement and Detection of Radiation. Hemisphere Pub.Corp., McGraw–Hill, New York.

van Deemter, J.J. (1961). Mixing and Contacting in Gas–Solid Fluidized Beds. Chem.Engng Sci., 13, 143–154.

van Deemter, J.J. (1980). Mixing Patterns in Large–Scale Fluidized Beds. in "Fluidization". Edited by Grace, J.R. and Matsen, J.M. Plenum Press, New York, 69.

van Swaij, V.P.M. (1978). The Design of Gas–solids Fluid Bed and Related Reactors. ACS Symp.Ser., 72, 193.

van Swaij, V.P.M. and Zuiderweg, F. J. (1973). Proc.Inter.Symp. on Fluidization and its Applications. Edited by Cepadues. Toulouse, France, 454.

De Vries, J., van Swaaij, W.P.M., Mantovani, C. and Heijkoop, A. (1972). Proc.5th–Europ.Symp.Chem.React.Engng, Amsterdam, B9–59.

Villermaux, J. (1993). Génie de la réaction chimique. 2e édition, Lavoisier, Paris.

Wakao, N. and Kaguei, S. (1982). Heat and Mass Transfer in Packed Beds. Gordon and Breach Science Publishers.

Werther, J. (1980). Mathematical modeling of fluidized bed reactors. Intern. Chem.Engng, 20, (4), 529.

CONCLUSION

The main objective of this work was to assess experimentally the feasibility of the catalytic combustion of natural gas in a fluidized bed as a zero NOx and CO emission technology. A pilot scale fluidized bed of 100 mm $I.D$ was designed and constructed to investigate the hydrodynamics and the reaction kinetics. The design parameters were based on the results of a simulation performed with the data obtained from the literature (kinetic and hydrodynamic parameters). A small tubular fixed bed reactor of 7 mm in diameter was used to evaluate the activity of the catalysts used in the fluidized bed.

Transient gas mixing experiments were performed in two different experimental setups of 100 mm and 200 mm $I.D$. The effective axial gas dispersion coefficient was used to determine the onset of slugging in the small bed for sand particles and the onset of turbulence in both beds for the FCC and sand particles. The bifurcation points thus determined were quite close to the values obtained from correlations found in the literature and the ones measured with a differential pressure tranducer. The FCC dispersion data in the larger bed were correlated in terms of the mean

bed voidage monitored by the capacitance probe. A second correlation related the Peclet number observed in both beds and for three particles to the characteristic dimensionless numbers. The two–phase model of *van Deemter* was also used to model the RTD data and the cross–flow mass transfer coefficient correlated as the Sherwood number.

The kinetics of the PSA catalyst was found to be inadequate for a high conversion combustion of methane in the turbulent bed. The $PC263$ was successfully used in the turbulent bed ($100\ mm\ I.D$) to achieve a high conversion and the conversion was higher than the one observed in the bubbling bed where the a perfect mixing model satisfactorily represented the data. In the turbulent regime the order of magnitude of the Peclet number derived from gas mixing experiments was enough for the prediction of our experimental data as well as a corrected cross–flow mass transfer coefficient for the model of *van Deemter*.

A self–sustained combustion in the bubbling and the turbulent regimes was realized up to $540°C$ and 100% conversion generating a power of about $5\ kW$ in the turbulent regime and about $3\ kW$ in the bubbling regime and no pollutants (NOx/CO) were recorded. With the parameters derived from this study, it was showed that a substantial amount of heat of the order of $50\ kW$ could be generated over this $PC263$ catalyst in a bed as small as $240\ mm\ I.D.$ with an inlet mixture of 5% in methane and a superficial gas velocity of the order of $1.5\ m/s$.

RECOMMENDATIONS

We have shown in this study that the catalytic combustion of natural gas in a $TFB2C$ is feasible as a zero NOx and CO emission technology. However, it is important to note that the $PC263$ catalyst used was made up of a noble metal which is very expensive. If this emerging technology has to know a bright future, a new catalyst with a comparable activity has to be developped. Once such a catalyst is available, a serious attrition and deactivation evaluation will be a prerequisite for the development of this process which operates at high velocities. The scale–up procedure will be contingent upon the development of an active, robust and cheap catalyst which is the battle horse of this technology.

BIBLIOGRAPHY

ABED, R. (1984). The characterization of Turbulent Fluidized Bed Hydrodynamics. In "Fluidization". Edited by Kunii, D. et Toei, R. Engineering Foundation, 137.

AHUJA, O.P., and MATHUR, G.P. (1967). Kinetics of Catalytic Oxydation of Methane: Application of Initial Rate Technique for Mechanism Determination. Can.J. Chem.Eng., 45, 367.

ASKINS, J.W., HINDS, G.P.Jr. and KUNREUTER, F. (1951). Fluid Catalytyst–Gas Mixing in Commercial Equipment. Chem.Eng.Prog., 47, (8) 401–404.

AVIDAN, A. (1982). Turbulent Fluid Bed Reactors Using Fine Powder Catalysts. A.I.Ch.E-CIESC Mtg Beijing.

AVIDAN, A. and EDWARDS, M. (1986). Modeling and Scale–up of Mobil's Fluid-bed MTG Process. In "Fluidization V". Edited by Ostergoard, K. and Sorenson, A. Engineering Foundation, New York, 457.

BARTOK, W., LYON, R.K., McINTYRE, A.D., RUTH, L.A. and SOMMERLAD, R.E. MARCH (1988). Combustors: Applications and Design Considerations.

Chem.Engng Prog., 54–71.

BRERETON, C.M.H. (1987). Fluid Mechanics of High Velocity Fluidized Beds. Ph.D. Thesis University of British Columbia, Canada.

BRERETON, C.M.H., GRACE, J.R. and YU, J. (1988). Axial Gas Mixing in a Circulating Fluidized Bed. Circulating Fluidized Bed technology II. Edited by BASU, P. and LARGE, J.F. Pergamon Press, Oxford, 209-212.

CAI, P. CHEN, S.P., JIN, Y. and WANG, Z.W. (1989). Effect of Operating Temperature on the Transition From bubbling to Turbulent Fluidization. A.I.Ch.E Symp.Ser., 37.

CHEHBOUNI, A. (1993). Frontières et structures du lit fluidisé turbulent, Ph.D. thesis, Ecole Polytechnique, Montréal.

CULLIS, C.F., KEENE, D.E., and TRIMM, D.L. (1971). Pulse Flow Reactor Studies of Methane Oxidation over Palladium Catalysts. Trans.Faraday Soc., 67, 864.

DE REYDELLET, A. (1989). Les mesures de réduction des émissions d'oxydes d'azote en aval du foyer. Rev.Gen.Therm., 28, 453.

DE SOETE, G.G. (1989). Mécanisme de formation et de destruction des oxydes d'azote dans la combustion. Rev.Gen.Therm., 28, 353.

FIRTH, J.G., and HOLLAND, H.B. (1969). Catalytic Oxidation of Methane Over Noble Metals. Trans.Faraday Soc., 65, 1121.

GELDART, D. (1973). Types of Gas Fluidization. Powder Technol., 7, 285.

GRACE, J.R. (1986). Chap. 11 in "Gas Fluidization Technology". Fluidized Beds as Chemical Reactors. Edited by Geldart, D. Wiley, London. 285.

GRACE, J.R. (1990). High Velocity Fluidized Bed Reactors. Chem.Engng Sci., 45, (8), 1953.

JONES, D.J, et SALFATI, S. (1989). Combustion catalytique et gaz naturel. Rev.Gen. Therm., 28, 401.

KAGAWA, H., MINEO, H., YAMAZAKI, R. and YOSHIDA, K. (1991). A Gas–solid Contacting Model for fast Fluidized Bed. Circulating Fluidized Bed Technology III. Edited by Basu, P., Horio, M. and Hasatani, M. Pergamon Press, Oxford, 551-556.

KLVANA D., VAILLANCOURT, J., KIRCHNEROVA, J. and CHAOUKI, J. (1994). Combustion of Methane over $La_{0.66}Sr_{0.34}Ni_{0.3}Co_{0.7}O_3$ and $La_{0.4}Sr_{0.6}Fe_{0.4}Co_{0.6}O_3$ prepared by freeze–drying. Applied Catalysis A: General 109, 181–193.

KUEHN, S.E. February (1994). Retrofit Control Technology Reducing NOx Emmissions. Power Engineering, 23–27.

KUNII, D. and LEVENSPIEL, O. (1991). Fluidization Engineering, second edition. Butterworth– Heinemann.

KUNII, D. and LEVENSPIEL, O. (1990). Fluidized Reactor Models. Ind.Eng.Chem.Res, 29, 1226–1234.

LEE, G.S. and KIM, S.D. (1989). Gas Mixing in Slugging and Turbulent Fluidized Beds. Chem. Engng Comm., 86, 91.

LI, J. and WEINSTEIN, H. (1989). An Experimental Comparison Of Gas Back-mixing In Fluidized Beds Across the Regime Spectrum. Chem. Engng Sci., 44, 1697–1705.

LI, Y and WU, P. (1990). A Study on Axial Gas Mixing in a Fast Fluidized Bed. Circulating Fluidized Bed Technology III, Proc. 3rd Inter. Conf. on Circulating Fluidized Beds. Edited by Basu, P., Horio, M. and Hasatani, M. Nagoya, Japan, 581.

MAY, W.G. (1959). Fluidized Bed Reactor Studies. Chem.Engng Progr.. 55, (12), 49–56.

MEZAKI, R., and WATSON, C.C. (1966). Catalytic Oxidation of Methane. I&EC Proc. Des.Dev., 5, 63.

MOLIÈRE, M.; COLAS, M.; FREIMARK, M. (1989). Des émulsions eau/fuel pour réduire les émissions de NOx de turbines à gaz. Rev.Gen.Therm., 28, 428.

PATIENCE, G.S. (1990). Circulating Fluidized Beds: Hydrodynamics and Reactor–Modelling, Ph.D. dissertation, Ecole Polytechnique de Montréal.

ROWE, P.N. and MacGILLIVRAY, H.J. (1980). The Structure of a 15 cm Diameter Gas Fluidized Bed Operated at up to 1 m/s and seen by X–Rays. In "Fluidization". Edited by Grace, J.R. and Matsen, J.M. New York, 545.

SALFATI, D.J., VAN DER WAL, W. (1989). Développement de nouveaux appareils utilisant la combustion catalytique du gaz naturel. Congrès A.T.G., Lyon.

SICARDI, S., SPECCHIA, V., and FERRERO, F. (1982). Kinetics of Combustion of Methane with Different Catalysts. Chimica Industriale, 3, 217.

THIEL, W.J. and POTTER, O.E. (1978). The Mixing of Solids in Slugging Gas Fluidized Beds. AIChE J., 24, (4).

TRIM, D.L., and LAM, C. (1980). The Combustion of Methane on Platinum–Alumina fibre catalysts–I, Kinetics and Mechanism. Chem.Eng.Sci., 35, 1405.

VAN DEEMTER, J.J. (1961). Mixing and Contacting in Gas–Solid Fluidized Beds. Chem.Engng Sci., 13, 143–154.

VAN DEEMTER, J.J. (1980). Mixing Patterns in Large–Scale Fluidized Beds. in "Fluidization". Edited by Grace, J.R. and Matsen, J.M. Plenum Press, New York, 69.

VAN SWAAIJ, W.P.M. (1978). The Design of Gas-solids Fluid Bed and Related Reactors. ACS Symp. Ser., 72, 193.

VAN DER VAART, D.R., DAVIDSON, J.F. (1986). The Combustion of Hydrocarbon Gas, Pre–Mixed with Air, in a Fluidized Bed. In "Fluidization V", Elsinore, Denmark. Engineering Foundation, New York, 539–546.

VAN DER VAART, D.R. (1988). Freeboard Ignition of Hydrocarbon Gas in Fluidized Bed. Fuel, 67, 1003–1007.

VAN DER VAART, D.R. (1992). Mathematical Modeling of Methane Combustion in a Fluidized Bed. Ind.Eng.Chem.Res., 31, 999–1007.

WEN, C.Y. (1984). Flow regimes and Flow models for fluidized Bed Reactors. In "Recent Advances in the Engineering Analysis of Chemically Reacting Systems". Edited by Doraisamy, L.K. Wiley Eastern, New Dehli, 256.

WISE, H., and QUINLAN, M. (1986). Elementary Processes in the Catalytic Combustion of Methane. Gas Research Institute Report, Chicago Il.

YANATA, I., MAKHORIN, K.E. and GLUKHOMANYUK, A.M. (1975). Investigation and Modeling of the Combustion of Natural Gas in a Fluidized Bed of Inert Heat Carrier. Int.Chem.Eng., 15, 68–72.

YERUSHALMI, J., and CANCURT, N.T. (1979). Further Studies of the Regimes of Fluidization. Powder Technol., 24, 187.

APPENDIX

APPENDIX A

Experimental Setups

A.1 Reactor 1

Figure A.1 shows the diagram of the 200 mm $I.D.$ column used for gas dispersion measurements. The orifices used to estimate the gas velocity are Eclipse–Bescom products $FOM43$, $FOM44$ and $FOM65$ and their calibration curves are presented in Figure A.2, Figure A.3, Figure A.4 respectively.

A.2 Reactor 2

Figure A.5 shows the diagram of the 100 mm $I.D$ with the equipment for data acquisition and the shielded $NaI(Tl)$ detectors. The reactor is made up of a preheater used only for hot experiments, a porous distributor that can withstand a maximum temperature of 600°C, a bed of about 1.2 m tall, a disengaging section of about 400 mm tall and 200 mm $I.D.$ and a reverse–flow cyclone.

Figure A.6 shows the same reactor with the features needed for the combustion of methane. A vibrator not shown in this diagram and tied below the cyclone was used to force sticky particles back into the reactor especially at high temperatures. The orifices $FOM43$ and $SBOG3$ used here are all Eclipse–Bescom products. Their calibration curves are presented in Figure A.2, and Figure A.7. Figure A.8 shows the calibration curve of the differential pressure transducer. The calibration curves of two rotameters from the same manufacturer and used on the methane line are presented in Figure A.9 and Figure A.10.

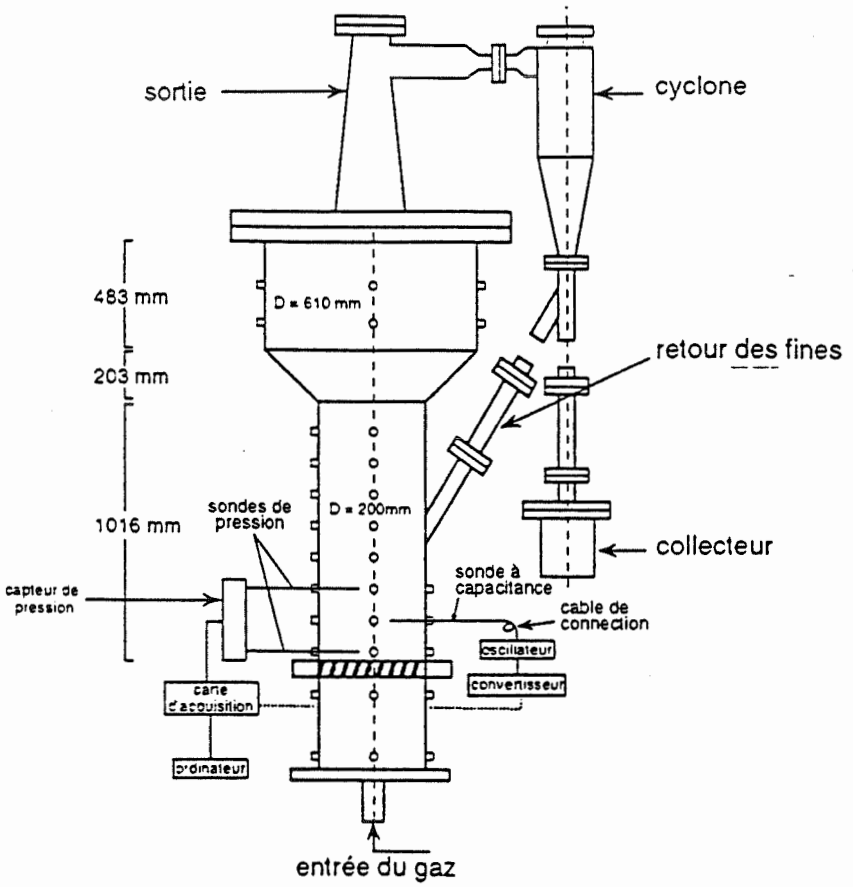

Figure A.1. Schematic diagram of the 200 *mm I.D.* Reactor

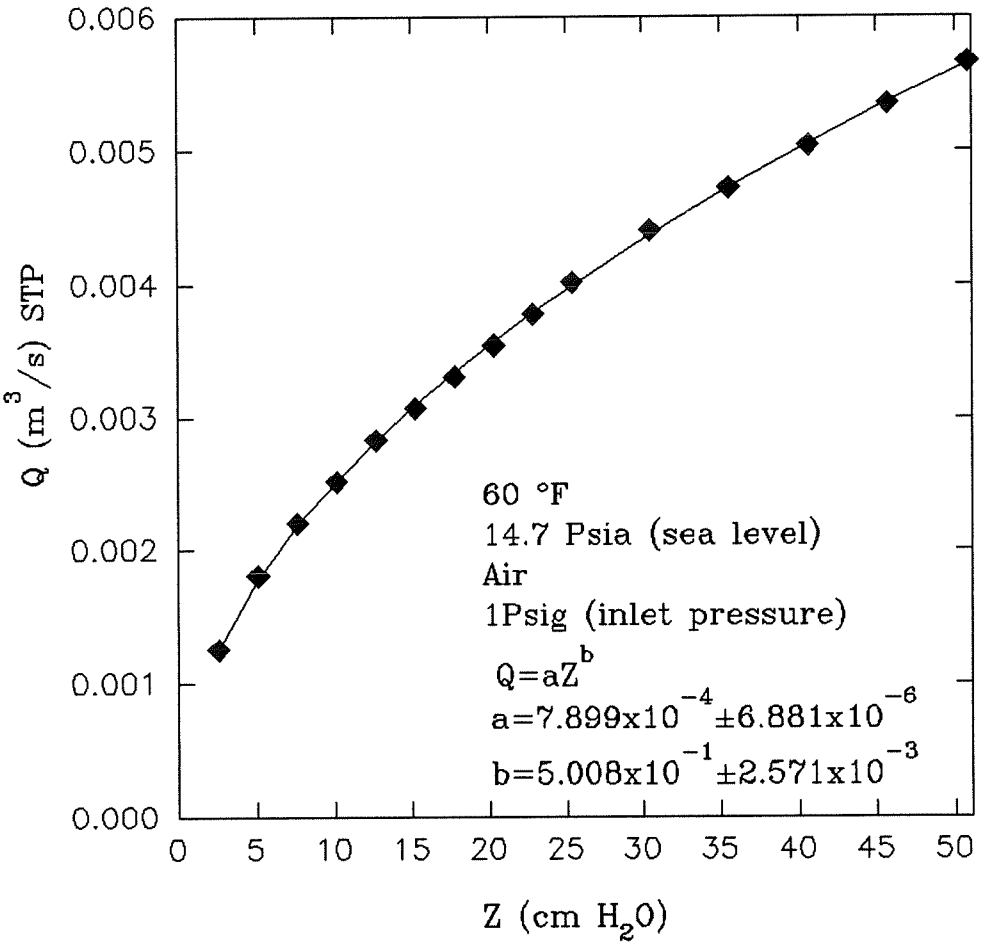

Figure A.2. Calibration of the orifice $FOM43$

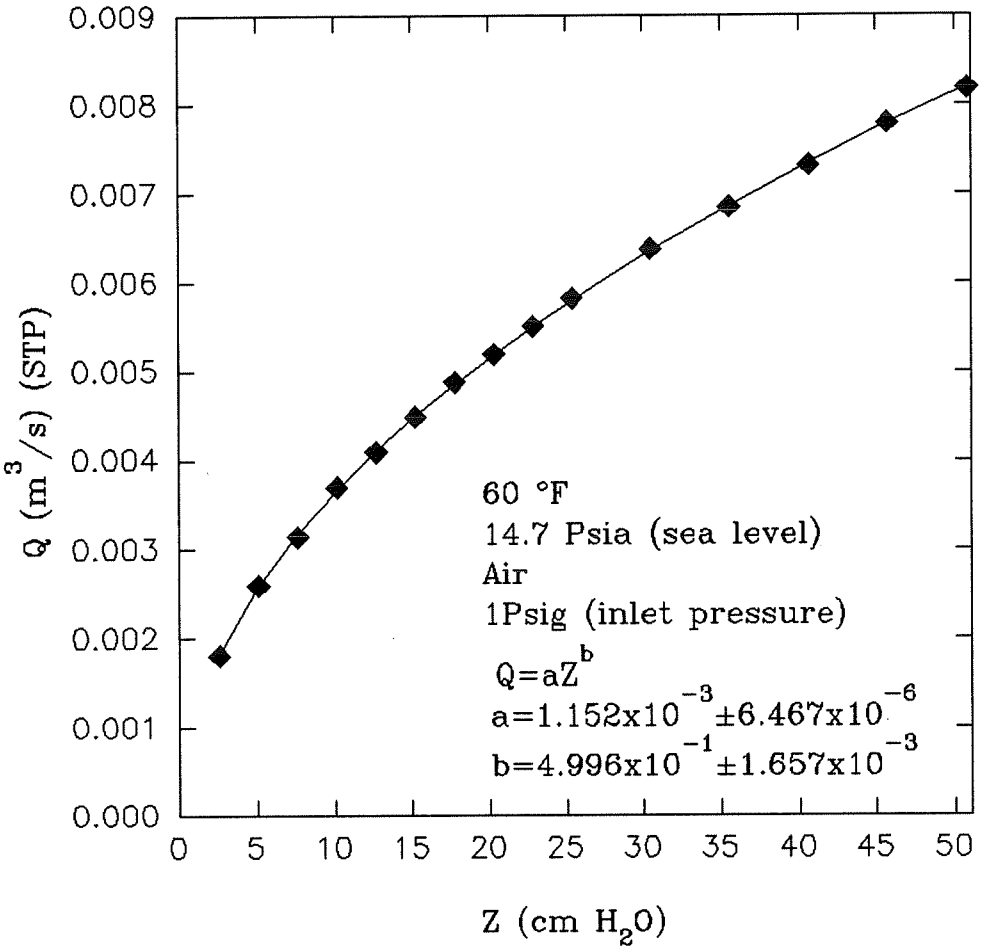

Figure A.3. Calibration of the orifice $FOM44$

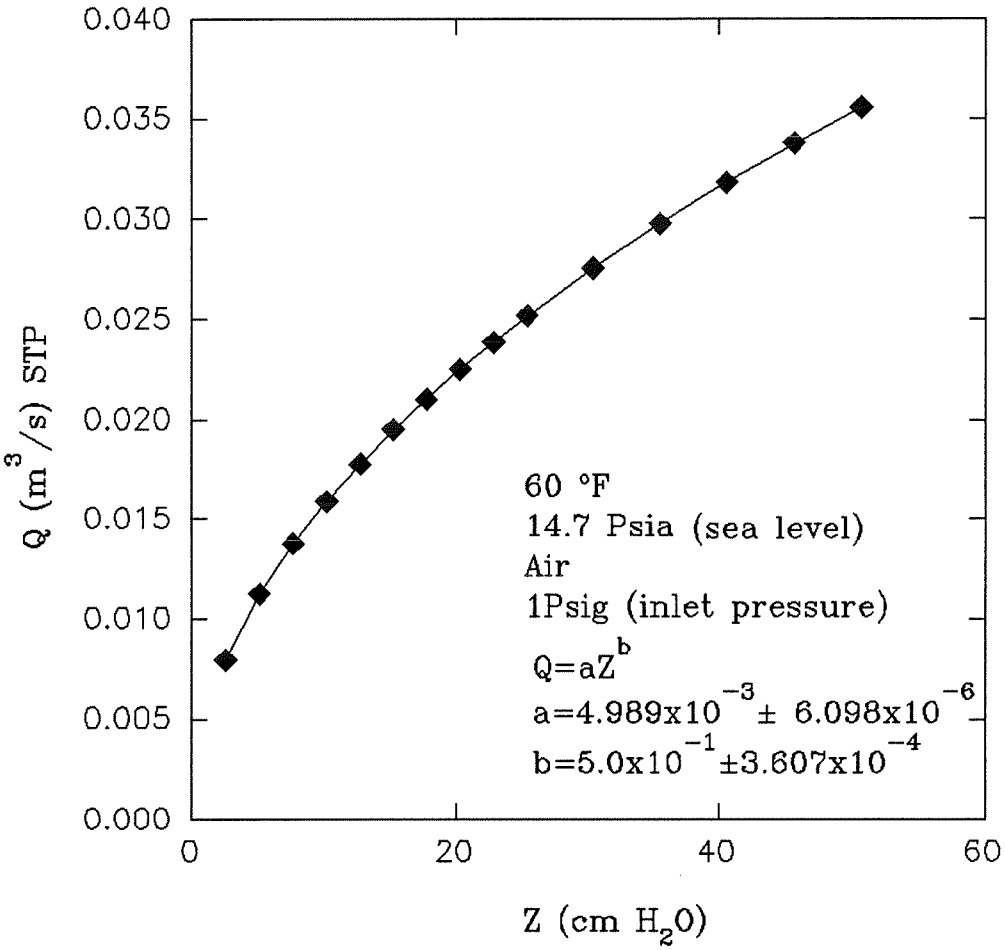

Figure A.4. Calibration of the orifice $FOM65$

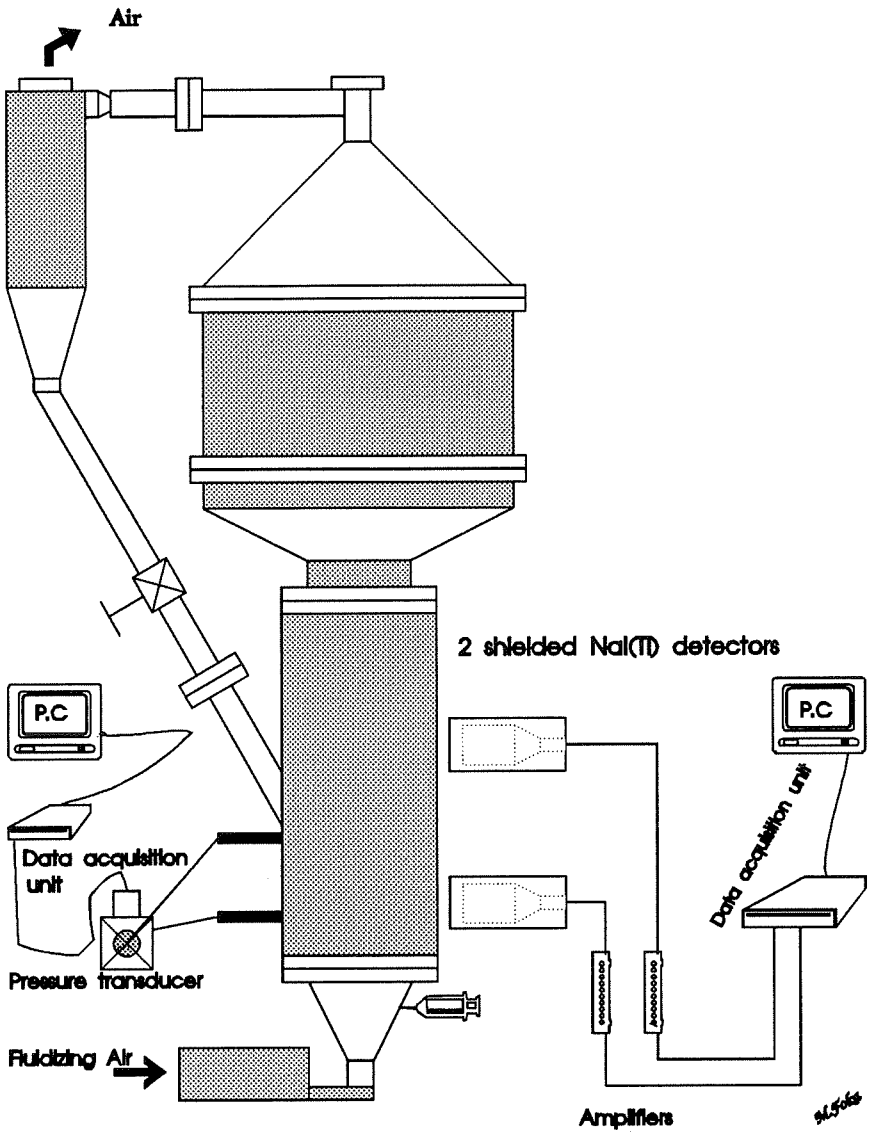

Figure A.5. Schematic diagram of the 100 *mm I.D.* Reactor as used for hydrodynamics investigations

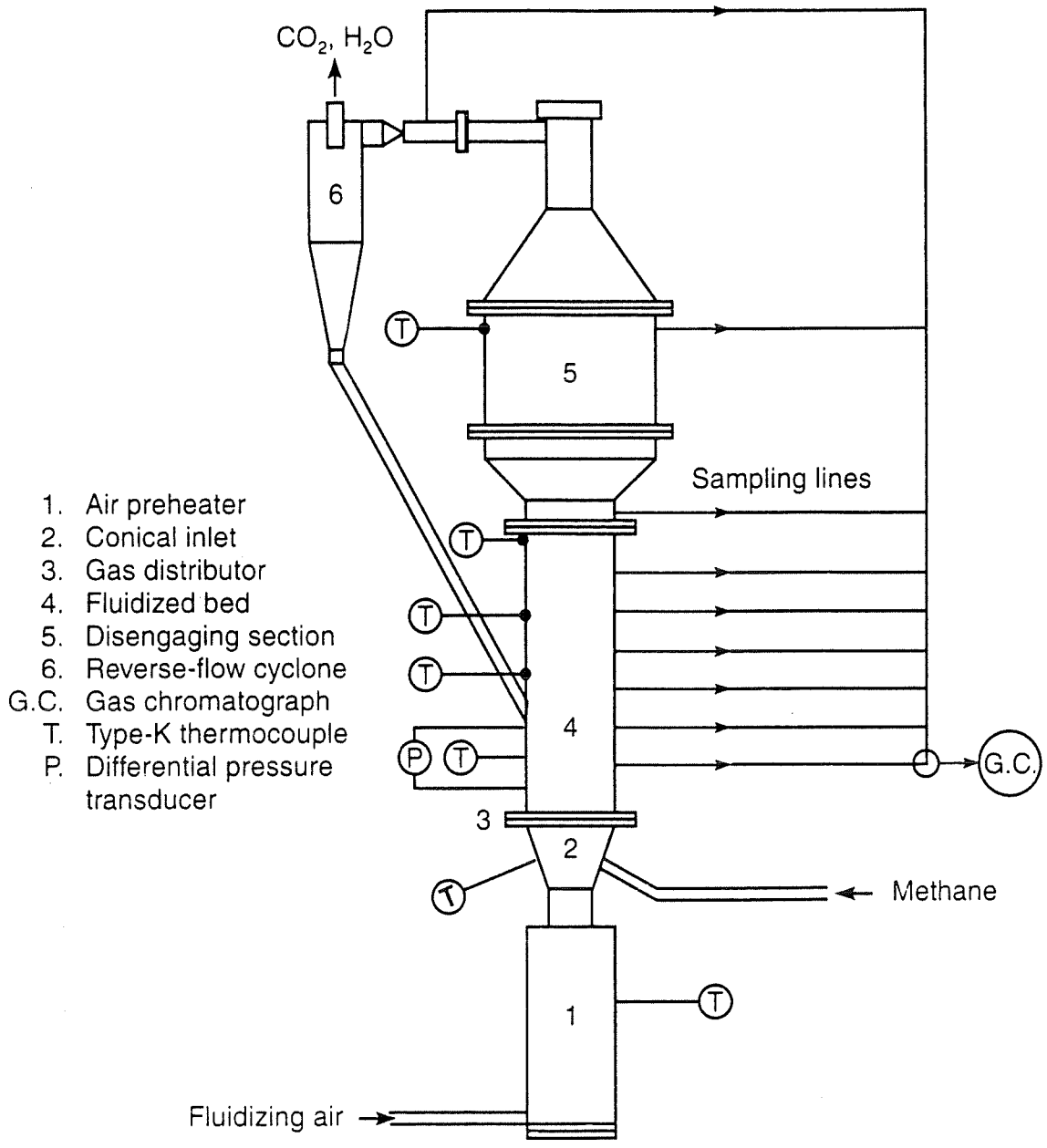

Figure A.6. Schematic diagram of the 100 *mm I.D.* Reactor as used for the combustion of methane

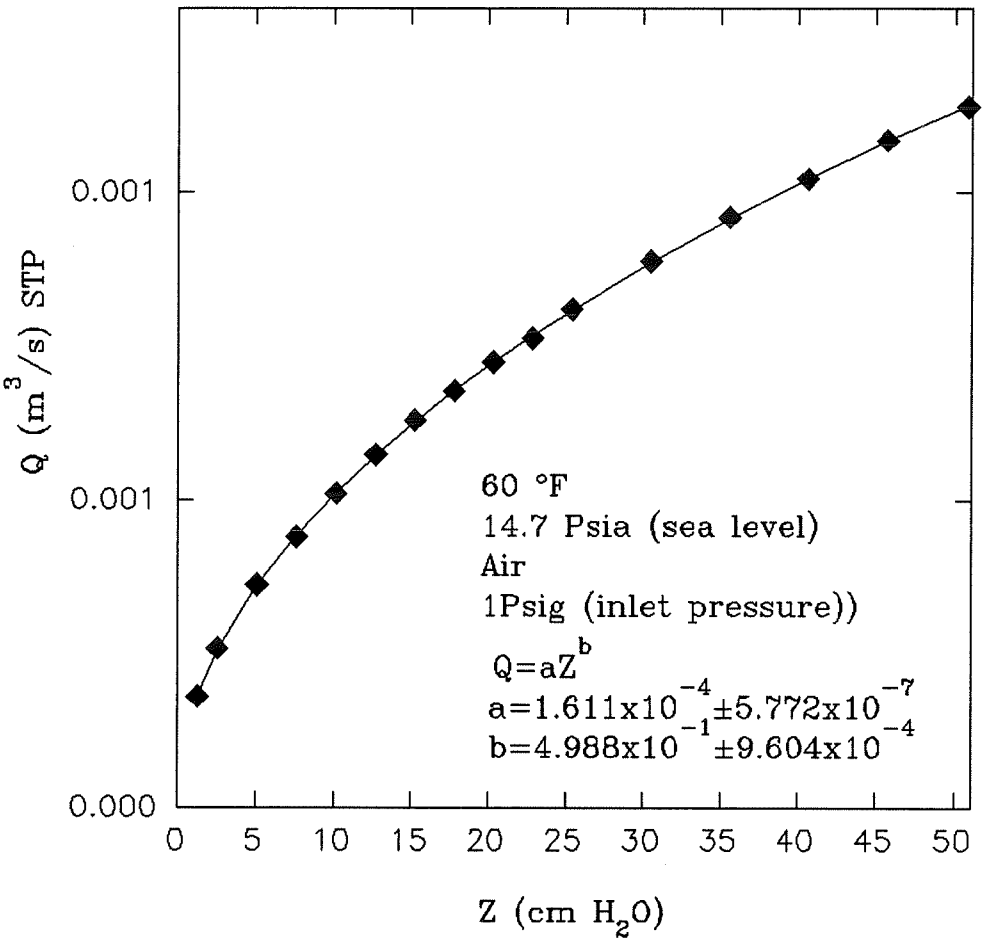

Figure A.7. Calibration of the orifice $SBOG3$

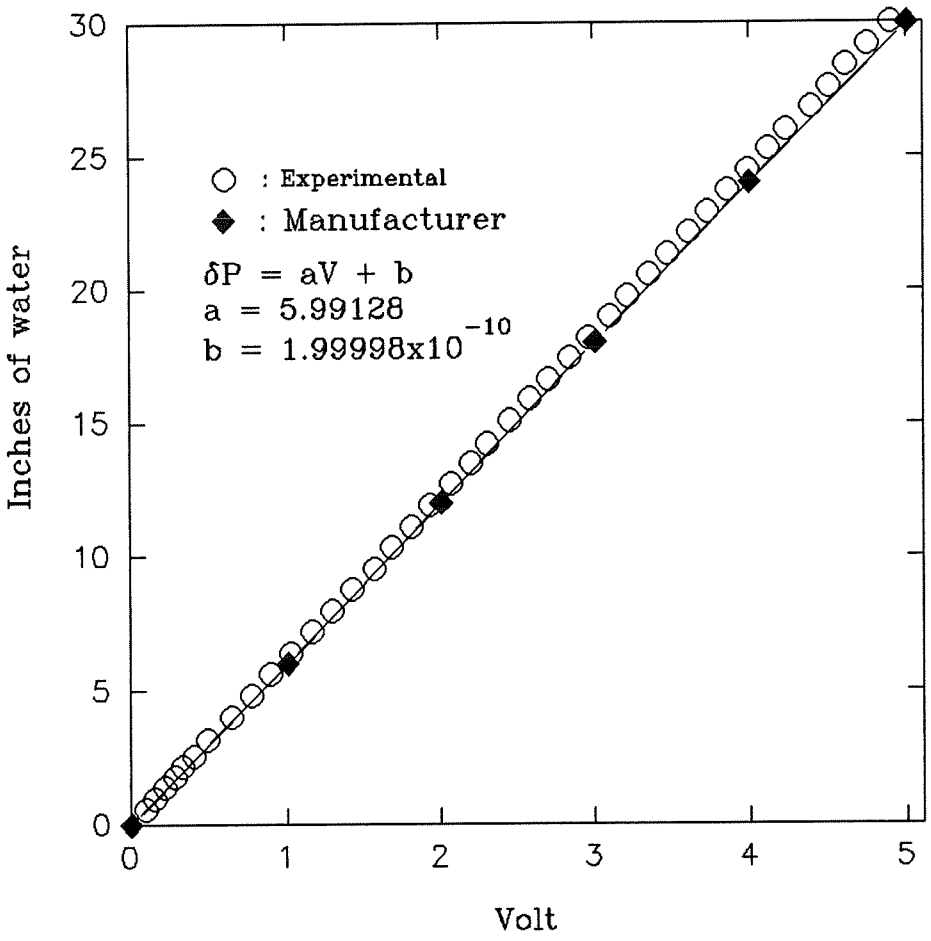

Figure A.8. Calibration of the differential pressure tranducer

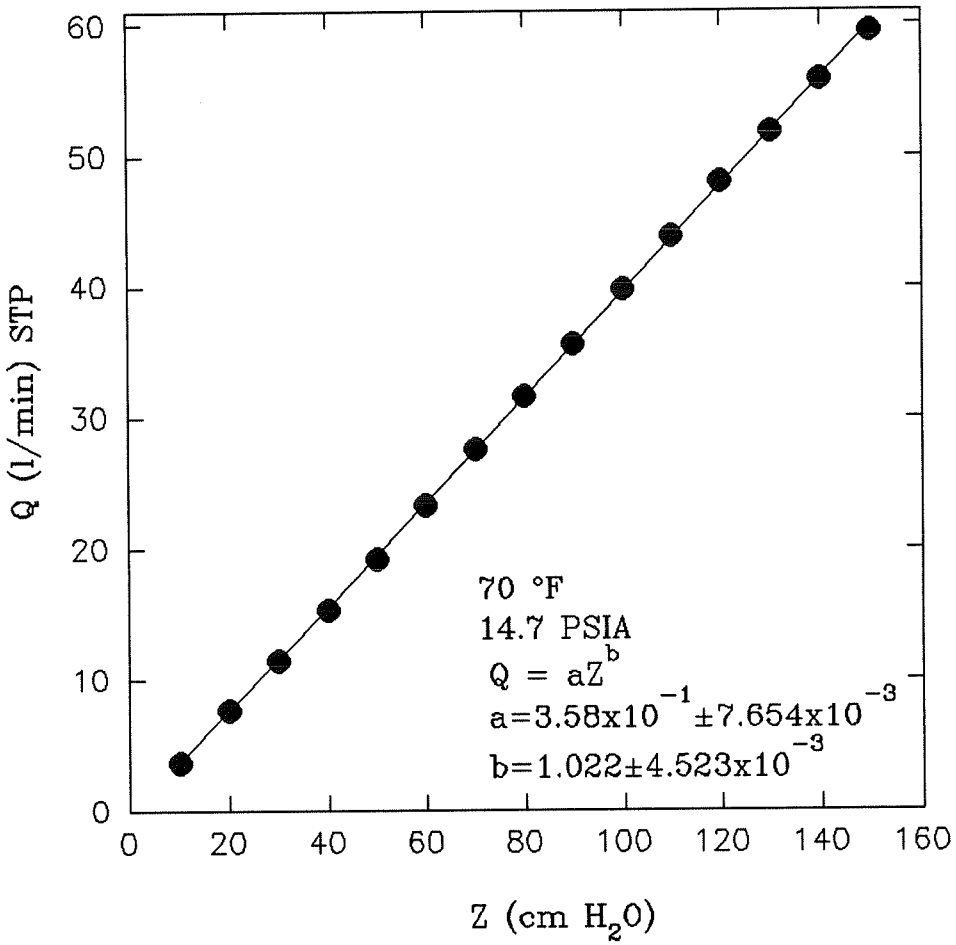

Figure A.9. Calibration of the rotameter $N044$

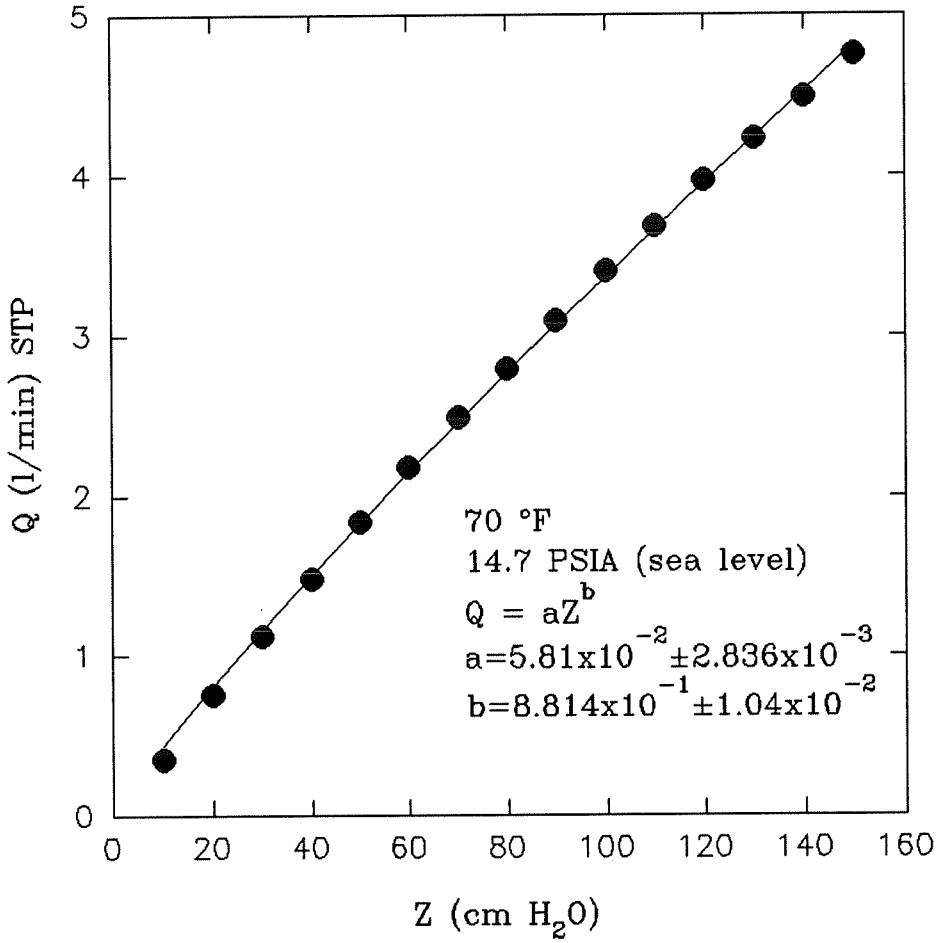

Figure A.10. Calibration of the rotameter $N092$

APPENDIX B

Experimental Procedure

B.1 Transition Velocity U_c

The transition velocity U_c is measured for every particle before any RTD and combustion measurement. Pressure fluctuations are measured with a dwell time of 20 ms and 2048 data points are analyzed over a wide range of velocities in terms of the standard deviation and the normalized standard deviation. Figure B.1, and Figure B.2 show two typical curves for pure alumina at ambient and high temperatures and for the $PC263$ catalyst at ambient temperature.

B.2 Gas Residence Time Distribution

Once the transition velocity are located at both ambient and high temperatures the RTD measurements are carried out in the appropriate flow regime. Figure B.3 shows the tracer response signals in the turbulent regime at $500°C$. Figure B.4 is

the prediction of the exit signal by the dispersive model using the transfer function in the real time domain.

B.3 Self–sustained Combustion

During the self–sustained combustion experiment the catalytic bed is preheated at the reaction temperature, then the solenoid valve controlled by the computer is opened and methane is allowed into the reactor through one of the rotameters of Figure A.9 and Figure A.10. The preheater is shut down when the temperature in the bed starts increasing. As the plenum cools down the temperature profiles in the equipment are similar to the curves in Figure B.5 and Figure B.6.

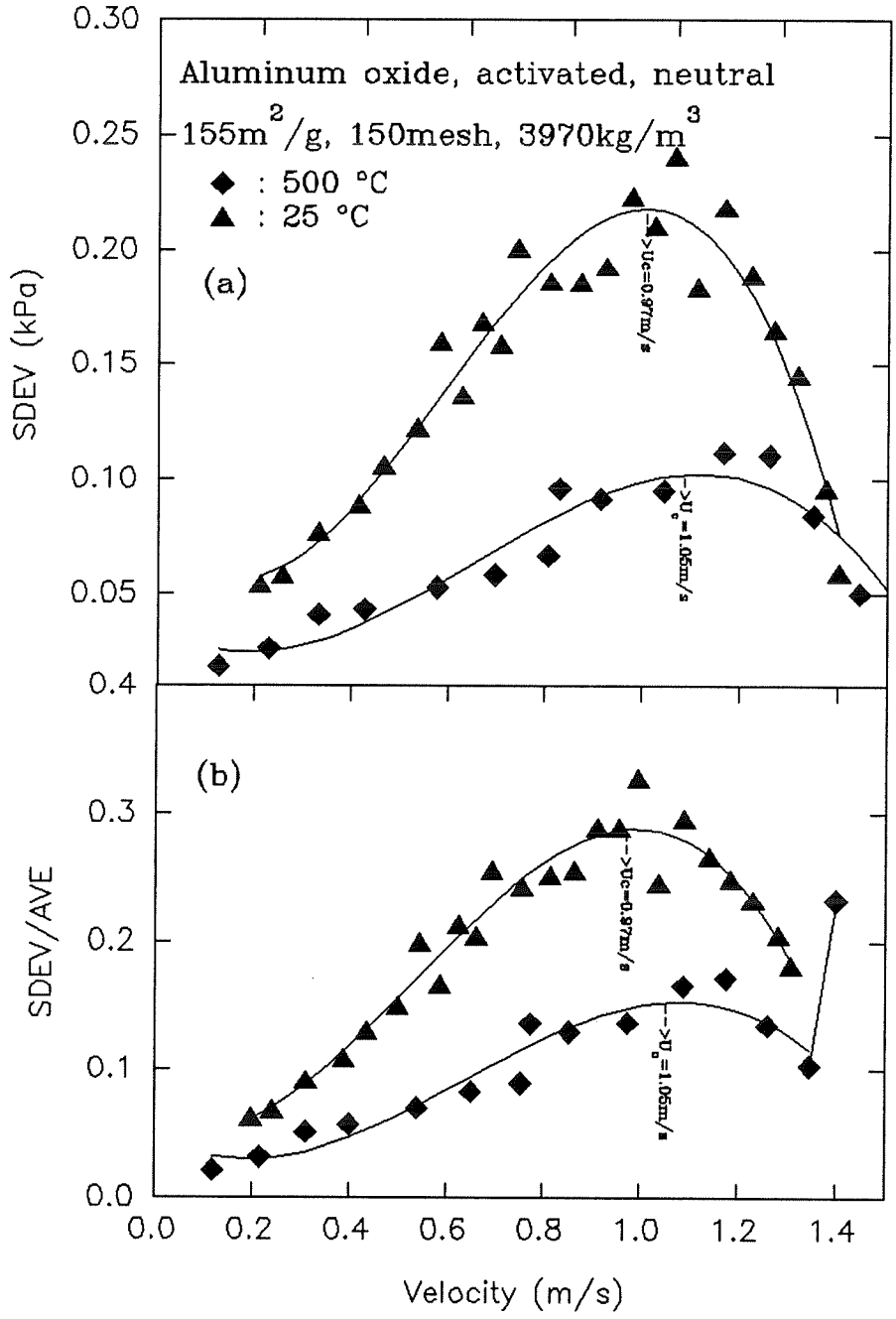

Figure B.1. Transition to turbulent fluidization at $25°C$ and at $500°C$.

Aluminum oxide particles

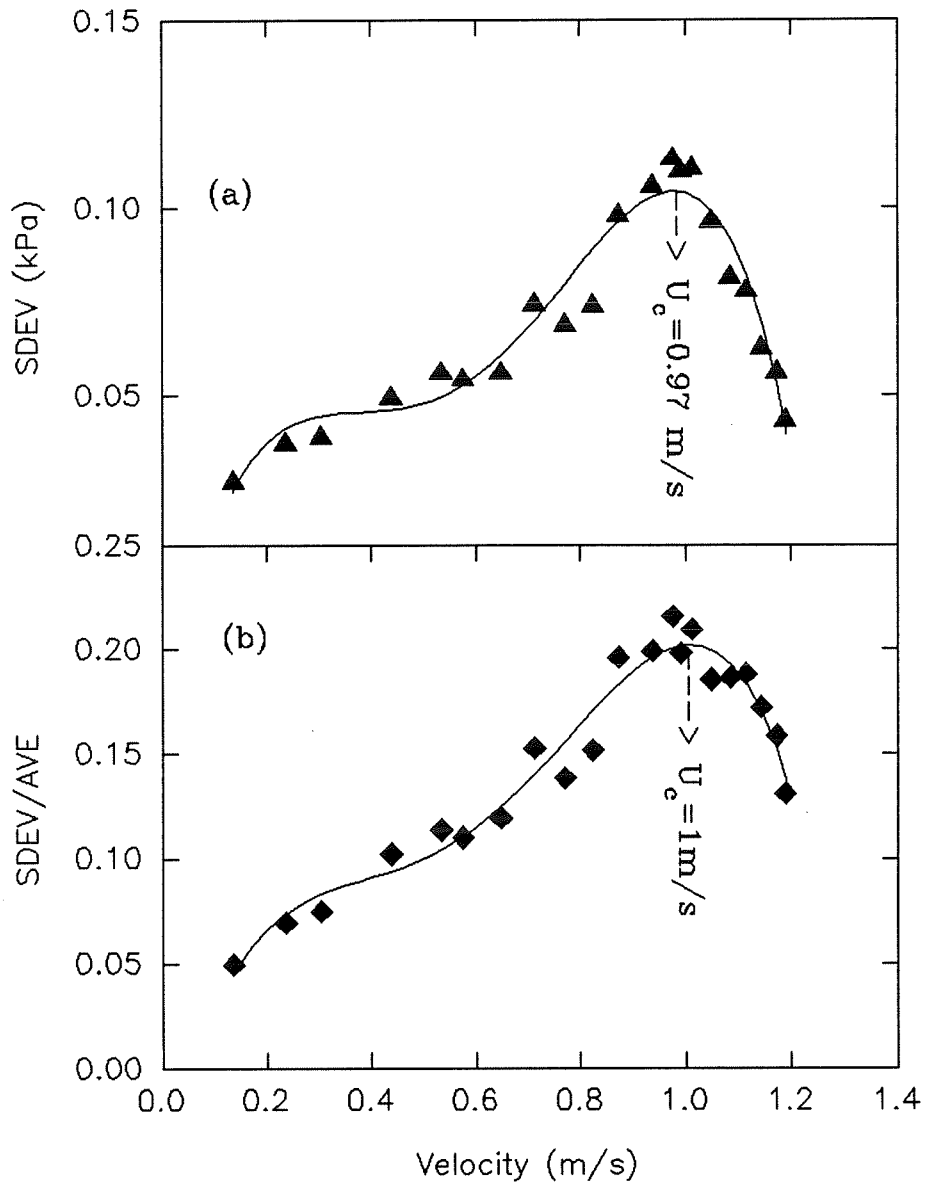

Figure B.2. Transition to turbulent fluidization at ambient temperature.

*PC*263 catalyst

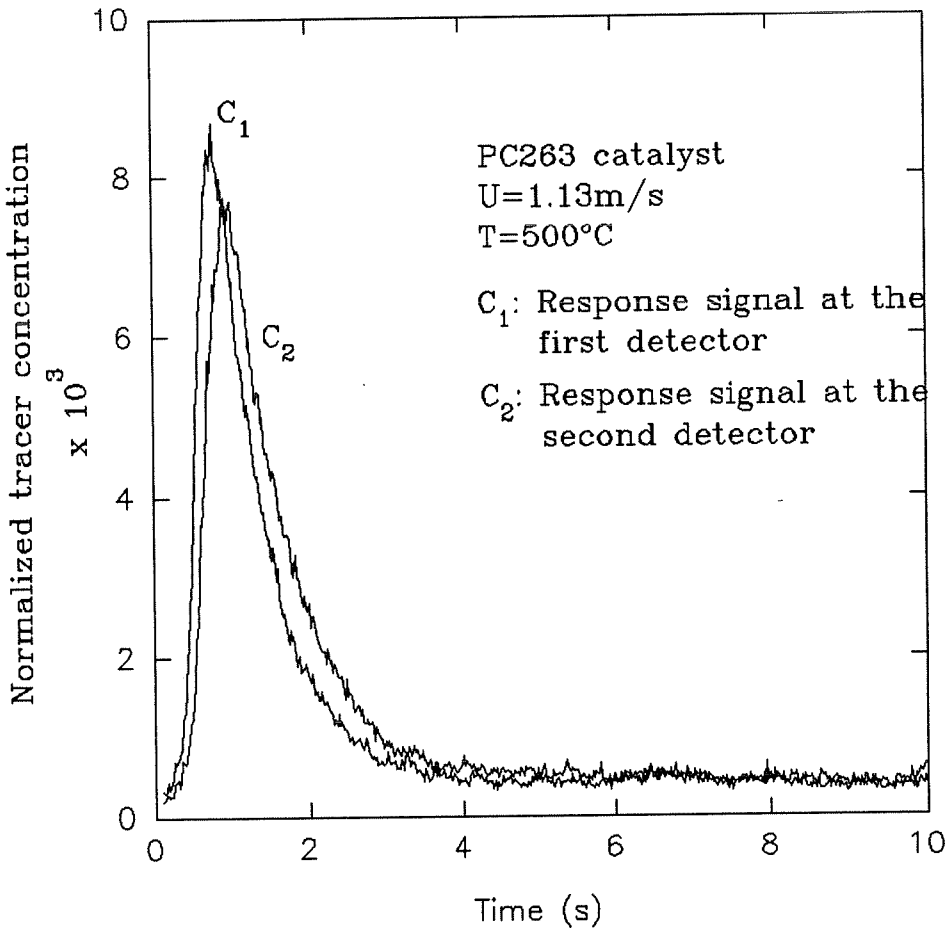

Figure B.3. Gas RTD with argon as tracer in the turbulent flow regime.

*PC*263 catalyst

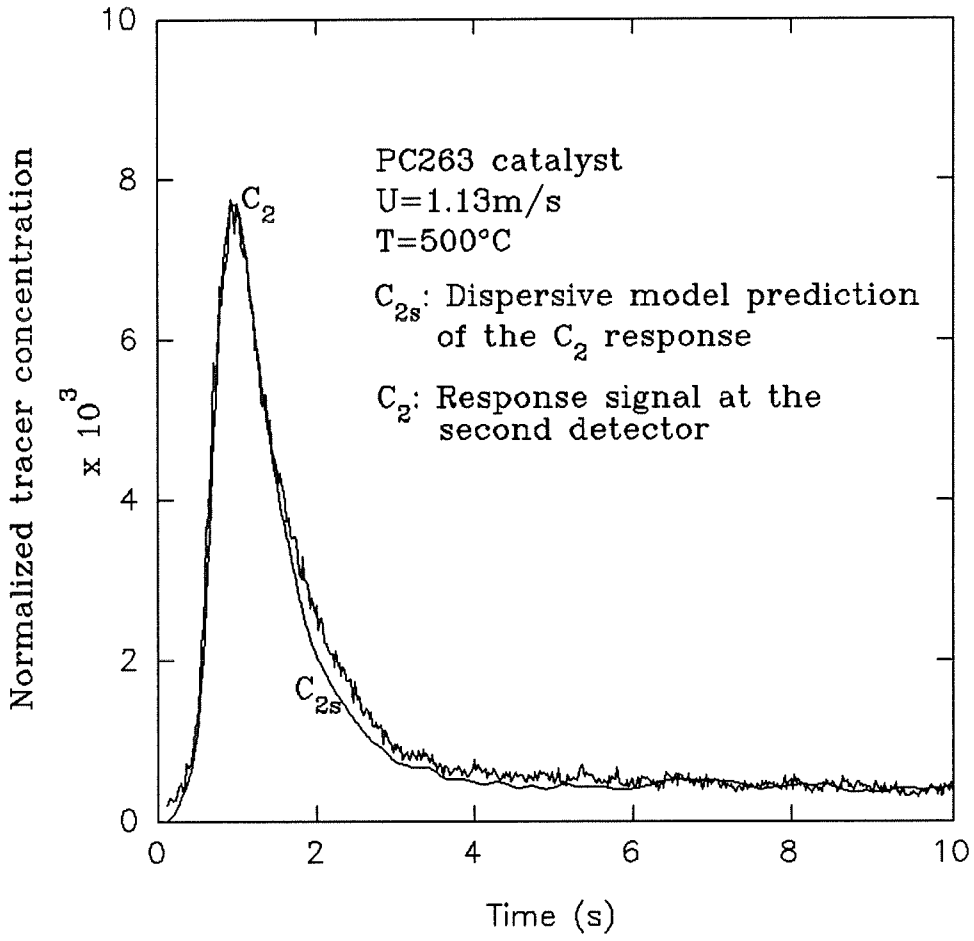

Figure B.4. Dispersive model prediction of the exit signal. $PC263$ catalyst

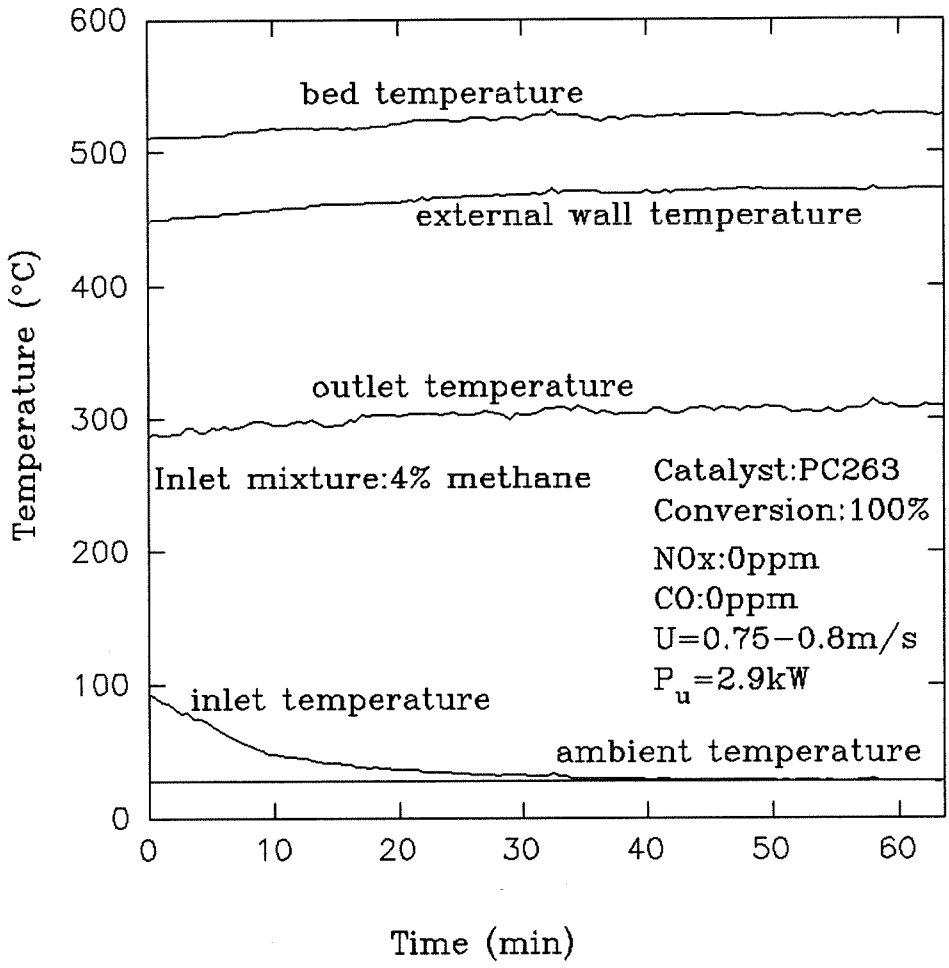

Figure B.5. Self–sustained combustion of methane in the bubbling regime

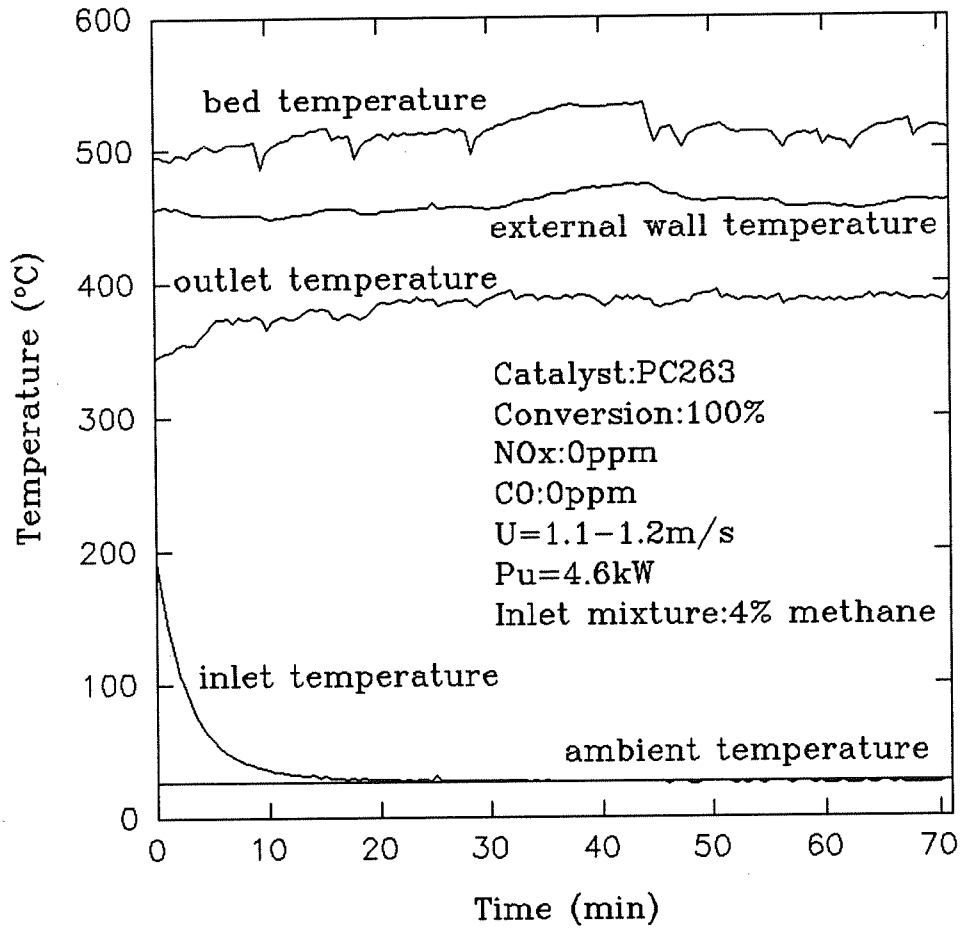

Figure B.6. Self-sustained combustion of methane in the turbulent regime